THE UNIVERSITY OF ASTON IN BIRMINGHAM

A DIAGNOSTIC STUDY OF A SADDLE FIELD ION SOURCE

Thesis submitted for the degree of

DOCTOR OF PHILOSOPHY

by

Thamir Numan MAWLOOD (B.Sc., M.Sc.)

Department of Physics

September 1980

ACKNOWLEDGMENTS

I would like to express my sincere thanks to my Supervisor, Dr. R.K. Fitch, for his continual help and invaluable encouragement throughout the period of this project.

Thanks are due to Professor S.E. Hunt, Head of the Department of Physics, for providing the facilities in his Department.

I express my gratitude to Mr. A.G. McKenzie, the Vacuum Laboratory Technician, for his considerable help in the construction of various parts of the apparatus.

Finally, my acknowledgments are also due to the Ministry of Higher Education and Scientific Research, Baghdad, Iraq, for supporting me during these studies.

SUMMARY

"A diagnostic study of a saddle field ion source"

Thamir Numan MAWLOOD

Ph.D - 1980

This thesis describes a diagnostic study of the spherical version of the saddle field ion source. It also includes a review of the development of the source and its importance in relation to other sources in various aspects of ion beam technology.

It has been shown that the source is easy to construct and operate and the properties of the source have been studied for argon, nitrogen and helium. The source is characterized by three principal modes of operation, the glow, transition and oscillating modes. Experimental studies and theoretical considerations have confirmed that the source efficiency is greatest in the oscillating mode. This occurs at low pressures when the mean free path for ionization by electron impact is greater than the radius of the source.

The source produces energetic ions, electrons and fast neutrals. An electrostatic deflecting system and an energy analyzer has been used to show that the electrons are of low energy and originate from the edge of the cathode aperture due to secondary emission by ion bombardment. These electrons surround the ion beam and do not appear to be important in application of the source to ion bombardment studies.

A simple probe technique has been developed to show that the fast neutrals are mainly confined to the centre of the beam. A crossed beam technique has been used to show that the neutrals have energies similar to that of the ions. A theoretical analysis supports the idea that the neutrals are produced by a resonance charge exchange process inside the source. The neutral/ion content varies from about 20% in the low pressure oscillating mode to as much as 90% in the glow mode. Advantage can be taken of this effect when it is required to etch electrically insulating materials.

Key words: ion, electron, neutral, energy, vacuum.

CONTENTS

LIST OF FIGURES

LIST OF TABLES

CHAPTER 1

DEVELOPMENT OF ION SOURCES

1.1 Introduction

The ion source is the most important single element in any ion beam system and probably began with the work of Thomson who developed an ion source operated at high voltage which produced ions with a large energy spread. It produced a low fraction of atomic ions and the stability of the gas discharge could not be continuously maintained.

Attempts were started to develop new ion sources with less spread of energy and lower power consumption. This work was stimulated to a great extent by the start of mass spectrometric research and the real development of ion sources began with the birth of nuclear physics in 1930-1933. Ion sources are becoming ever more extensively applied in various fields of science and technology. The basic function of an ion source is to produce an ion beam of the required intensity, energy and gas pressure. In ion implantation, milliamperes of current for a wide range of solid ions are required. Thus the design of the ion source, acceleration, shaping of the ion beam, separation of the chosen ions from other ions and atoms, and the energy of the ions are all important parameters in the implantation in semiconductors.

In sputtering processes, which is the removal of atoms during ion bombardment, the ion current density must be high and the mean free path of ions and sputtered atoms, large compared with the tube dimensions. Furthermore the energy spread of the incident beam must be minimal and the ionization condition should be such as to minimise the production of multiply charged states.

The achievement of very intense ion beams of a few amperes is

still important in technology and scientific research. In space propulsion, heavy ions with long life times and high ionization efficiencies with ion energy several keV are required. In particle accelerators a high proportion of atomic ions with respect to molecular ions, low consumption of gas, long life time, low consumption of electric power and uniform energy distribution are all features required in accelerator technology. However, fusion plasma ion sources are passing through a fast development at the present time as there is a need for high density ions of 10^{13} to 10^{15} cm^{-3} with small divergence which is necessary for heating the plasma. Some experimental work needs multiply charged ions to produce high energy heavy ions which, for example, are needed in particle and nuclear research. In medical research and health physics application of heavy ion beams is being pursued in many areas.

It can be seen from the previous discussion that there are many wide and varied applications of ion sources, each purpose having appropriate requirements thus presenting some unique problems in (1) the design of the ion source to produce the required ions with appropriate energy and species, (2) the transport and focusing system and (3) the interaction of the beam and the target. The important characteristics of ion sources are thus beam intensity, current stability, mass discrimination, energy spread, ion species, fragments and sensitivity ratios of ions produced to neutrals present.

A variety of mechanisms exist by which sufficient energy may be imparted to gaseous atoms or molecules to cause ionization. The gas may be ionized thermally by a high voltage discharge, by a radio frequency field or by electron impact where electrons are derived from a hot filament or by secondary emission from a cold cathode. These methods of producing ions have given rise to ion sources of various types each having its own characteristics of design,

properties and applications. These are designed to eliminate the problems in producing the ionization and to achieve the adequate intensity of ions of the required energy spread. A considerable amount of developmental effort has been expended over the past thirty or more years to evolve improved types of ion sources. It is thus rather difficult to classify them and to state the precise requirements and principles of all types of ion sources in use today. In the next section an attempt is made to discuss the most important types, namely, electron impact, low voltage arc discharge, high frequency gas discharge, thermal ionization and bombardment ion sources.

1.2 Ion sources

A. Electron impact ion source

In the ion sources utilizing bombardment by electrons, the atoms or molecules of the analyzed element are ionized by inelastic collision with electrons. The number of ions depends on the following parameters: The ionization cross section, current density of the electron beam, the number of atoms or molecules to be ionized per unit volume and the effective volume of the ionization. Nier[1] and Bleakney[2] developed an ion source with a low intensity ion beam with a small energy spread as shown in figure 1.1 for their electron impact ion source.

The ionizing electrons are emitted from an oxide cathode and pass through the chamber with energy 100 eV. The ions thus formed are extracted from the ionizer by a 2kV voltage applied to the extracting electrode and reach the ion beam analyzer by a focussing system. The ion current extracted from the ion source varies from 1 to 30 μA with an operating pressure 10^{-4} Torr and giving an energy spread of 0.05 eV. The ion source is suitable for experiments in mass

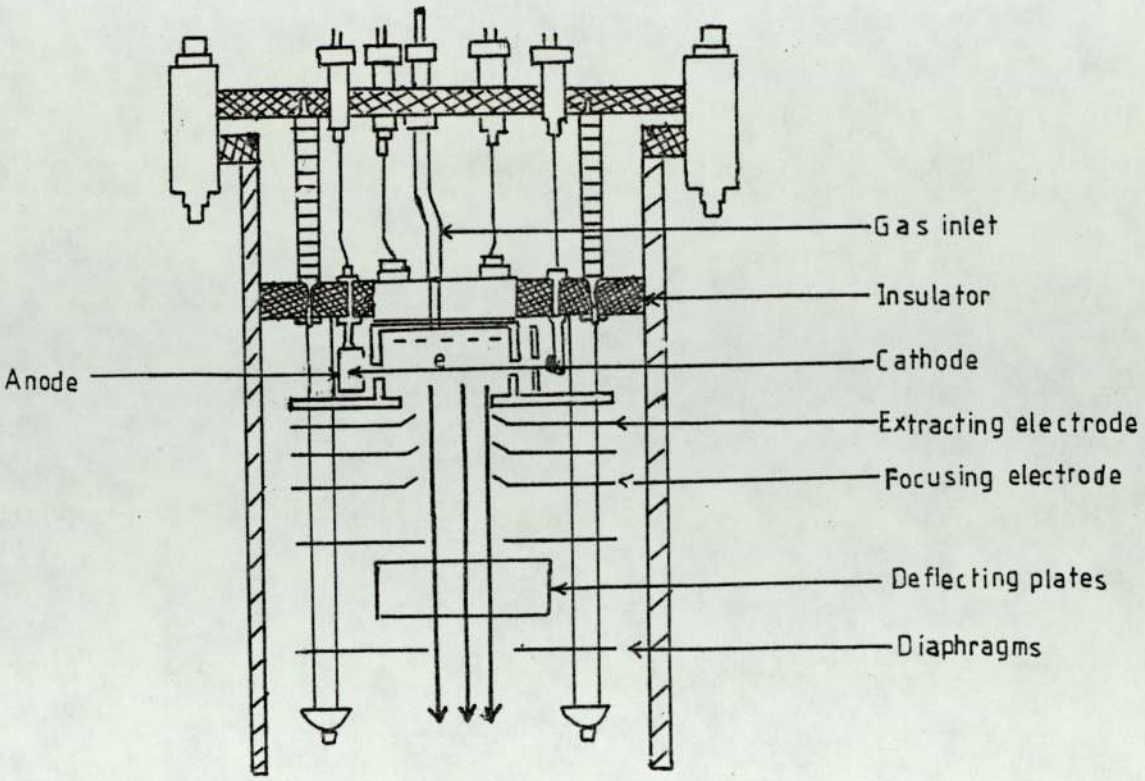

Figure 1.1 Electron impact ion source for production of gas ions

spectrometer. The specified parameter of the ionizer is its efficiency, which can be defined as number of ions to the number of neutral atoms per second. The efficiency increases if the electron density and effective volume are increased and Pierce[3] and Slabospitskii et al[4] used a multicathode ionizer to increase the efficiency.

B. Low voltage arc-discharge ion sources

The arc discharge process takes place at discharge currents greater than 0.1A. Low gas pressure arc discharges are characterised by three regions. Firstly, a fall in the potential during the discharge and the value of this fall is only slightly below that of the total potential difference in the discharge. Secondly, a region of the quasi-neutral plasma, the positive column of arc-discharge which extends almost over the entire space between the anode and cathode and in this region the potential fall is very small. The third region is anode fall where the potential fall is small. The

potential difference required to bring about the discharge in the cathode fall depends on whether the electrons are obtained from the cathode by cold or thermal emission.

(1) Hot cathode electron emission:-

(a) Plasmatron

The plasmatron is the source which utilizes hot cathode electron emission. Ardenne et al[5] used a helical cathode of tungsten wire mounted in the interior of the intermediate electrode. The anode was placed at the end of the intermediate electrode. In this source the plasma sphere with high ion concentration appears at the end of the intermediate electrode in front of the electron emitter and the outlet aperture through which the ions are being extracted. Ion currents of the order of 10 mA can be obtained from this assembly at a gas pressure 2 to 5 x 10^{-2} torr, arc currents between 0.3 to 2A, applied voltages between 30-80V and extracting voltages from 50 to 70 kV. The energy spread of this source is not more than a few electron-volts. These sources are therefore preferably used in experiments which require an intense ion beam of homogeneous energy.

Another advantage of this type is the low power consumption, since they can be operated at a few hundred watts. These sources are limited by the lifetime of the hot filament and poor atomic contribution of about 20 percent to the extracted ion beam. Thus sources of this type are employed only if the ion sources are operated in magnetic or radio frequency fields. In a homogeneous magnetic field version Baily et al[6] used a solenoid surrounding the ion source to produce the magnetic field with a gas consumption 8 cm^3 hr^{-1} and with a field of 100 mT and a molecular ion current of 100 μA.

Atterling[7] used a hot cathode arc-discharge ion source without

high intensity oscillating electrons and this source can be utilized in the cyclotron. Ion currents from 50 to 100 mA can be extracted from this source at a gas consumption rate of 60 cm^3 hr^{-1}.

(b) Duoplasmatron

The duoplasmatron is a hot cathode arc-discharge ion source in an inhomogeneous magnetic field. Moak et al[8] used a cathode which was prepared from a barium oxide coated platinum or iridium band.

The cathode is heated directly with a current of 30 to 60A at 2 to 3 volts. The magnetic field is generated by an electromagnet which produces an inhomogeneous field generated between the peak of the intermediate electrode and the support of the anode. The value of the magnetic induction at the point of maximum field intensity can be 2 to 6 mT. The magnetic coil, the intermediate electrode and the environment are cooled using liquid coolant. Figure 1.2 shows the duoplasmatron type ion source with electromagnet.

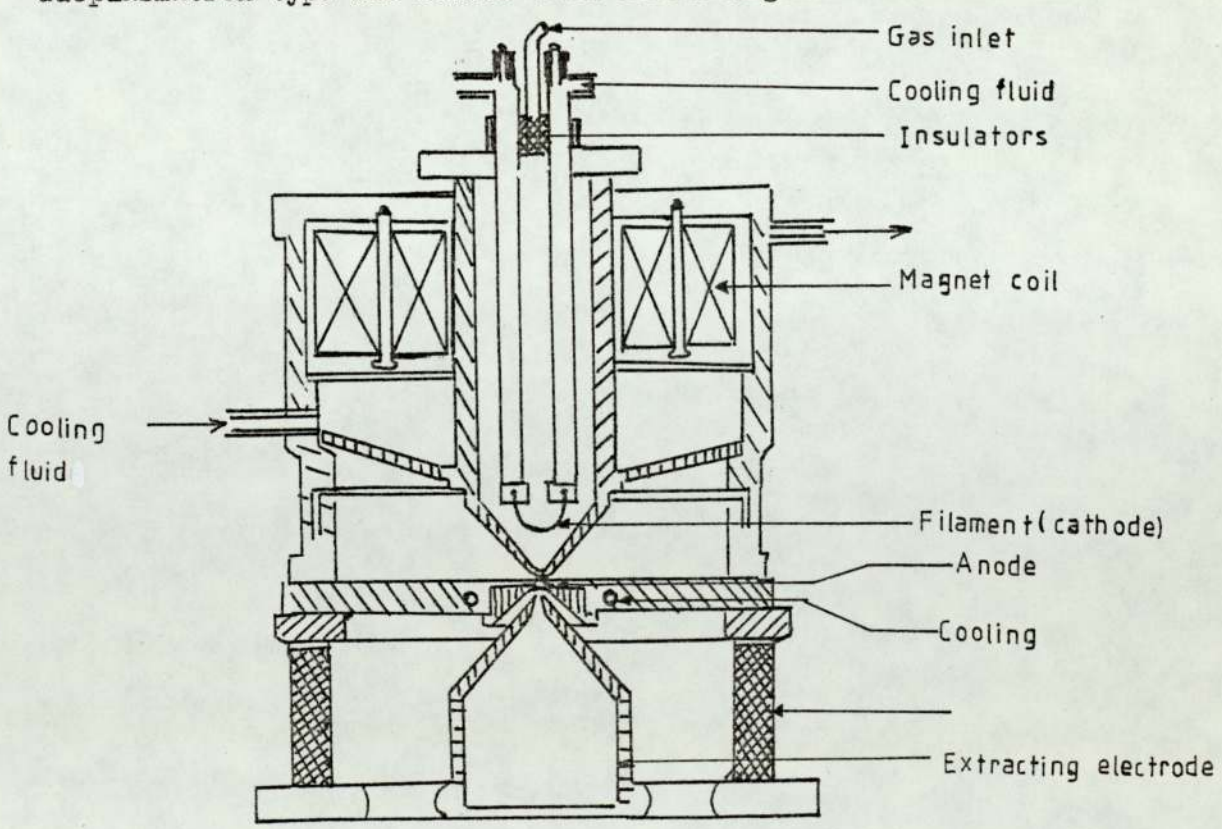

Figure 1.2 Moak's duoplasmatron type ion source with electromagnet.

The source uses ion currents of a few mA and an arc current about 2 mA and the useful lifetime of the assembly can be 600-1000 hours. The value of the extracted ion current depends on the discharge current as shown in figure 1.3 (Ciuti)[9].

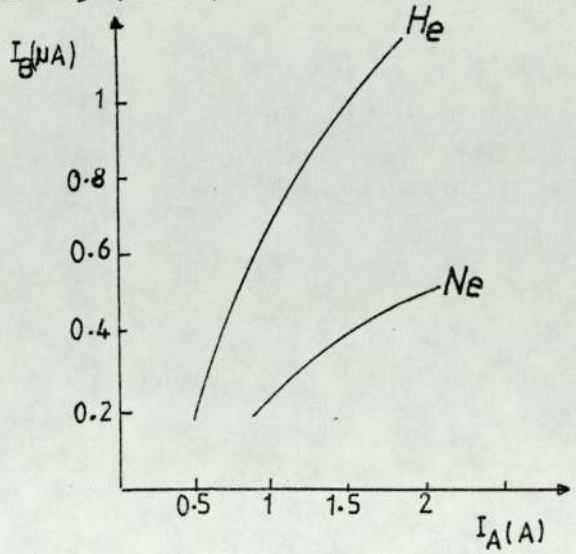

Figure 1.3 Dependence of ion current on arc discharge current in low voltage duoplasmatron ion source.

In the hot cathode arc-discharge ion source with oscillating electrons both homogeneous and inhomogeneous magnetic fields can be applied. This type of source is useful in either linear or cyclic accelerators and in isotope separators. The cathode lifetime limits that of the ion source and the construction of the assembly is also complicated by the use of heated cathodes and thus the cold cathode ion source is preferable.

(2) Cold cathode emission ion sources:-

These sources are designed on the Penning type discharge[10] phenomena in which a self-maintained discharge can be operated at low pressures. The electrons which fly on a nearly helical trajectory under the action of the electric field generated between the electrodes, oscillate at the same time in the direction parallel to that of the magnetic field and to the discharge axis. The material of the cathode, the quality of the cathode and ion energy are

important in the production of secondary electron emission. Consequently the formation of a self-maintaining discharge may be influenced by the proper choice of the cathode material and the cathode surface. The ions are extracted from the source either axially, which is, in the direction parallel to that of the discharge axis and of the magnetic field, or transversely in the direction normal to the axial direction. The first version is preferred for low intensity ion beams, while the second is mostly used for high intensity beams.

With axial ion extraction, Keller[11] used a permanent magnet for the generation of the magnetic field. The cathodes are hollow to improve the stability of the discharge and the cathodes of this type are made of iron with the poles of the permanent magnet attached to the iron. The ions are extracted from the discharge volume at the anticathode aperture 1 to 2 mm in diameter. The ion current obtainable from this source varies from 0.1 to 1 mA. The anode is a ring made of iron or magnesium and the anode voltages from 470 to 520 volts and the discharge current is in the range 10 to 120 mA. The magnetic field applied to the discharge volume is usually about 100 mT. Prelec et al[12] used a solenoid to generate the magnetic field, the cathodes of this source are made of 3 mm thick tantalum. Figure 1.4 shows the cold cathode ion source and axial ion extraction.

The ions are extracted through a slit in the anticathode. The anode is made of stainless steel and consists of two cylinders screwed together and attached to a metal disc soldered between isolating rings. With this source singly or multiply charged ions of carbon, nitrogen, neon, argon and xenon can be produced. The ion current extracted from the source varies from 2.5 to 5 mA with an extracting voltage of 16 kV with the parameter values being typically

V_A = 5 to 6 kV, I_A = 0.5 to 1.5A and the magnetic intensity 27 mT.

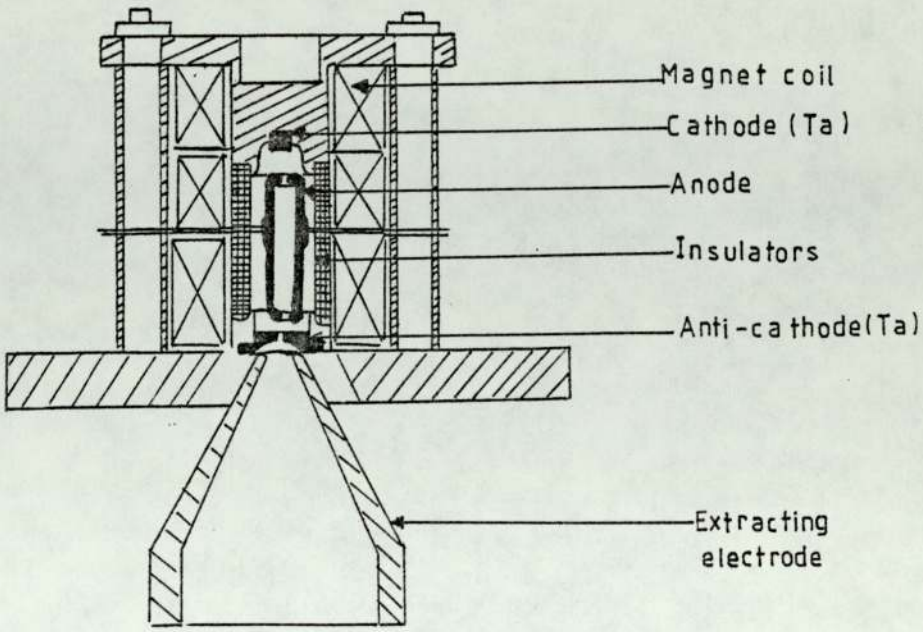

Figure 1.4 Prelec version of a low intensity ion source with cold cathode and axial ion extraction.

The energies of ions extracted in this source are usually equal to the energy corresponding to the cathode fall potential. This value depends on the material of the cathode and equal to 70 to 80% of the anode voltage. The energy spread of ions depends on the fluctuations in discharge current and the amplitude of ion oscillations taking in the discharge. Nagy[13] has shown the ion energy spread for an aluminium and an iron cathode as shown in figure 1.5. The full width of the energy spectrum obtained with the aluminium cathode is between 45 and 50 eV with a half-width value of 16 eV and if iron cathodes, the energy spread shows the total width being 240 eV with a half-width value of 45 eV.

With transversal ion extraction, Anderson et al[14] used ion extraction suitable for the production of high intensity beams. The tantalum cathodes of the source are of cylindrical shape and they can

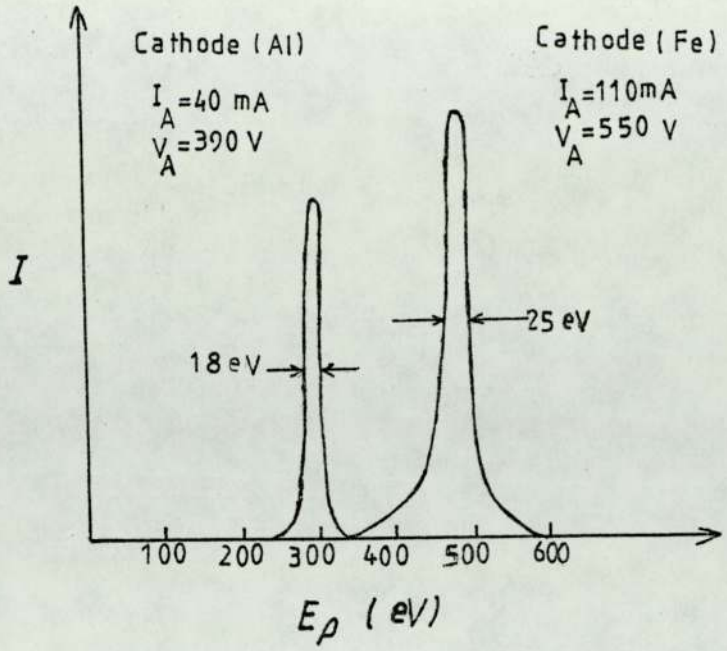

Figure 1.5 Energy spread of ions extracted from cold cathode Penning type discharge for aluminium and iron cathodes.

be screwed into the base plate of the cathode. The ion currents which can be extracted with the use of a magnetic field of 0.44 T and extraction voltage 18 kV with different discharge currents and different gas consumption as, for example, with helium I_A = 1.4A, V_A = 2 kV, gas consumption 6cm^3/min and ion current 29 mA.

C. High frequency gas discharge ion sources

These types of sources utilize the oscillator to generate the high frequency discharge. The collision frequency in the discharge depends on the gas pressure such that higher gas pressure is associated with higher frequency and lower gas pressure with lower collision frequencies. The most precise geometry is required by the ion extraction system and two types of extraction system are applied.

The first is done with a probe and in the other with the aid of a diaphragm which is a thin disc with a hole in the centre. In the first system the anode is mounted at one end of the discharge tube while the cathode is mounted at the other end. In the diaphragm

system both electrodes are mounted at the same end of the discharge tube. In both systems the two electrodes are shielded by glass or quartz to decrease the rate of recombination. Thonemann[15] used a probe extracting system, the discharge chamber of this source is made of pyrex glass. Two electrodes are mounted inside the discharge tube and the potential difference between two electrodes is variable from 2 to 5 kV. The oscillator frequency is 20 MHz and with a gas consumption of 7.5 $cm^3\ h^{-1}$ and an ion current of 500 μA can be obtained. Figure 1.6 shows the high frequency ion source with probe-type extraction.

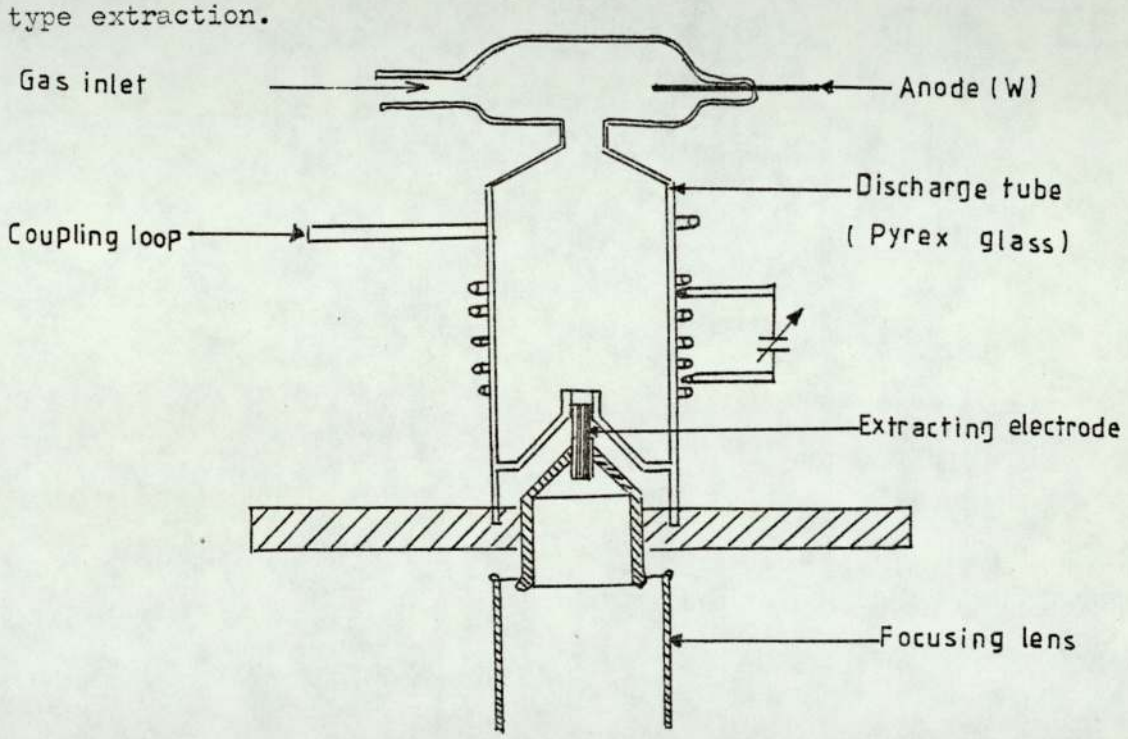

Figure 1.6. Thonemann's low current high frequency ion source with probe-type extraction.

Vâlyi[16] and Harrison[17] used the diaphragm extracting system at high frequency. The extracting assembly consists of a plane electrode with a bore mounted above an extracting electrode. An electromagnet, mounted close to the extracting electrode, generates a field of 70 mT in the ion channel. The high frequency discharge is generated by an inductively coupled oscillator operating at a frequency of 100 MHz and an output power of 400W. The ion current

obtained was measured as 49 mA for a gas consumption of 100 $cm^3\ h^{-1}$ with the extractor voltage 10 kV.

D. Thermal ionization sources

The operation of these sources, depends on the evaporation of the atoms or molecules from the surface. Datz and Taylor[18] have shown the ratio of ionized to neutral atoms is given by

$$\frac{n^+}{n_o} = A \exp\left[\frac{\acute{Q}-E_i}{kT}\right]$$

Where A is constant, $\acute{Q}$ the work function of the surface, E_i the ionization energy of the atom, k Boltzman's constant and T the absolute temperature.

Metals will emit their own ions when the temperature is sufficiently high and for $\acute{Q} - E_i >> kT$ nearly complete ionization will occur as observed for the vapours of alkali metals in contact with heated tungsten and nickel surfaces[18]. The evaporation of the sample occurs by a heating process which utilizes two methods either by single filament which comprises simply a wire or ribbon on which the sample is placed, or the other a multiple filament[19,20] using one filament or the sample and an ionizer in contact with a second heated filament.

The advantages of this method are to maintain the ionizing filament at the optimum temperature for thermal excitation and the evaporating filament can be independently controlled to promote a reasonable evaporation rate. In multiple filament sources, formation of ions on the hot filament must be considered. To eliminate this effect it is usual to apply a small negative potential or arrange for a focusing lens system which accepts ions from the central ionizing filament but defocuses ions from the evaporator

filament. The ionization filament potential is 6 kV for an ion current of a few mA.

E. Ion bombardment ion source

This is basically sputtering of ionic species of a given sample when it is bombarded by ions of another species. This source does not utilize a filament or magnetic field. The advantage of this type of source is that the current is stable and the energy spread is not very large.

The principle disadvantage is, however, that an ion source and focusing system is required for the primary beam and a further analyzer and energy selector for the secondary beam. Liebl et al[21] used a duoplasmatron to produce a preliminary argon ion beam of 10 to 12 keV of 1 mA intensity. Secondary emission coefficients are such that the ejected ion current is only of the order 10^{-8} to 10^{-7} A.

It can be seen from the previous discussions that the development of ion sources has been carried out by separate groups of people at different times and in different places concerning the practical requirements associated with different applications. Some require light ions, other heavy ions, some require high energy, others high current. For example; for surface analysis (1-10 μA, 10 eV to 20 keV), and for relatively high current density systems for sputtering and gas phase collision studies (100 μA to 10 mA, 1-10 keV) and for larger scale accelerators for surface study and modification 1 μA to 1 mA, 5-200 keV) beam energy are the typical values (Hurley)[22].

Some important parameters are considered in the design of the source, like using magnetic field or electrostatic field to increase the degree of the ionization by increasing the electron path length.

Some sources are using a cooling system for the anode to reduce the power dissipation. The electrons are emitted from a cold cathode or hot cathode but with ion sources there are many factors which can limit the operation of the source.

1.3 Practical limitations of the characteristics of the ion beam

The previous section provided a description of several ion sources. It is important to discuss a number of fundamental practical limitations on the characteristics of the ion beam which affect the design of the beam generation system and the use of the ions in various applications. Wilson and Brewer[23] discussed in detail the factors that can limit the beam characteristics, namely, space charge effect, thermal of transverse velocities and aberration of the ion optical system.

In space charge effects an electric field will be created from the charge in the beam resulting in a transverse outward force causing expansion in the diameter of the beam. When the beam contains a mixture of ions of different species, the heavier ions have a greater effect on the space charge than the lighter ions assuming they have the same current and energy. To minimize this effect, a neutralization of space charge is a well-known treatment (Barford)[24]. The achievement of space-charge neutralization of long electron beams by trapping ions in them has been discussed by Hines et al[25].

In the effect of transverse thermal velocity, the spread in the ion beam is due to the transverse components of the velocity of the ions that are emitted from the source. As a practical matter in order to focus an ion beam at a certain angle, some of the emitted current must be collected on a defining aperture, i.e. those ions with a high transverse thermal velocity must be removed from the beam. A source with high current density capability and low energy spread,

low equivalent thermal temperature is essential to attain a well-focused beam.

The size and shape of a focused beam can be strongly influenced by imperfection in several ion optical elements which make up the beam transport system. Klemperer[26] described the imperfection of the optical system. The aberrationsare spherical, chromatic and astigmatic as well as diffraction through the aperture. Well collimated intense ion beams with small diameter which are required in the apparatus utilizing an ion source can be obtained only from sources equipped with an ion extracting system. The properties of the ion beam extractable from the ion source depends on the ion concentration in the source, the area of the ion emitter surface and on the ion optical properties of the extraction system.

In spite of these limitations in ion beam production, the ion sources have been used successfully in a variety of scientific experiments and technologies. More recently, they have emerged into use in engineering applications and even in production as shown, for example, by the use of sputtering deposition and removal in semiconductor device manufacture (Hall)[27], for fine surface polishing and for ion-implantation. Furthermore, there has been considerable interest shown in ion etching carried out in-situ in the specimen chamber of scanning and transmission electron microscopes and this has placed further restrictions on the type of ion sources that can be used. Under these conditions it is necessary that the source should operate at low pressure without the need of a magnetic field which would effect the electron beam.

It is also preferable that the source should be small but still produce an intense beam of ions without the complexity of additional extracting and focusing electrodes. A new type of ion source which is very suitable for these applications has recently been developed

from the idea of McIlraith[28] for an electrostatic charged particle oscillator. This source is the main subject of this thesis and its earlier development and properties will be discussed in the next Chapter.

CHAPTER 2

THE DEVELOPMENT OF SADDLE FIELD ION SOURCES

2.1 Introduction

In 1966 McIlraith[28] found that if a steel ball is released on a rubber sheet stretched across a circular support in which a pair of rods are pressed into it, then the ball oscillates between the rods many times before finally colliding with one of them. He used this idea to develop an oscillator for charged particles to oscillate within a limited volume by means of an electrostatic field alone. Thus, if a positive voltage is connected to a pair of parallel wires mounted in an evacuated cylinder, the equipotentials within the cylinder take the form as shown in figure 2.1 in which a saddle point X is produced midway between two anodes. It can be shown that an electron starting from rest within the shaded region follows a long oscillatory path between the two anodes before finally being collected by one of them.

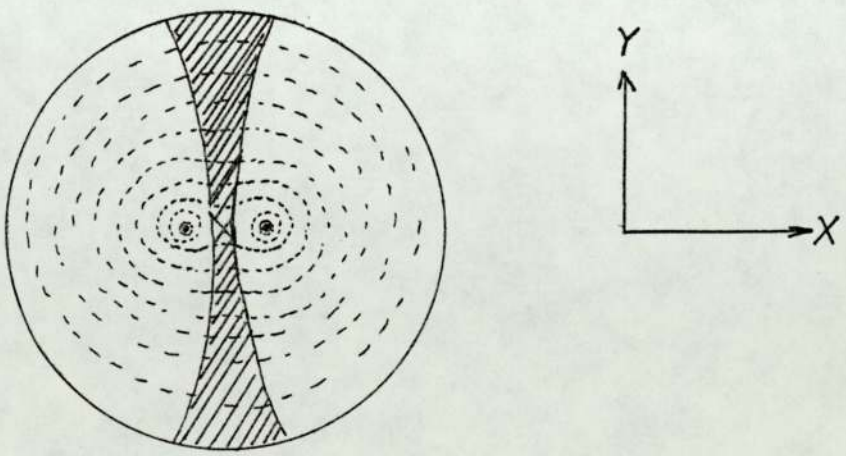

Figure 2.1 A cross-section of the oscillator showing the equipotentials and saddle point X.

McIlraith stated that the type of motion may occur in the gravitational field of stars where the asteroids could be held in the oscillatory motion between the stars.

However, the long electron path makes possible a number of applications of the oscillator, notably amongst them being a vacuum gauge[29], an ion source, a sputter-ion vacuum pump and molecular detector analyser[30] of moderate resolution. In this Chapter, the discharge mechanism of the saddle field ion source and the development and the application of the sources will be discussed.

2.2 The discharge mechanism of the saddle field ion source

It has been shown that the electrons oscillate between the two anodes many times, before they are collected by the anodes. When the volume has enough neutral particles, then each oscillating electron has a large number of elastic or non-elastic collisions between the electron and thermal neutrals. If the electron energy E_e is higher than the ionization energy, E_i, the neutral may be ionized. With the large electron path a high density plasma can be produced even at low pressures. If we assume that the initial electron current, i_e, can Produce N_i pair of ions before being collected by one of the anodes, then (N_i+1) electrons will strike the anode and N_i ions bombard the cathode. Thus γN_i secondary electrons will be emitted where γ is the secondary electron coefficient which depends on the type and energy of the ions and cathode material.

It should also be mentioned that during this process neutral atoms and sputtered ions are emitted from the cathode so that the cathode target produces neutral particles or causes recombination of ions and secondary electrons. As a result of this electron

transition from higher to lower energy levels, photons will also be emitted. Now in the next ionization process between the two poles (N_i+1) electrons will cause $N_i(N_i+1)$ electrons and $N_i(\gamma N_i)$ ions and so on in third and fourth collision etc.

Therefore

$$\frac{I_c}{I_e} = (N_i+1) + (N_i+1)\gamma N_i + (N_i+1)\gamma^2 N_i^2 \ldots\ldots\ldots$$

$$I_c = I_e(N_i+1)(1+\gamma N_i+\gamma^2 N_i^2 \ldots\ldots \gamma^n N_i^n)$$

where I_c is the ion current.

Since N_i depends on the electron energy, the gas pressure and the type of the gas used and γ depends on the cathode material as well as the kind of positive ions, therefore, I_c will depend on these parameters too as it is expected. Rushton[31] used aluminium and stainless steel cathodes and obtained different oscillator characteristics.

The oscillator can maintain a cold cathode discharge at low pressures without magnetic field or thermionic source of electron. Thus a discharge can be sustained at considerably lower pressures than in conventional cold cathode discharge tube.

The particle trajectories are of two types - stable and unstable. In the case of a stable trajectory the oscillating particle passes between the two electrodes and in the unstable trajectories it orbits around them as shown in figure 2.2. The positive ions will be moving towards the Y-axis giving two etched regions in the cathode. Therefore, one or more holes in either side of the cathode will allow some of the ions to escape out of the source in the form of energetic ion beams without using any extraction system (self extraction). This idea led to the

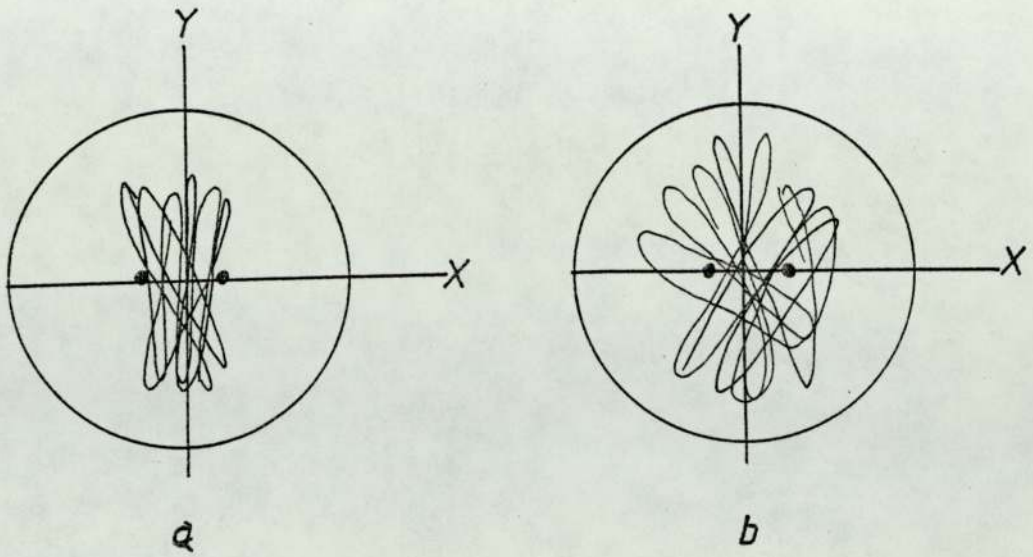

Figure 2.2 Diagram showing (a) stable and (b) unstable electron trajectories.

development of saddle field ion sources.

2.3 Development of saddle field ion sources

Two forms of these sources have now been produced using either cylindrical or spherical geometry and the development of these will now be given.

2.3.1 Cylindrical source

Ion currents of about 100 μA cm^{-2} were produced at a pressure of 5×10^{-4} Torr by the original form of the saddle field ion source described by Fitch et al[32]. It consists of a cylindrical cathode surrounding two anode wires which are symmetrically disposed about the axis of the cylinder as shown in figure 2.3.

An electron starting from rest within a specified region follows a long oscillatory path between the wires, thus a cold cathode discharge can be maintained without the application of magnetic field. The cathode was 200 mm long and 54 mm internal diameter, with end-plates of copper gauze. The anodes were springloaded tungsten wires of 0.3 mm diameter. The discharge is concentrated

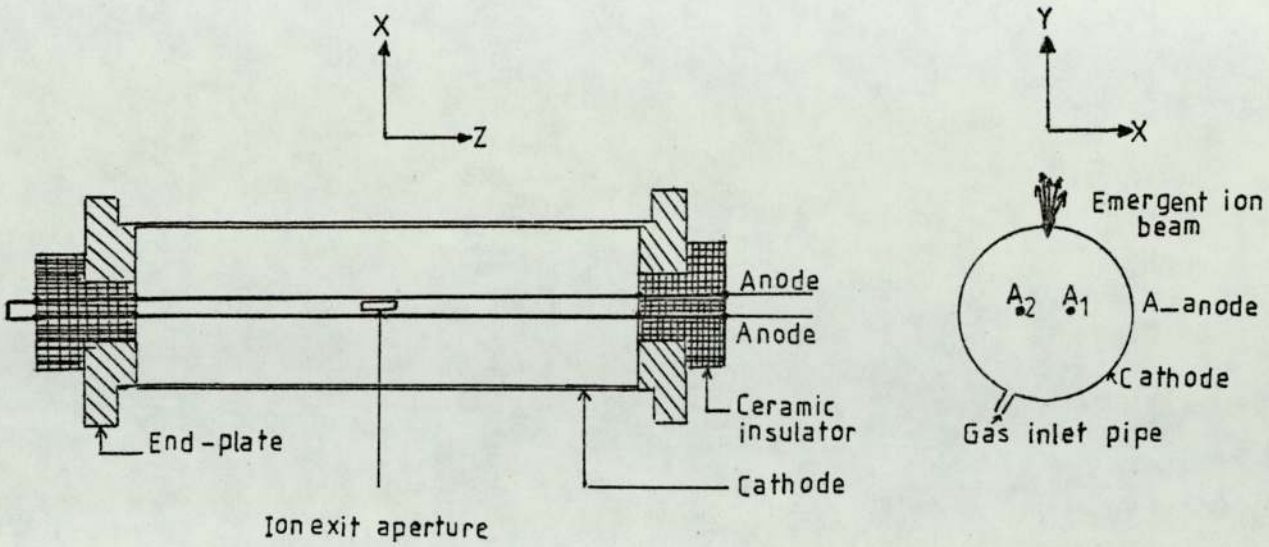

Figure 2.3 Schematic diagrams of the ion source in the xy and xz planes.

about an axial plane normal to the plane of the anode wires. Ions generated in the discharge were allowed to escape from the source through a rectangular slot 25x5 mm in the cathode positioned above the plane of the anode wires which allowed a wedge-shaped ion beam of angle 5^{o} to emerge. The ion beam was used for etching a specimen of O.F.H.C.copper and gave a sputtering yield about 5 atoms per ion.

An improvement from this source was described in 1971 by Rushton et al[33]. Figure 2.4 shows the discharge characteristics of anode current vs anode voltage at various pressure using dry air. It can be seen that the cut-off voltage for the discharge is pressure dependent.

The performance of this ion source depends on the anode separation. It was found[33] that the anode current increased when the anode separation is decreased to 6 mm but then decreases with further decrease in anode separation. At a separation of 4 mm it was not possible to obtain a discharge. This "cut-off" at small

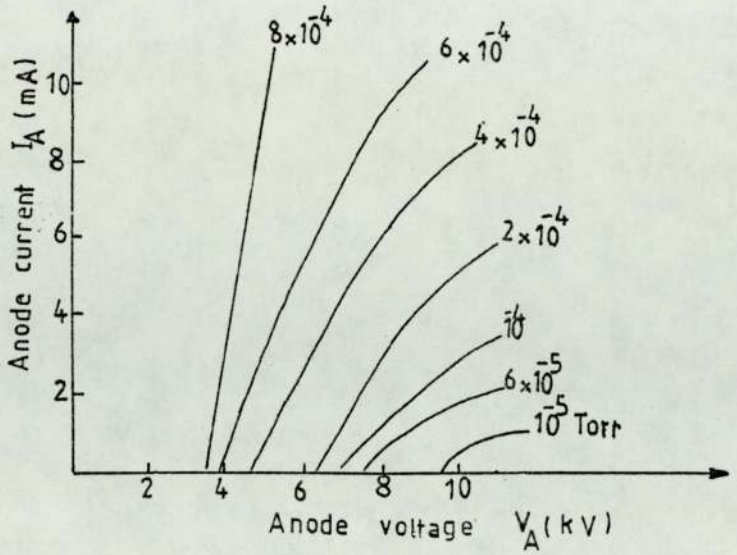

Figure 2.4 Cold cathode discharge characteristics

separations is believed to be due to the secondary electrons emitted from the cathode having a component of initial velocity parallel to the plane of the anodes. This causes the electrons to be captured by one of the anodes before a useful ionizing collision occurs. This source was used to etch alloys and plastic specimens including one case in which chemical etching had been found to be unsuitable. They also studied the effects of magnetic field upon the performance of this source, that the anode current decreased when the magnetic field increased along the Z axis. In 1973 Rushton et al[34] showed three main modes of operation, namely, an "oscillating mode", a "transition mode" and a "general glow discharge mode", and advantage was taken of these effects with the variation of the pressure. This was done by observing the shapes of ion-etched regions produced on the inside surface of the cathode by ion bombardment at different chamber pressures. The uniformity of the ion beam at these modes was studied as shown in figure 2.5 for the oscillating and transition modes.

In 1973 work was done by Rushton et al[35] for the "twin anode

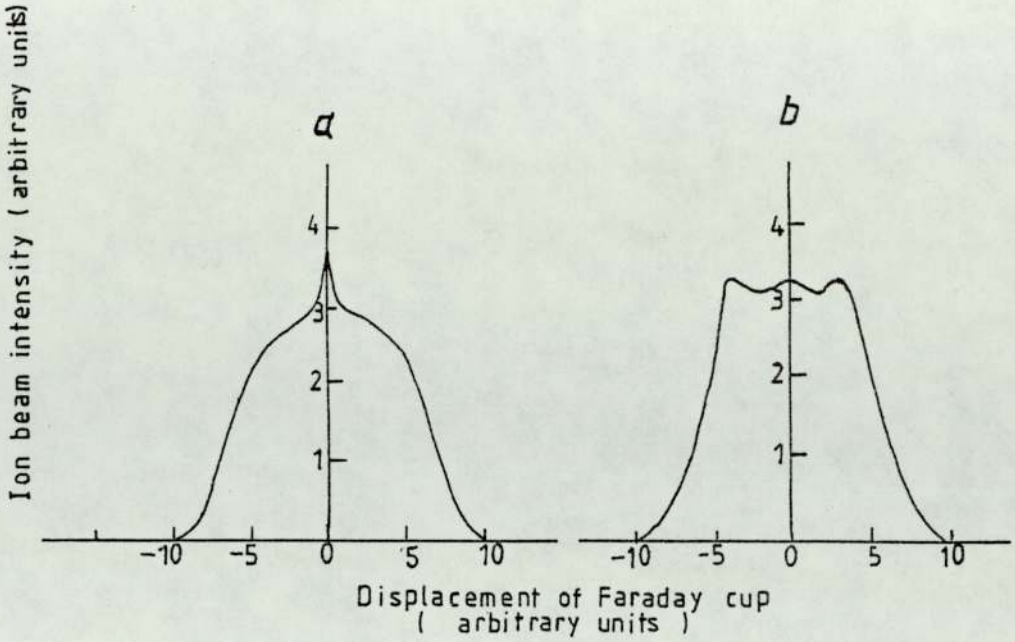

Figure 2.5 The ion beam density profiles obtained from (a) the oscillating mode and (b) the transition mode.

electrostatic ion gun with thermionic electron impact". In this work, the energy of emerging ion beam had been reduced and thus the ions will produce less structural damage to any specimen under ion bombardment. The thermionic version of the ion gun should extend the range and the type of applications that are possible and could include, for example, ion cleaning in U.H.V. and surface physics applications such as Auger spectroscopy. In 1974 Clark et al[36] determined the charge states of the ions produced by the oscillating electron electrostatic ion source. They used different gases, H_e, H_2, N and Ar to produce He^+, H_2^+, N^+, Ar^{2+} but higher charge states were seen and these increased with increasing source power.

The spectrum for argon is given in figure 2.6 in which Ar^{2+} in the dominant species and Ar^+ and Ar^{3+} are present in only small proportions. The ions were accelerated up to 50 kV, by a linear accelerator in order to increase the resolution of the analysing system.

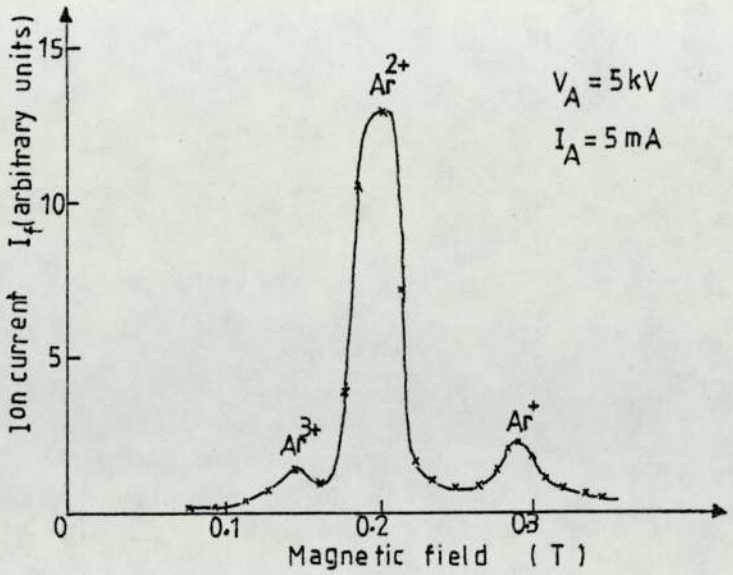

Figure 2.6 The spectrum for argon at a pressure of 2×10^{-5} Torr.

Another design was followed, which has been described by Fitch et al[37]. This involved water cooling by constructing a spiral tube to cool the cathode at higher input powers. It was observed that the temperature rise of the target could be reduced by at least 50% using this source. Another advantage with water cooling is that the anode current I_A remains constant and it was also observed that the source is much more stable in operation and much higher current densities can be obtained. The application of this source was used to ion etch various specimens such as electron beam welds, superconducting wire, human teeth, plastic and field emitting tips.

2.3.2 Spherical source

It has previously been shown that the cylindrical source produces a wide beam but sometimes a fine beam is required. Furthermore, the dimensions of this source are relatively large making it difficult in some applications in which only a small space is available in the experimental chamber. In the cylindrical source end plates which are at cathode potential are necessary to

reflect the electrons along the axis, and these end-effects are undesirable. Thus Franks[38] in 1972 showed that if the cathode is made spherical and the anode rods are replaced by a ring anode, then the saddle line becomes a saddle point and the end effects are eliminated. Franks[39] described and designed a saddle field ion source of spherical geometry by making the cathode from two aluminium hemispheres, and the anode from a stainless steel annulus. In order to retain the true spherical geometry he added two guard rings at earth potential placed either side of the anode. These were isolated from the anode by four ceramic insulators and the ion beam emerged through a hole in the cathode.

A schematic diagram of this source is shown in figure 2.7a. In a later version he simplified this by using tubular cathodes as shown in figure 2.7b to simulate the spherical field. The equipotential distribution in this source is shown in figure 2.8 which illustrates that the saddle point potential was found at about 70 to 80% of the anode potential.

Ghander[40] showed how the characteristics were effected by variation of the anode hole diameter, and he showed that as the anode hole diameter is decreased the saddle point potential increases. He therefore determined the appropriate anode hole diameter in relation to the cathode diameter in the same way as Rushton et al[33] did to optimise the anode separation in the cylindrical source.

Later, Khorassany et al[41] used a retarding field energy analyser to measure the energy distribution of the ions produced by the spherical source as well as the cylindrical one for different gases. They showed that ions occur at an energy equivalent to about 75% of the anode potential with a peak half-width of about 10% of the anode potential as shown in figure 2.9a. They also showed that with the cylindrical ion source the distribution is broad but always

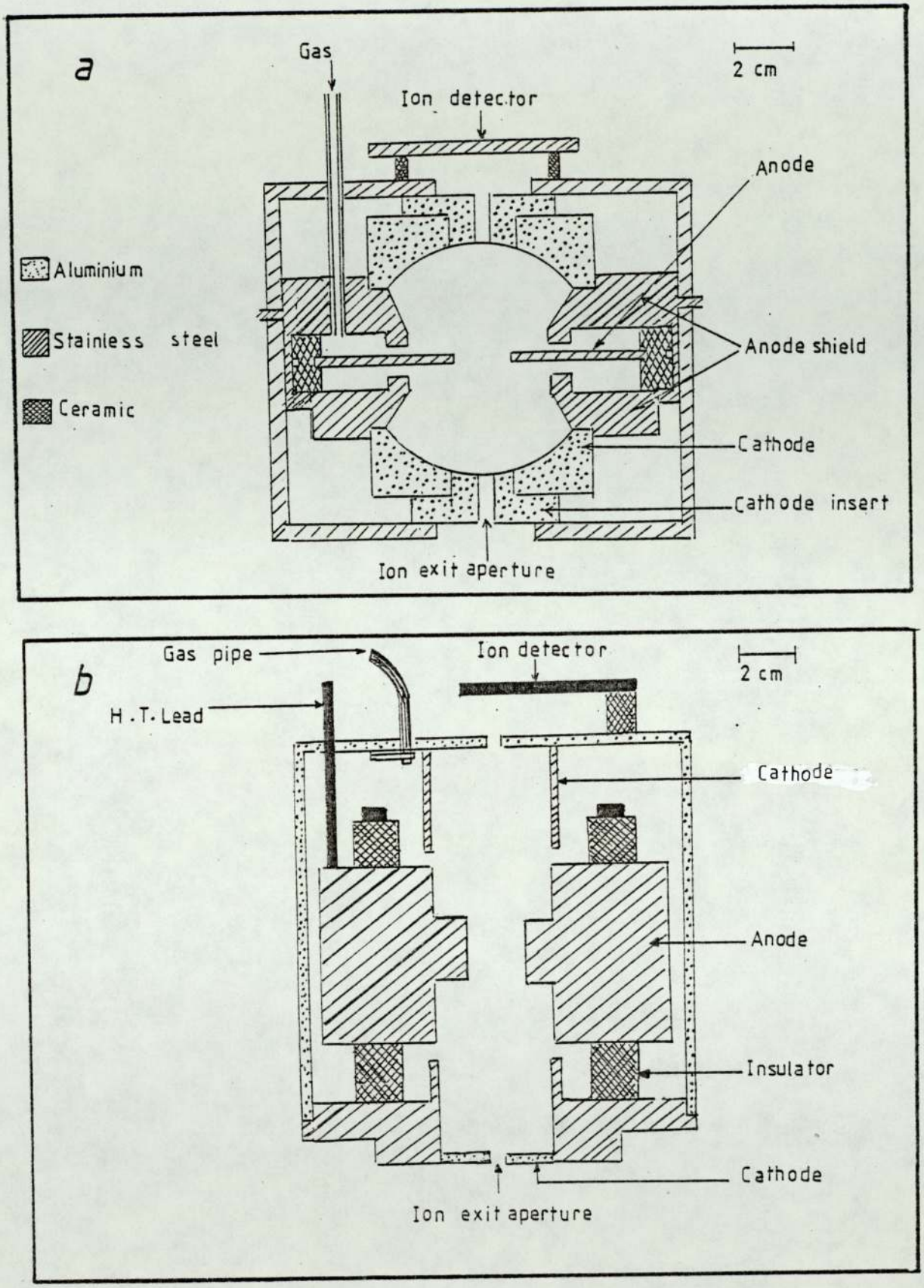

Figure 2.7 Schematic diagram of the (a) spherical source and (b) B11 fine beam ion source.

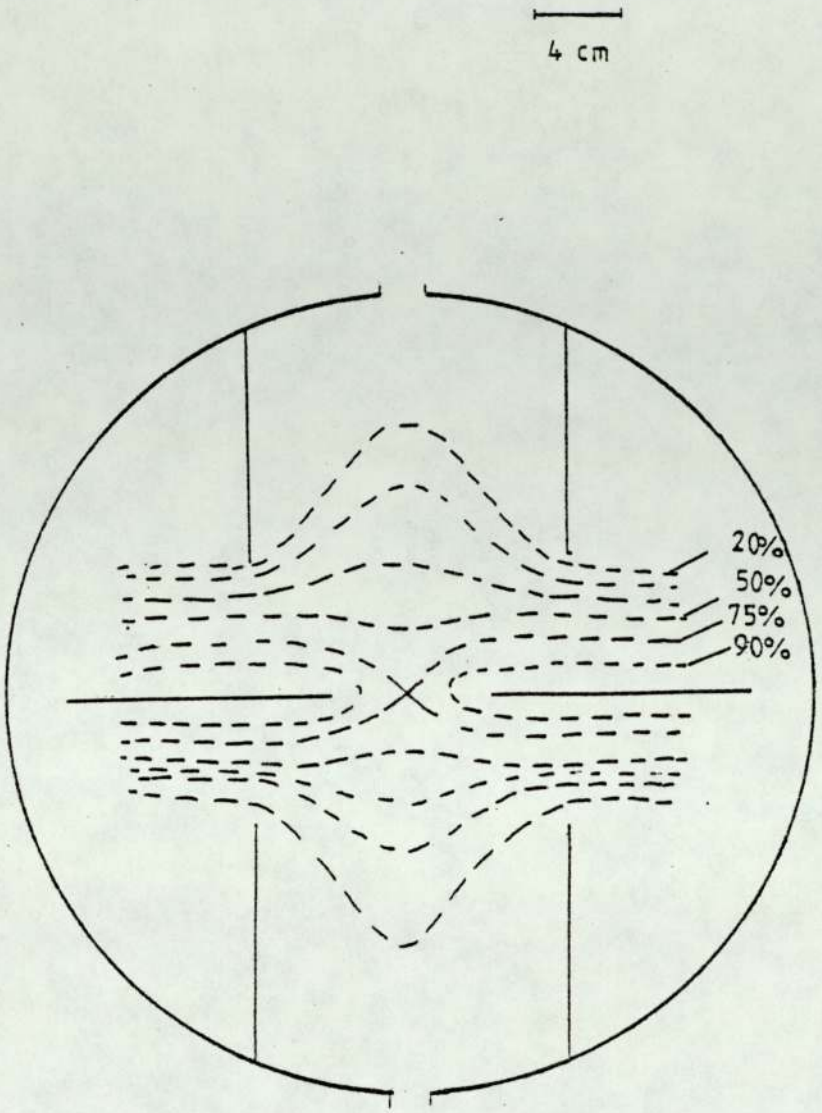

Figure 2.8 Potential distribution in the spherical source

contains two distinct peaks at energies equivalent to about 35% and 75% of the anode potential as shown in figure 2.9b. They also found that the proportion of higher energy ions in the beam decreases towards the edge of the beam for both sources.

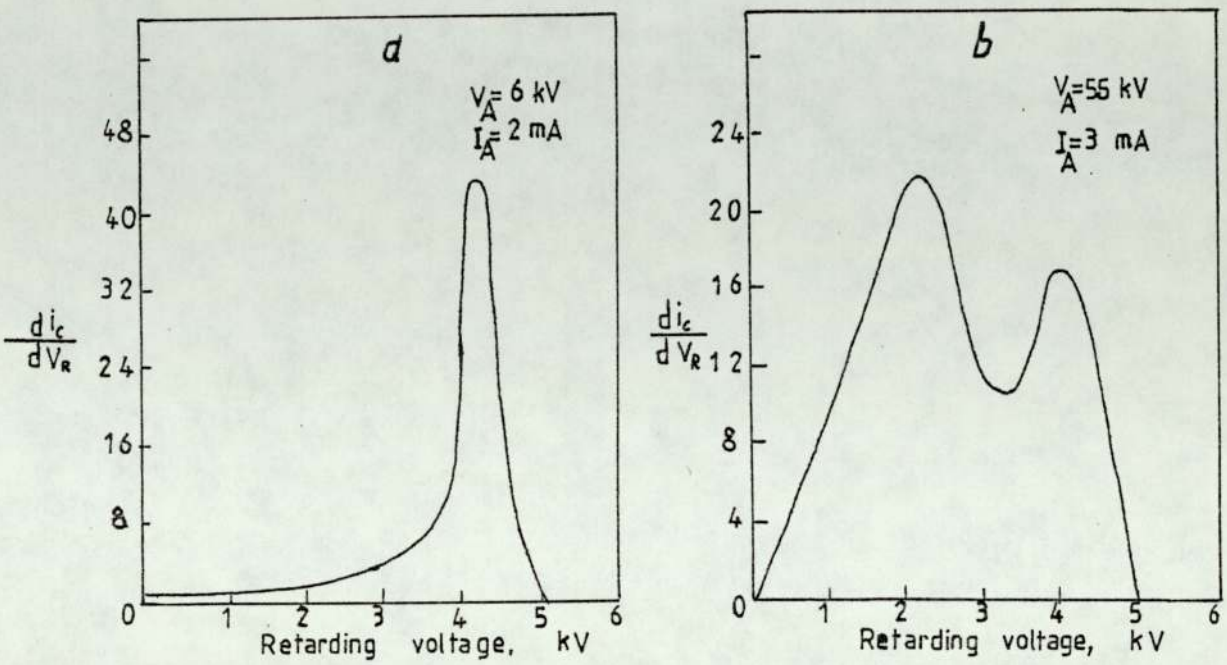

Figure 2.9 Energy spectrum for (a) spherical and (b) cylindrical source for argon.

Fitch et al[42] found that there is a percentage of energetic neutrals in the emerging beam which increases from about 20% to 70% as the chamber pressure increases as the anode voltage reduces from about 7kV to 2kV. More recent work has been done by Fitch et al[43] who measured the charge state of the ions produced by the spherical source using a magnetic analyser and an Einzel lens to focus the ion beam into a Faraday cup. They found that the ionic species for Hydrogen, Neon, Nitrogen, Oxygen and Argon were H_2^+, H^+, He^+, N_e^+, N_e^{2+}, N_2^+, N^+, N^{2+}, O_2^+, O^+, O^{2+}, Ar^+, Ar^{2+} and the percentage of charge states varies with pressure. They determined the yield of sputtered aluminium and various dental

materials after considering the presence of multi-charge ions and energetic neutrals.

Both designs of the saddle field ion sources are in the use in various applications in different aspects of vacuum technology. In general, the cylindrical source should be used if a wide ion beam with a broad energy spread is required but if a fine beam of much lower energy spread is necessary, then the spherical source is more suitable. In the following section, a wide application of saddle field ion source will be discussed.

2.4 Applications of saddle field ion sources

Since the development of the saddle field ion source in this laboratory in 1970, these sources are being used in various applications and they are preferred to other sources because of their small size, lower operating pressure, which is suitable for sputtering and cleaning of materials, and these sources do not use a magnetic field and are therefore suitable for use in the scanning electron microscope (S.E.M.).

Fitch et al[44] used a cylindrical source using argon ions to etch nickel, molybdenum, copper and acrilonitrile butadiene styrene (ABS) plastic. Ghander et al[45] used a cylindrical source with a focusing electrode at negative potential in respect to the cathode. They used this improved source for ion etching and they found the etching rates of copper film increased from 0.4 μmh^{-1} to 10 μmh^{-1} when the focusing electrode potential increased from zero to 5 kV. However the sources have been successfully used to ion etch field emitting tips and human tooth enamel. Fitch et al[37] used a technique in which the tip is rotated in the ion beam. It has advantages over other techniques in that it can be used to sharpen and re-sharpen all types of materials and appears to be a

reliable process.

Franks et al[46] used a spherical source with about 2 mA cm^{-2} current density for ion thinning. He showed that both the cylindrical and spherical sources are compatible with ultra high vacuum equipment and may be used for cleaning surfaces prior to analysis by Auger electron microscopy (A.E.S.) or electron spectroscopy for chemical analysis (E.S.C.A.). In a very recent paper Franks[47] showed that this source in particular is suitable for use in an ion beam deposition system for shadowing materials for examination in the S.E.M. and transmission electron microscope (T.E.M.).

In one study Dhariwal et al[48] observed artefacts on dental tissues during ion etching when the specimen was examined in an S.E.M. and he measured the temperature of the enamel and the growth of cones during ion bombardment. Dhariwal et al[49] used also the spherical source to study the structure of metals alloys and sinters. In addition to its use with plastics, glass, and resins, biological materials such as enamel and dentine have been successfully etched.

The use of the saddle field ion sources has not been confined to this laboratory and there are several uses which have been reported from other laboratories for various applications and for different purposes. For example, in the Metallurgy Department, the cylindrical is used in the specimen thinning of transmission electron microscope. In the field emission laboratory the spherical source is being used successfully to remove the oxide layer from a titanium target in high voltage breakdown and in thin film research the spherical source has proved to be a suitable tool to remove the oxide layer from aluminium samples in ellipsometry.

From previous discussions it was shown that the saddle field ion sources are successfully used in various applications which present good evidence that these sources are reliable and efficient

and are sometimes preferable to other sources because of its relatively simple construction and operation, easy cleaning and is suitable for ion bombardment of conducting and non-conducting materials. It is evident from the above that these sources, and in particular the spherical version, are finding increasing use in the many different technologies. However, future development and applications are dependent on a better understanding of the mechanism contributing to more efficient design and further knowledge of the nature of the particles produced by the source.

In this work a study has been made of the modes of operation of the source and the nature and energy of the particles emerging from the source including ions, electrons, thermal and fast neutrals.

CHAPTER 3

DESCRIPTION OF THE ION SOURCE, VACUUM SYSTEM, ELECTRICAL CIRCUIT AND BEAM MONITORING TECHNIQUES

3.1 Description of the ion source

The spherical source used in this investigation was a modified form of the B11 source produced by Ion Tech Ltd. In this device the spherical configuration is produced by using two stainless steel cylinders of length 8.5 mm and diameter 10 mm spaced either side of the stainless steel anode of aperture of diameter 5 mm and thickness 7 mm. The ends of two cylinders are closed with two aluminium cathode discs of diameter 10 mm and thickness 1.5 mm. The ion beam is allowed to escape through 1.5 mm diameter holes in each disc such that the source produces two identical intense beams. The anode assembly is isolated from the cathode body by using glazed ceramic insulators. The H.T. lead is fitted in the stainless steel anode and the other end is mounted on the cylindrical Duralumin body through ceramic insulators. To monitor the beam, a nickel plate 2 cm length and 1 cm width is placed opposite one of the apertures. A stainless steel pipe 3 cm length and 5 mm diameter is connected to the body to admit gas into the source. Components of the source are shown in figure 3.1a.

A simple improvement was made by extending the H.T. lead to avoid breakdown when the source was operated at high anode voltages (> 8 kV) and lower chamber pressures ($< 6 \times 10^{-6}$ torr). Materials used in the construction of the source are stainless steel grade 321 for the anode and shield electrodes, aluminium alloy HE30 for the body and aluminium alloy S/A for the cathodes. In order to maintain the source efficiency it was necessary to pay particular attention to the cleaning processes prior to assembly.

During the operation of the source, the cathodes were gradually sputtered away and aluminium was deposited on the shield electrodes, the anode and insulators. The effect of the deposition was to reduce the anode current due to the distortion of the field in the vicinity of the anode. The ion source was normally cleaned by using an effective agent such as acetone after removing any contamination with waterproof silicon carbide paper grade 180 C. When the source was required for re-assembly it was important to ensure that the anode and shield were concentric. This was conveniently achieved using a centering tool which was made to fit closely inside the anode and cathode apertures. As a result of the ion bombardment of the cathode discs this eventually caused a widening of the apertures and thus a change in operating condition and in order to avoid this the apertures were replaced when necessary throughout the course of the experimental work.

3.2 Mounting of the ion source

The source was mounted on a solid aluminium flange (5x5x1 cm) inside a 34 mm diameter hole so that it was easy to rotate the source to select the adequate position of the gas inlet pipe. The source was located in the flange with a fixing screw. The complete flange and source was supported on an aluminium stand 23 cm length, 19 cm width and 6 cm height. There were several holes and slots on the sides of the stand to fit other accessories when required such as the Faraday cup. This stand is portable, convenient and easy to mount in the experimental chamber in the required position. The photograph (3.1b) shows the source mounted on the stand with the Faraday cup.

3.3 Electrical circuit and beam monitoring facilities

A schematic diagram of ion source and its associated electrical circuit is shown in figure 3.2. A voltage was applied to the anodes

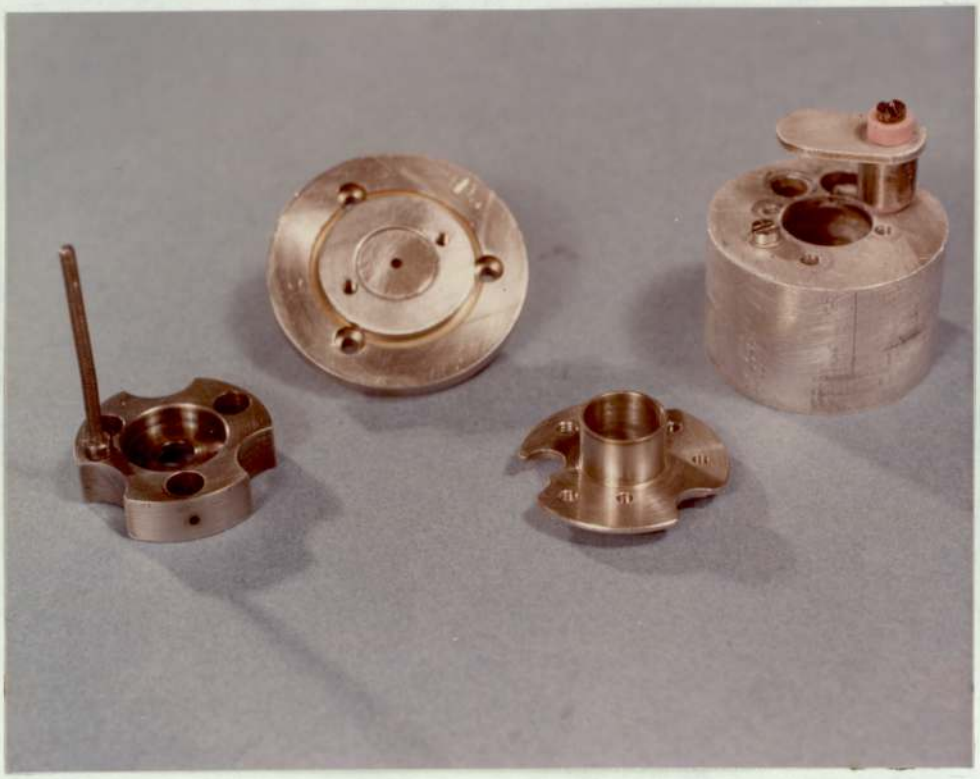

Figure 3.1a Photograph shows the components of the source

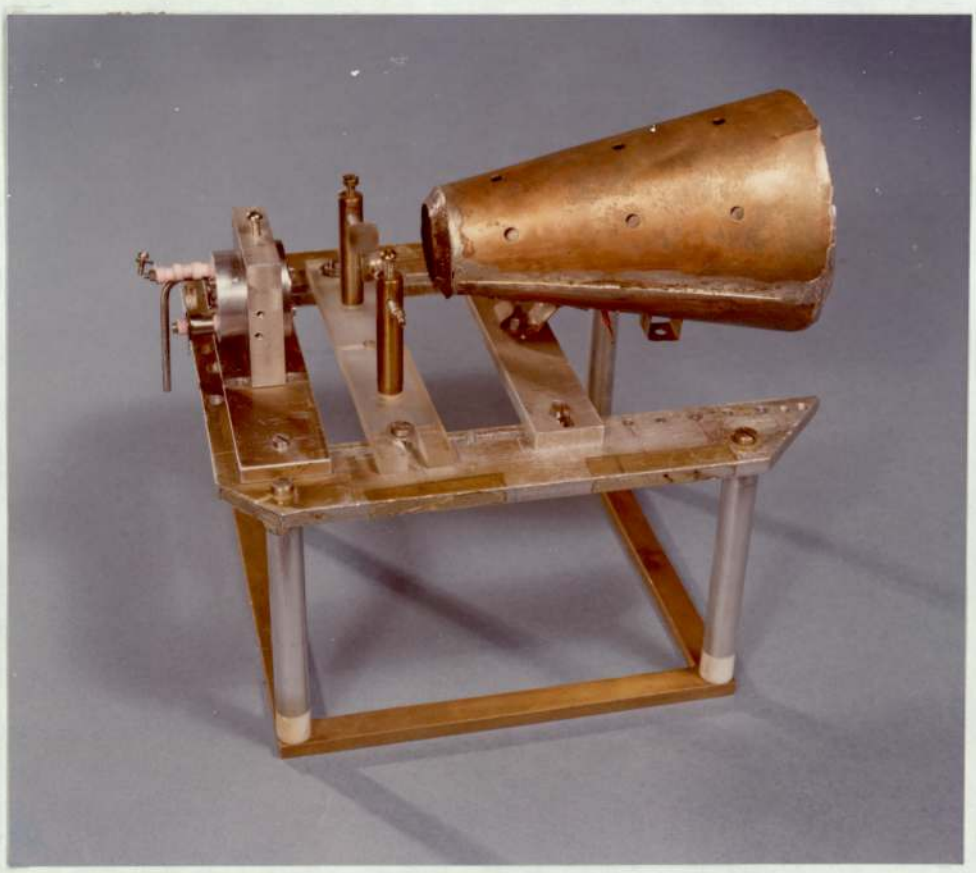

Figure 3.1b Photograph shows the source mounted on the stand with Faraday cup

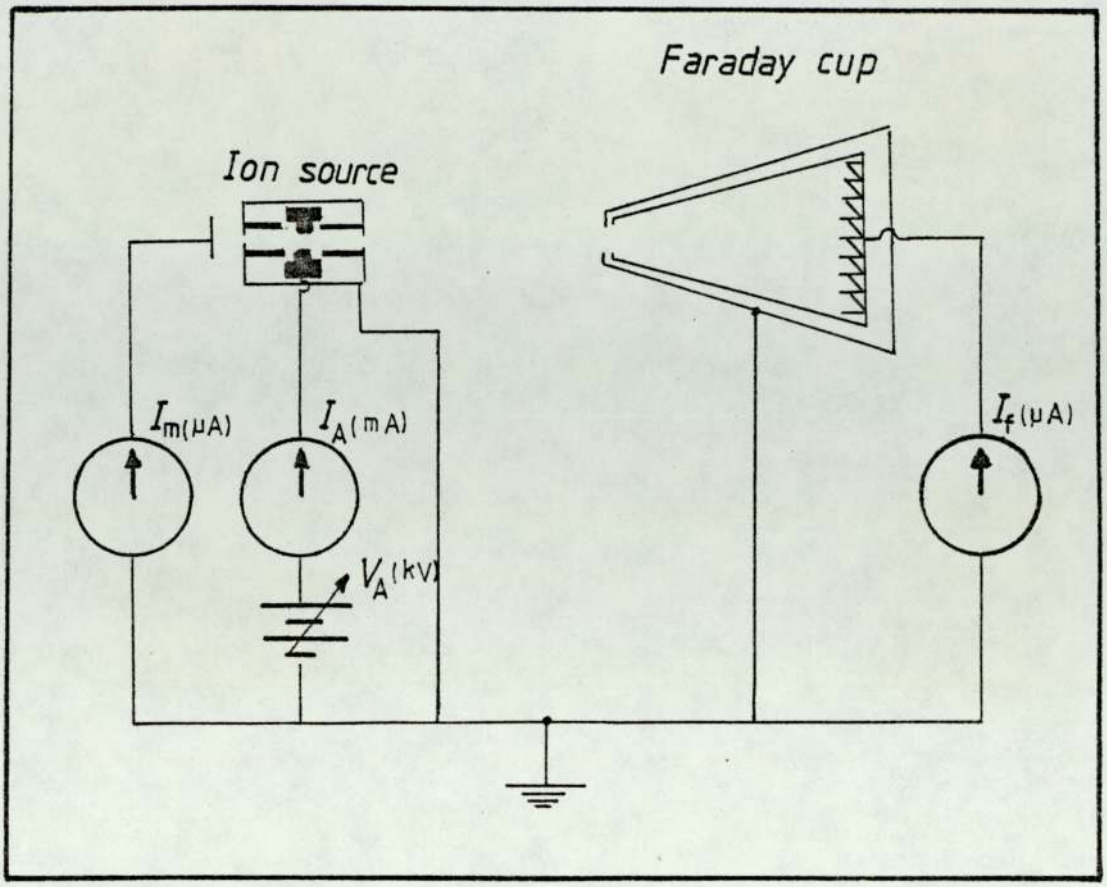

Figure 3.2 Schematic diagram of the ion source and electrical circuit.

via the H.T. terminal connection on the source from a stabilised power supply capable of providing up to 50 mA at 20 kV. Monitoring facilities for the anode voltage and current were built into the power supply. The experimental chamber, along with the cathode of the ion source, were kept at earth potential. The ion beam is an essential parameter of the source and therefore the design of the ion collector is a very important aspect of the diagnostic techniques. In order to obtain an efficient collector consideration should be taken into account that the collector will retain any secondary electrons produced by the ion beam whilst still incorporating a relatively large entrance aperture to admit the total ion beam at

large distances from the source. The modified Faraday cup shown in figure 3.2 was developed in this laboratory by Khorassany[50]. This collector is constructed from nickel and the conical shape length 12 cm and entrance aperture 2.5 cm which is more than the maximum ion beam diameter at 7 cm from the source. An earthed screen was constructed around the collector to eliminate any collection of low energy and reflected ions in the experimental chamber. The ion beam was measured using a multirange three digits microameter with an accuracy 0.5%. A small piece of nickel sheet was used to monitor the beam current and was mounted on the back of the source but isolated from the cathode body.

3.4 Vacuum system and experimental procedures

In all the programs of the experimental work discussed in this thesis, the measurements were undertaken in a conventional high vacuum system shown schematically in figure 3.3. It consists of a combination of a rotary pump, water cooled diffusion pump, experimental chamber and gas supplies. The rotary pump was used down to pressures of about 10^{-2} torr, measured by a Pirani gauge and a water-cooled oil diffusion pump model E04 of rated speed 600 litre/sec manufactured by Edwards Vacuum Ltd using "Santovac 5" fluid. This system gave an ultimate pressure of less than 10^{-6} torr. "Santovac 5" has a low backstreaming rate and a very low vapour pressure and is capable of producing ultimate pressures in the range of 10^{-10} torr without the use of a liquid nitrogen trap. "Santovac 5" has unusually high thermal and oxidation stability, non-corrosive and non-toxic at normal operating temperatures. It significantly reduces these major causes of vacuum system contamination. In addition, films of "Santovac 5" which are accidently adsorbed on to the surface of the work chamber are easier to remove than silicon films because "Santovac 5" contains

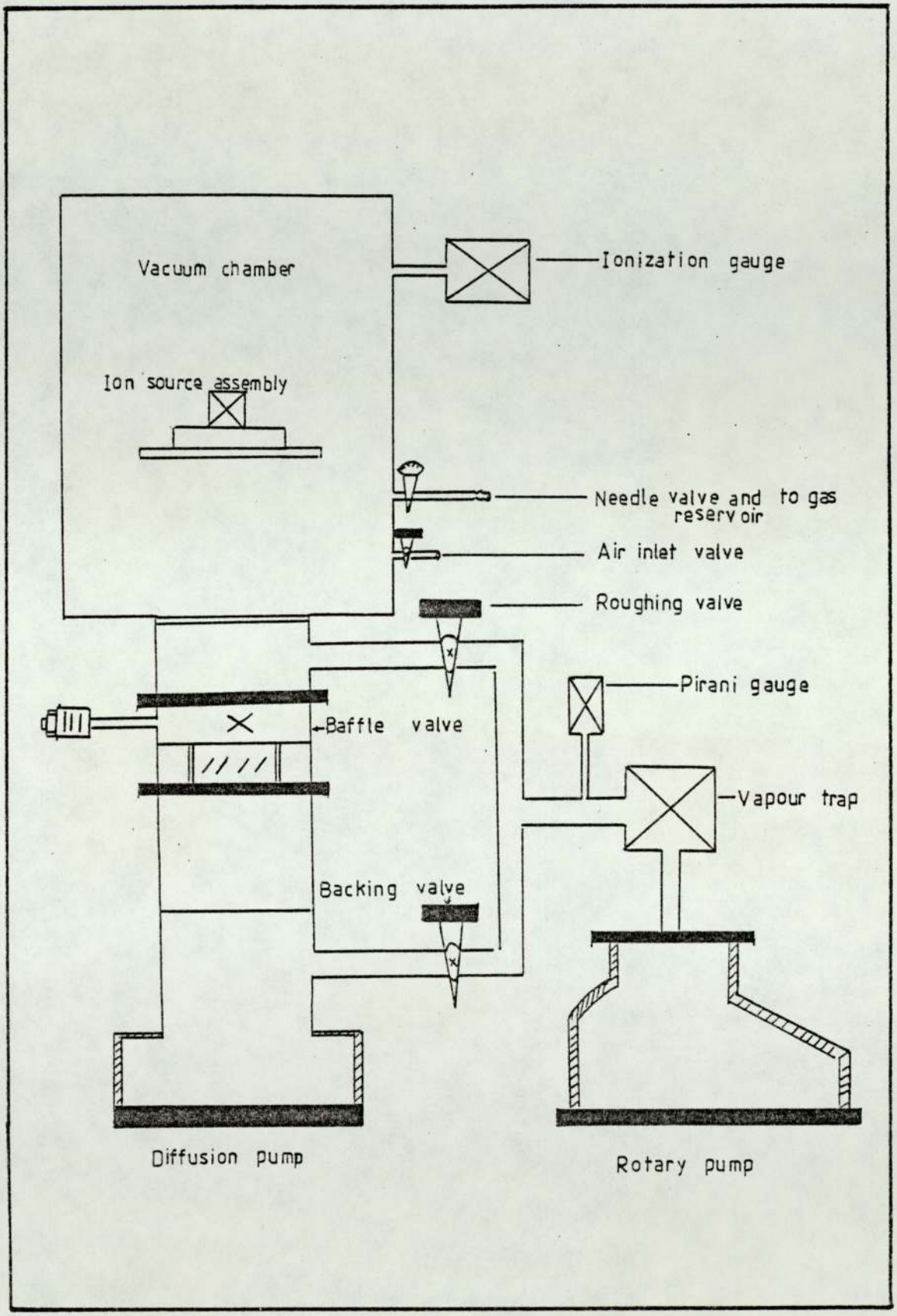

Figure 3.3 Schematic diagram of the vacuum system

only carbon, hydrogen and oxygen.

On the other hand silicone fluid can deposit an amorphous residue which may need chiselling or sandblasting to effect its removal. Furthermore, these silicone deposits can be electrically insulating and hence a variation of potential can arise due to build of charge from any incoming ions or electrons. The chamber contains three flanges carrying ten high voltage and current lead-throughs two glass viewing windows, a Mullard IOG 12 head and a Penning gauge. The gas could be admitted to the source by a needle valve through a P.T.F.E. tube of diameter 5 mm and the chamber pressure was measured by both the Penning gauge and the ionization gauge in the range 10^{-6} to 10^{-3} torr. The use of these two gauges will be justified in the following section.

3.5 Calibration of the gauges

The Penning gauge was used for most of the measurements because the ionization gauge is less suitable for continuous use at high pressures. However, it is known that significant errors can arise in pressure measurements with the Penning gauge and in many experiments it was important to have a fairly precise measurement of the pressure. In a Penning gauge the cathode metal is sputtered at high pressures (10^{-3} torr) producing a pumping action and furthermore dissociation of pumping fluid by electron bombardment can cause the discharge to become unstable.

In order to confirm that the pressure measured by the Penning gauge was a reasonable estimate of the chamber pressure, an ionization gauge was fitted into the chamber near to the existing Penning gauge. Preliminary experiments showed that the readings on the gauges were not affected when their positions were interchanged. The ionization gauge which is used in these experiments is the Mullard IOG 12. This

gauge was degassed for twenty minutes before the measurements were taken and a comparison between the readings of the two gauges for nitrogen is shown in figure 3.4. It is believed that the departure from the expected 45° slope is due to the inaccuracy of the Penning gauge rather than the ionization gauge. Thus the ionization gauge was used as the standard.

An attempt was tried to investigate the true pressure in the chamber and to overcome any discrepancies in pressure measurement due to the gauge position. Another ionization gauge was placed inside the chamber in a position similar to that of the ion source when in normal use. A comparison between two readings of the ionization gauge inside the chamber and the ionization gauge fitted in the chamber wall was made and is shown in figure 3.5. It can be seen that the pressure inside the chamber is apparently higher than that measured outside. This is because the gauge inside the chamber is nearer to the position where the gas is admitted into the chamber, thus causing a pressure differential between the central region of the chamber and external ionization gauge. It will be seen that this is important when quantitative measurements are required. However it has already been pointed out that it was more convenient to use the Penning gauge. Hence, unless otherwise stated, any reference to the chamber pressure, p_c, will be that recorded by the Penning gauge mounted on the side of the vacuum chamber. In addition the true pressure, taking into account the variation of the gauge sensitivity for different gases, will only be given when necessary.

3.6 Measurement of the effective pump speed

The effective speed of the pump in the chamber was measured in two ways - namely the constant volume and constant pressure methods for argon, nitrogen and helium. In both cases the pressure was measured

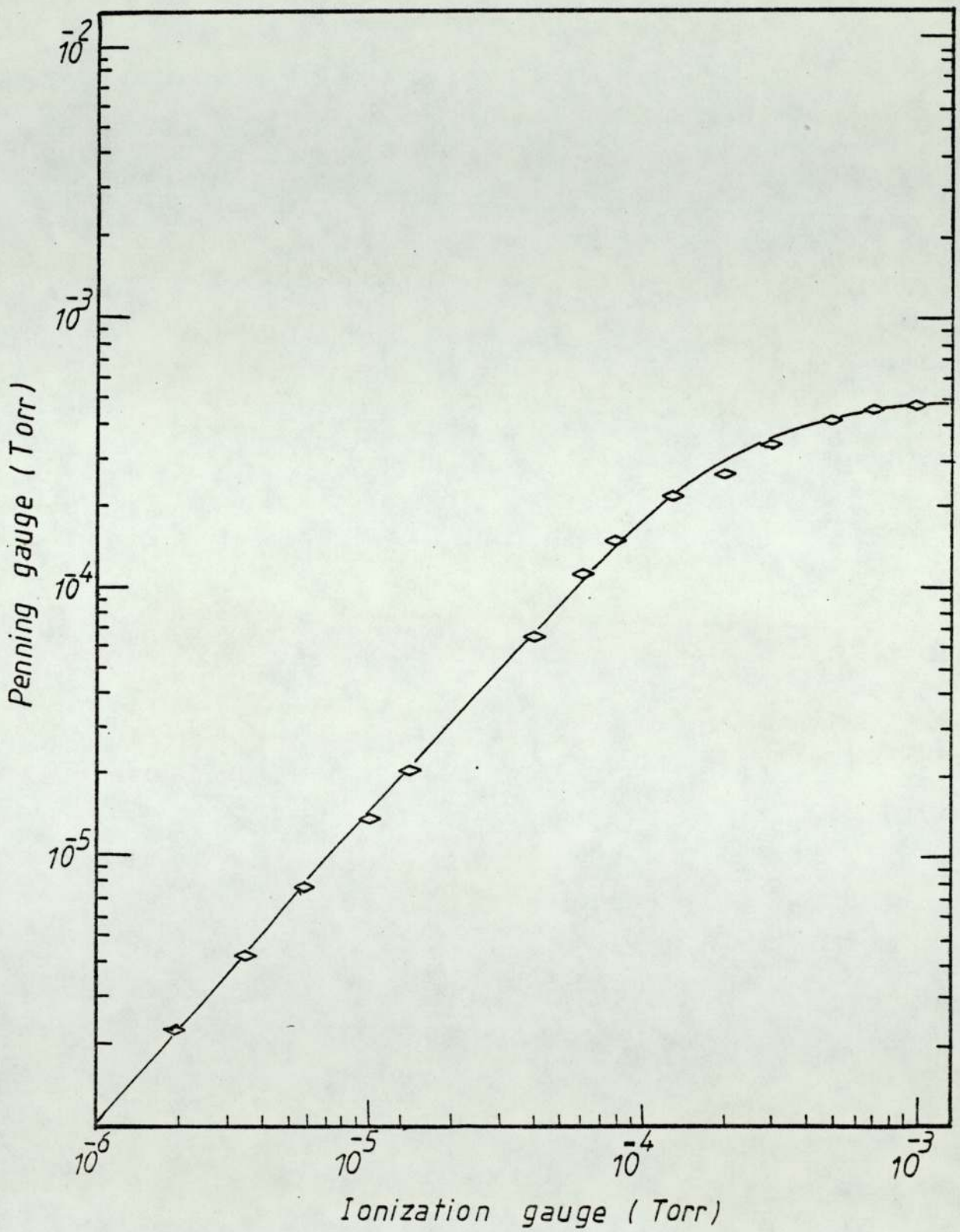

Figure 3.4 Calibration of ionization gauge against Penning gauge using nitrogen.

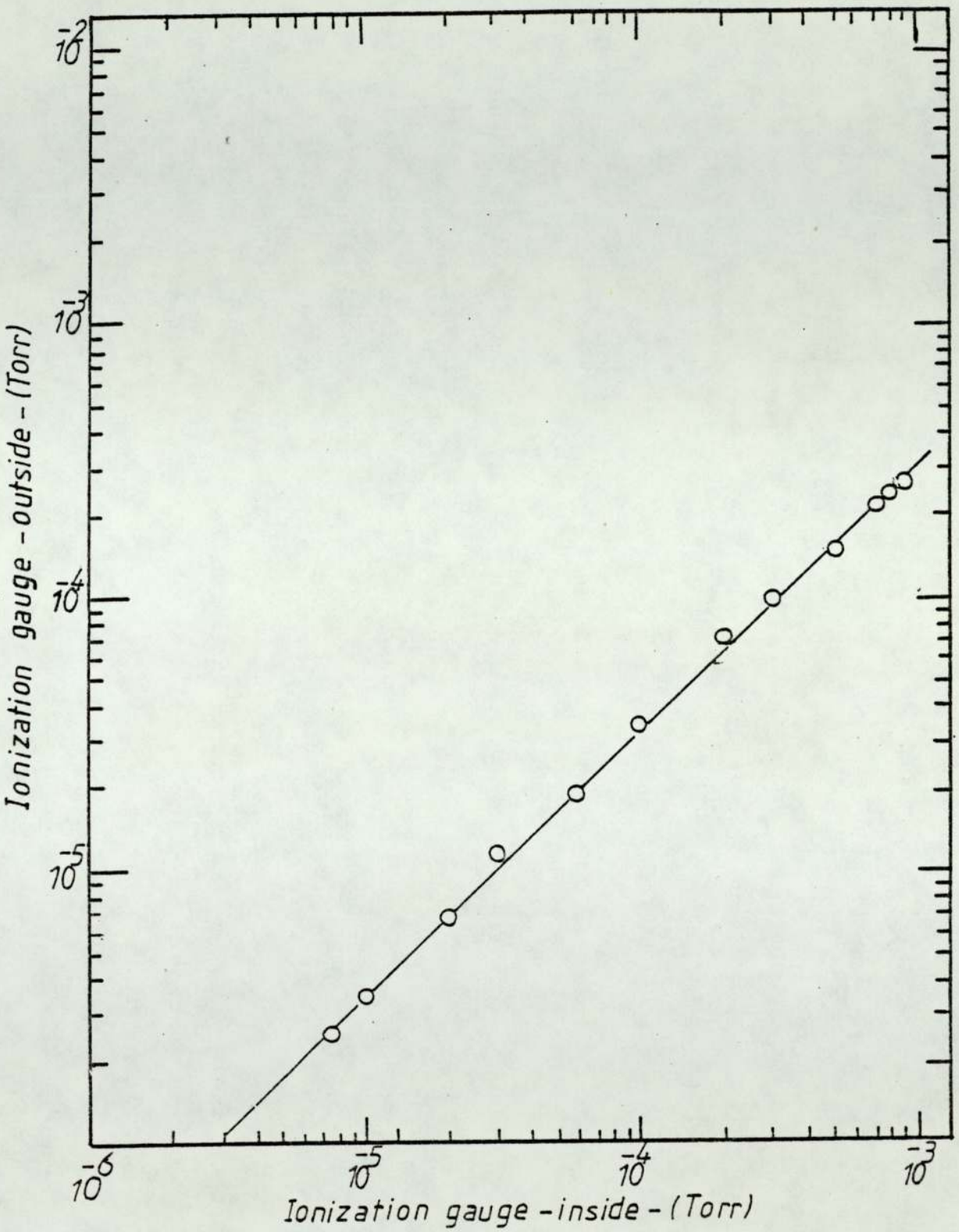

Figure 3.5 Calibration of pressures inside and outside the experimental chamber.

with the ionization gauge.

(a) Constant volume method:

An equilibrium pressure p_e was established for a constant leak into the chamber through the normal gas inlet valve and the rise in the pressure after isolating the diffusion pump was recorded, thus the effective speed of the pump S_E is given by:-

$$S_E = \frac{V}{p_e}\frac{dp}{dt} \qquad \ldots\ldots\ldots (3.1)$$

where the volume of the chamber, V, is equal to 35 l. The results given in table (3.1) show the expected difference between all three gases.

(b) Constant pressure method:

In this method it is necessary to measure the flow-rate of the gas directly and a flow-meter was constructed from glass and filled with fluid of the same type as used in the diffusion pump as shown in figure 3.6. For a particular flow of gas, Q, an equilibrium pressure p_e is produced and the effective speed, S_E, is given by:-

$$S_E = \frac{Q}{p_e}$$

Q is determined from a measurement of the volume, $\acute{V}$, of the fluid raised in a time t. Hence as one side of the flow-meter is at atmospheric pressure p_a, then:-

$$Q = \frac{p_a \acute{V}}{t}$$

and hence

$$S_E = \frac{p_a}{p_e}\frac{\acute{V}}{t}$$

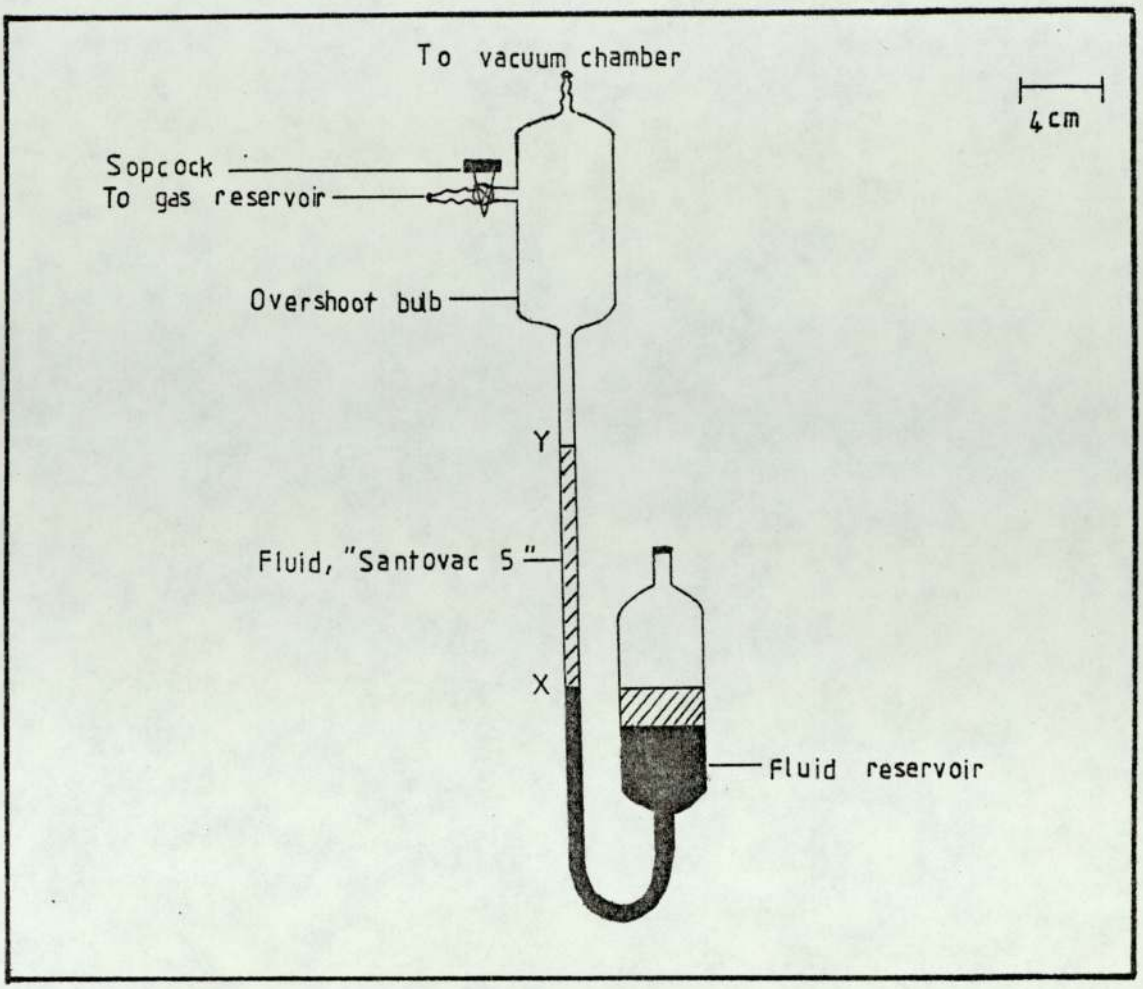

Figure 3.6 Displacement type flow-meter

The results for the constant pressure method are also shown in Table (3.1) and show similar values of S_E found with the constant volume method.

The table also shows the ratio of the speeds for argon and helium relative to that of nitrogen for each method and the theoretical values of these ratios, $\acute{R}$, are also given in the Table. The values of $\acute{R}$ have been determined using the equation

$$S_E \propto \sqrt{\frac{T}{M}}$$

where T and M are the temperature and molecular weight respectively. Therefore the values of $\acute{R}$ at constant temperature are given by:-

$$\acute{R} = \sqrt{\frac{M_N}{M_A}}$$

Table 3.1 Comparison of the measured and theoretical pumping speed for argon, nitrogen and helium.

Type of information	Type of gas		
	Argon	Nitrogen	Helium
Speed of the pump at constant volume (litre per sec)	90 ± 6	100 ± 6	220 ± 12
Speed of the pump at constant pressure (litre per sec)	110 ± 12	130 ± 16	205 ± 25
Ratio of speed relative to nitrogen (constant volume method)	0.9 ± 0.1	1	2.2 ± 0.3
Ratio of speed relative to nitrogen (constant pressure method)	0.85 ± 0.2	1	1.6 ± 0.4
Theoretical ratio of speed relative to nitrogen	0.84	1	2.65

The Table shows that the relative speeds as measured with the constant volume method are in better agreement with the theoretical values than those obtained from the constant pressure method. These results are perhaps not surprising since, firstly, the constant volume method has the advantage that it is independent of the gauge sensitivity. Furthermore, with the constant volume method, the pump is isolated and thus one would expect the pressure in the system to be reasonably uniform in all parts of the chamber. On the other hand it has already been shown that when we have constant pressure arising as a balance between the pump speed and the gas flow rate, a pressure

differential can exist in the chamber. Of course the constant volume method suffers from the disadvantage that the pressure can be influenced from sorption and desorption processes but this is not likely to be important at the relatively high pressures used in these measurements. In addition it was found as indicated in Table 3.1, that the uncertainties in the measured speed was less using the constant volume method. It was thus decided to use the measured values of speed determined by the constant volume method in all subsequent calculations.

CHAPTER 4

SOURCE CHARACTERISTICS AND MODES OF OPERATION

4.1 Introduction

The characteristics of the ion source were studied for argon, nitrogen and helium. This involved recording the variation of anode current, I_A, with anode voltage, V_A, and the variation of beam current, I_B, with I_A as a function of chamber pressure, p_c. Before any measurements were taken the system was pumped to its normal ultimate pressure of 1×10^{-6} torr. The chamber was flushed several times with the particular gas in order to reduce the effect of any other residual gases. The source was outgassed before any measurements were recorded by operating the source at high anode voltage and anode current for about 15 minutes and even longer if the source had been previously cleaned with organic agents.

4.2 Characteristics of the ion source

Figure 4.1 shows the $V_A \rightarrow I_A$ characteristics for argon over the pressure range 3×10^{-4} torr to 3×10^{-5} torr. It can be seen that when the pressures increase the anode current increases and the corresponding anode voltage decreases. Figure 4.2 shows the $I_B \rightarrow I_A$ characteristics over the same range of pressure and it is evident that I_B increases as the pressure decreases for a given anode current. Similar characteristics for nitrogen and helium are shown in figures 4.3 to 4.6.

It is thus clear that the chamber pressure, anode voltage and anode current are important parameters in the determination of the source characteristics. However there is another parameter, namely the source aperture, which is also important. The size of the

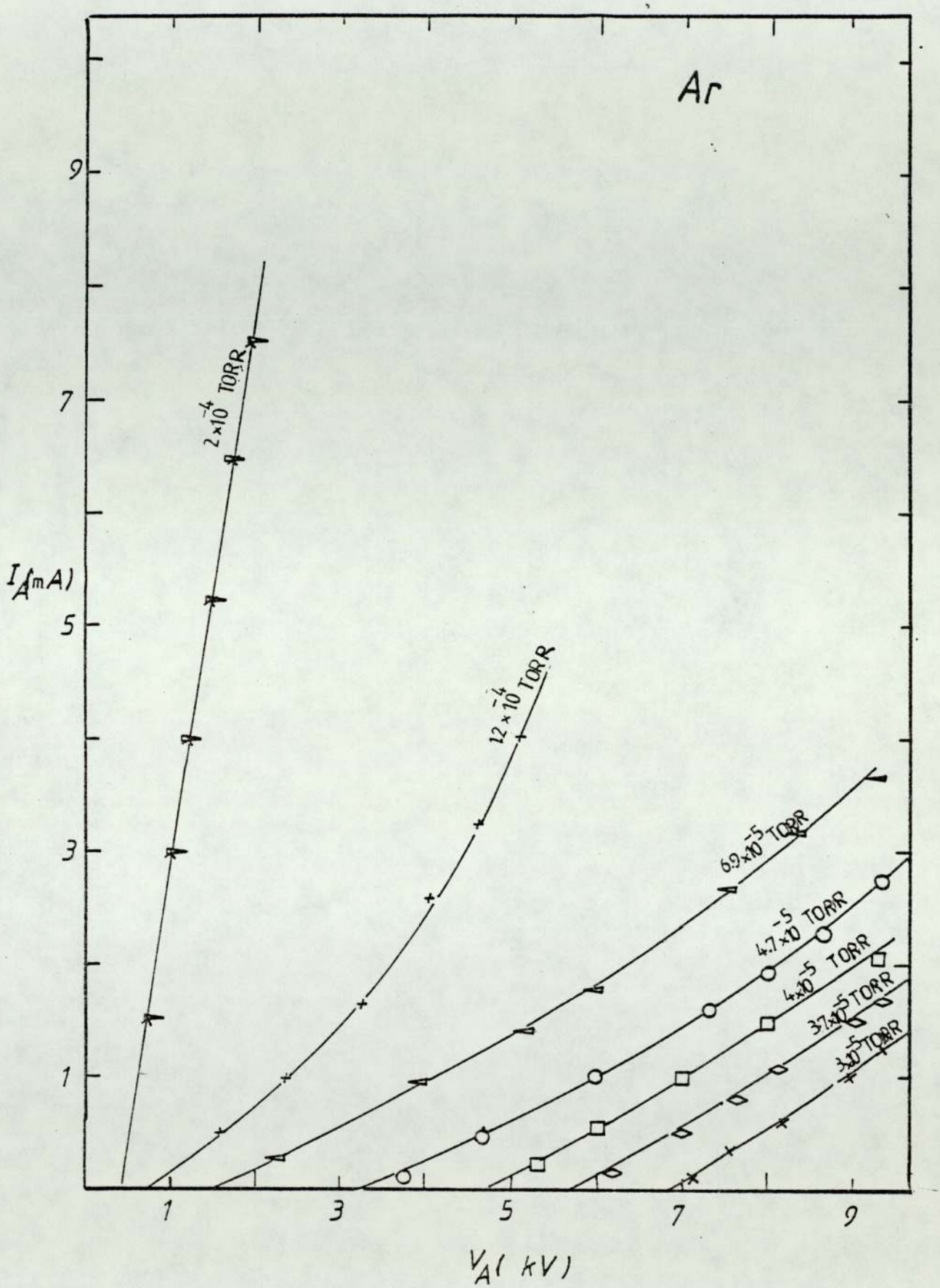

Figure 4.1 Variation of anode current, I_A with anode voltage, V_A using argon.

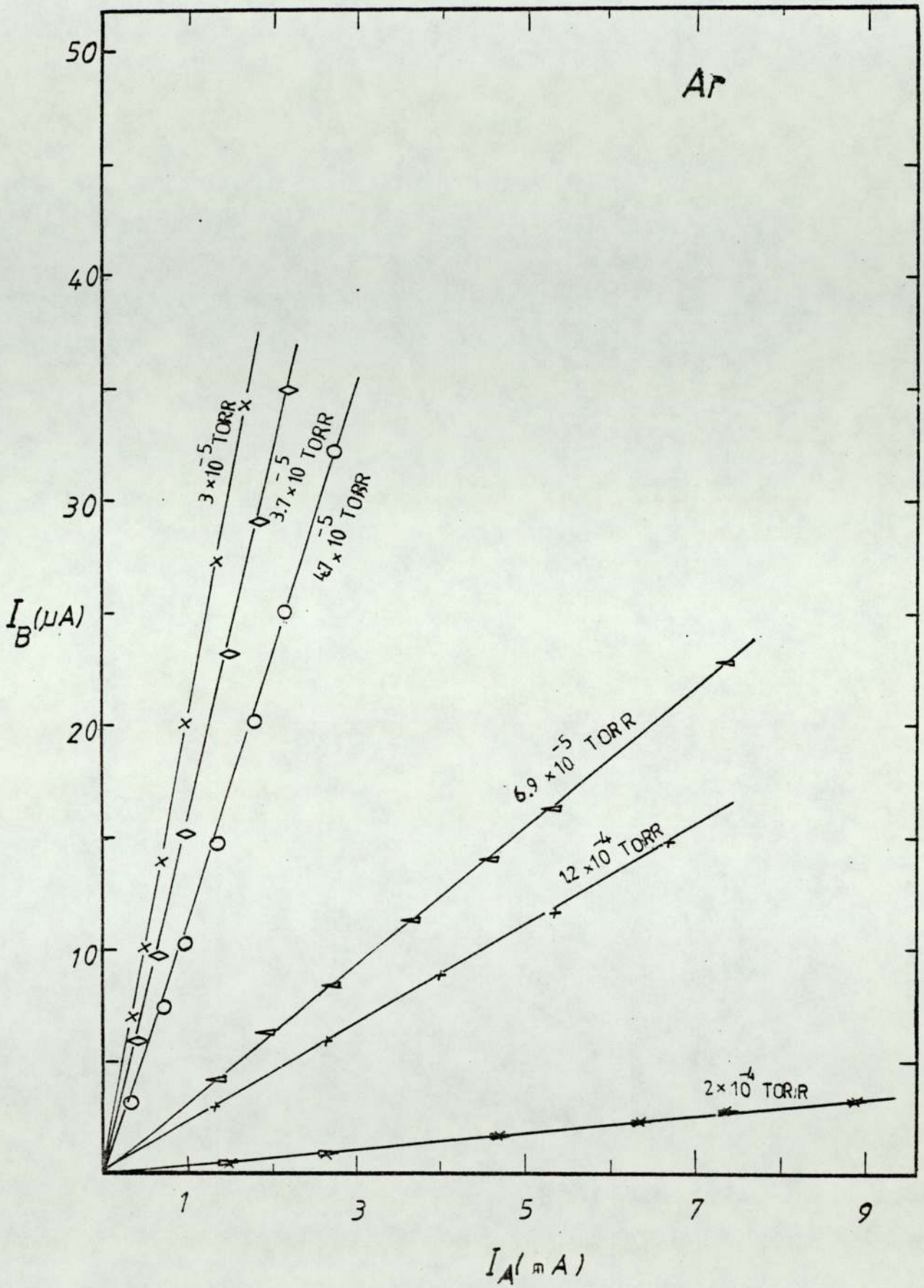

Figure 4.2 Variation of ion beam current, I_B with anode current I_A using argon.

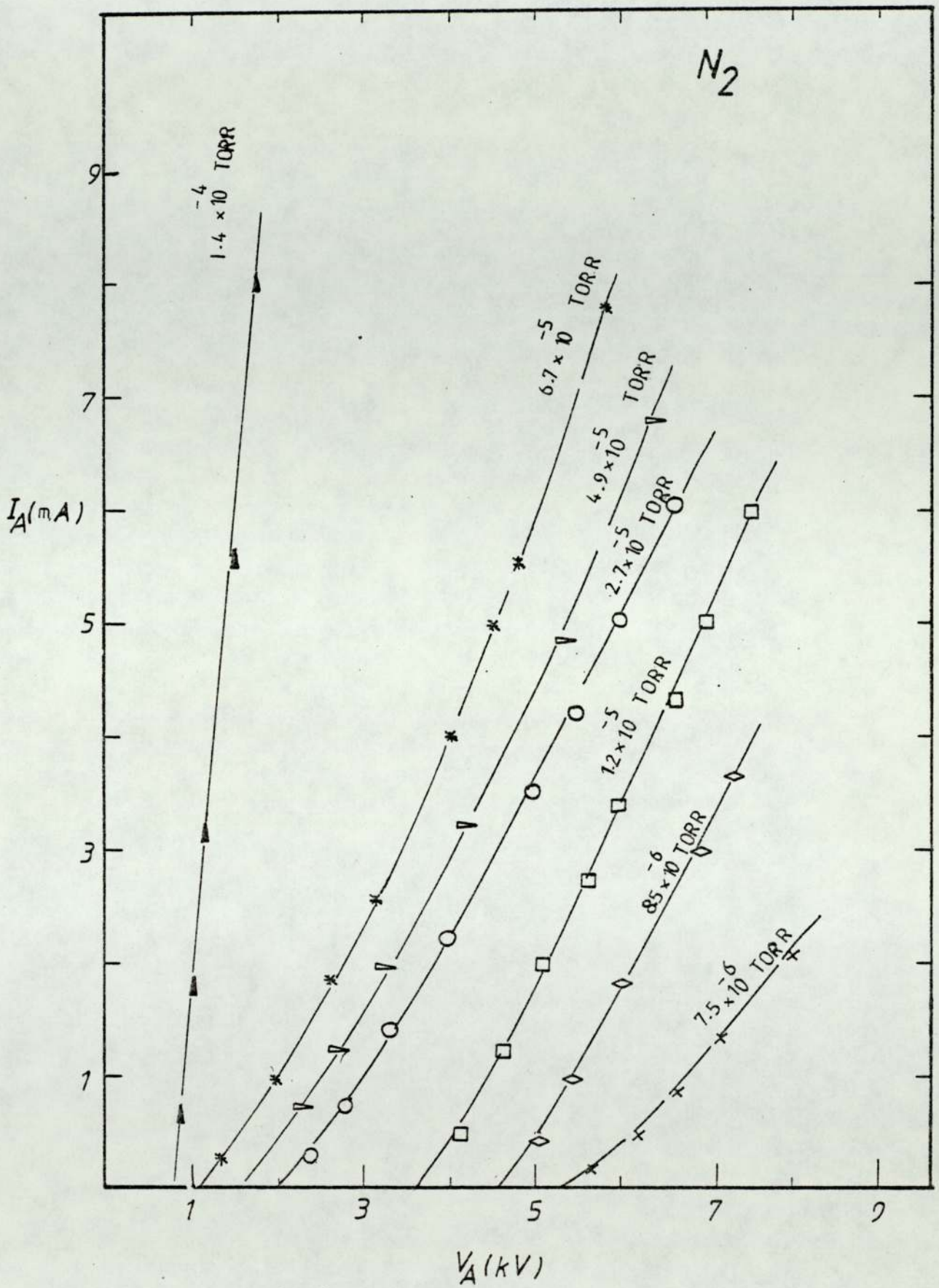

Figure 4.3 Variation of anode current, I_A with anode voltage, V_A using nitrogen.

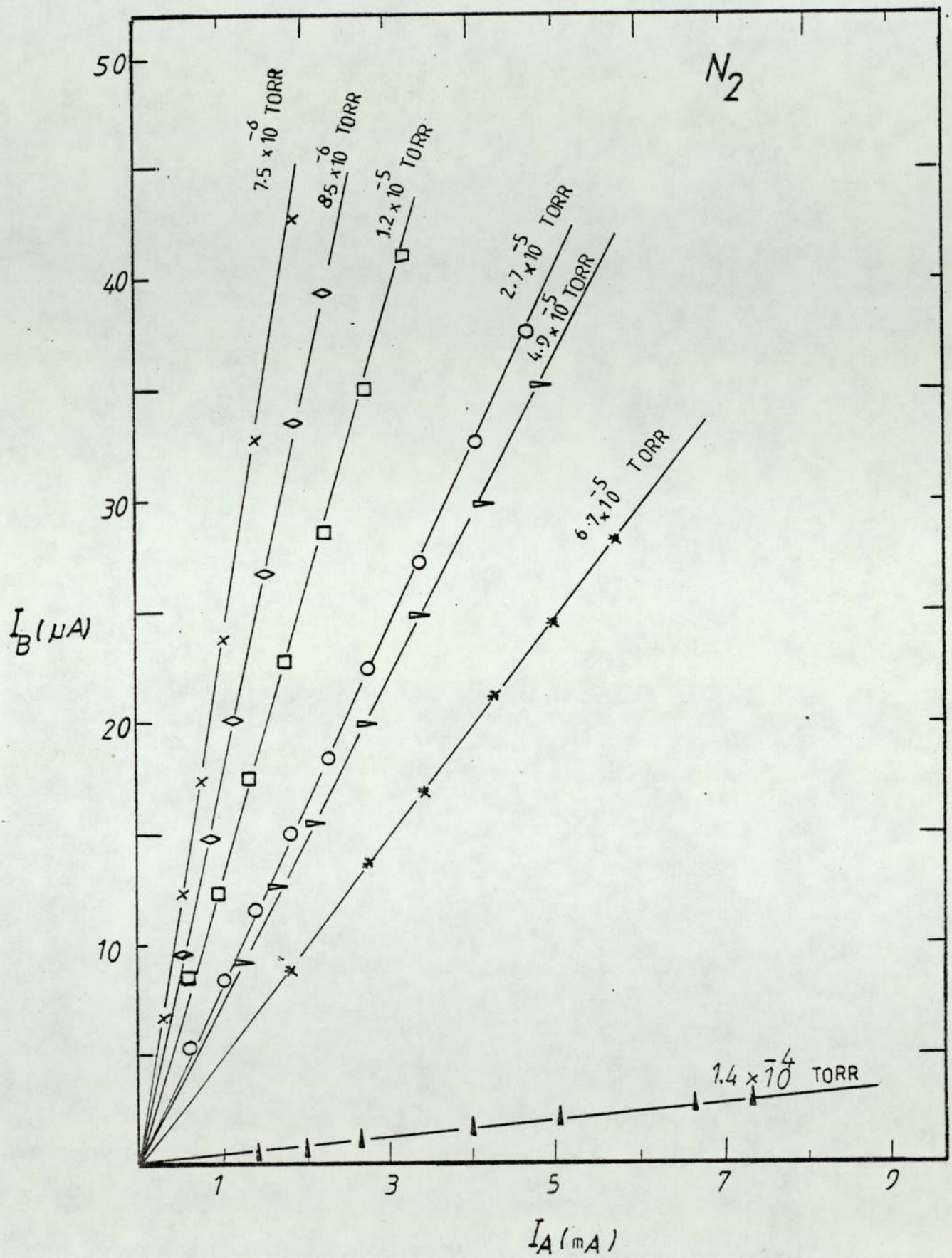

Figure 4.4 Variation of ion beam current, I_B with anode current, I_A using nitrogen.

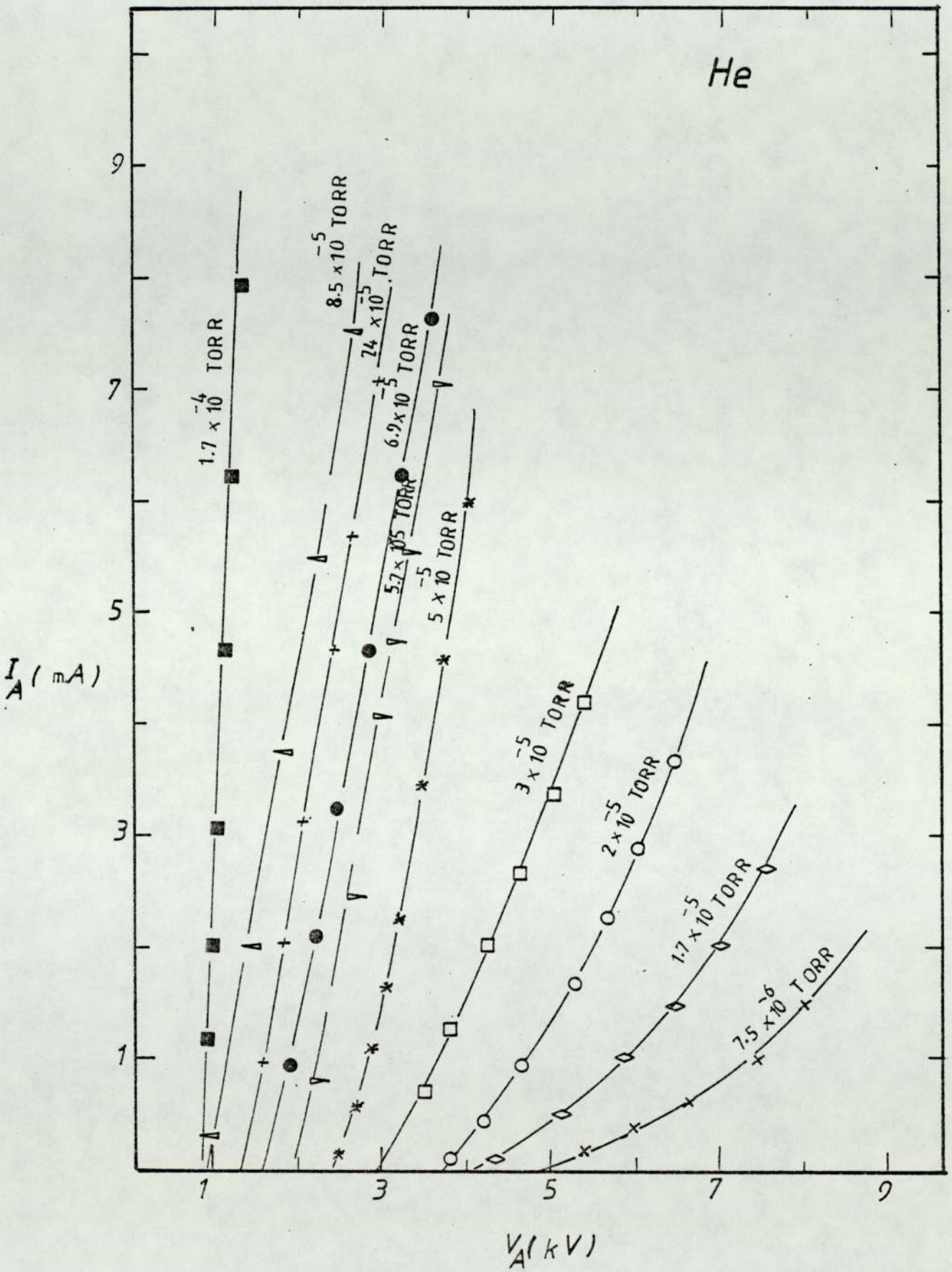

Figure 4.5 Variation of anode current, I_A with anode voltage, V_A using helium.

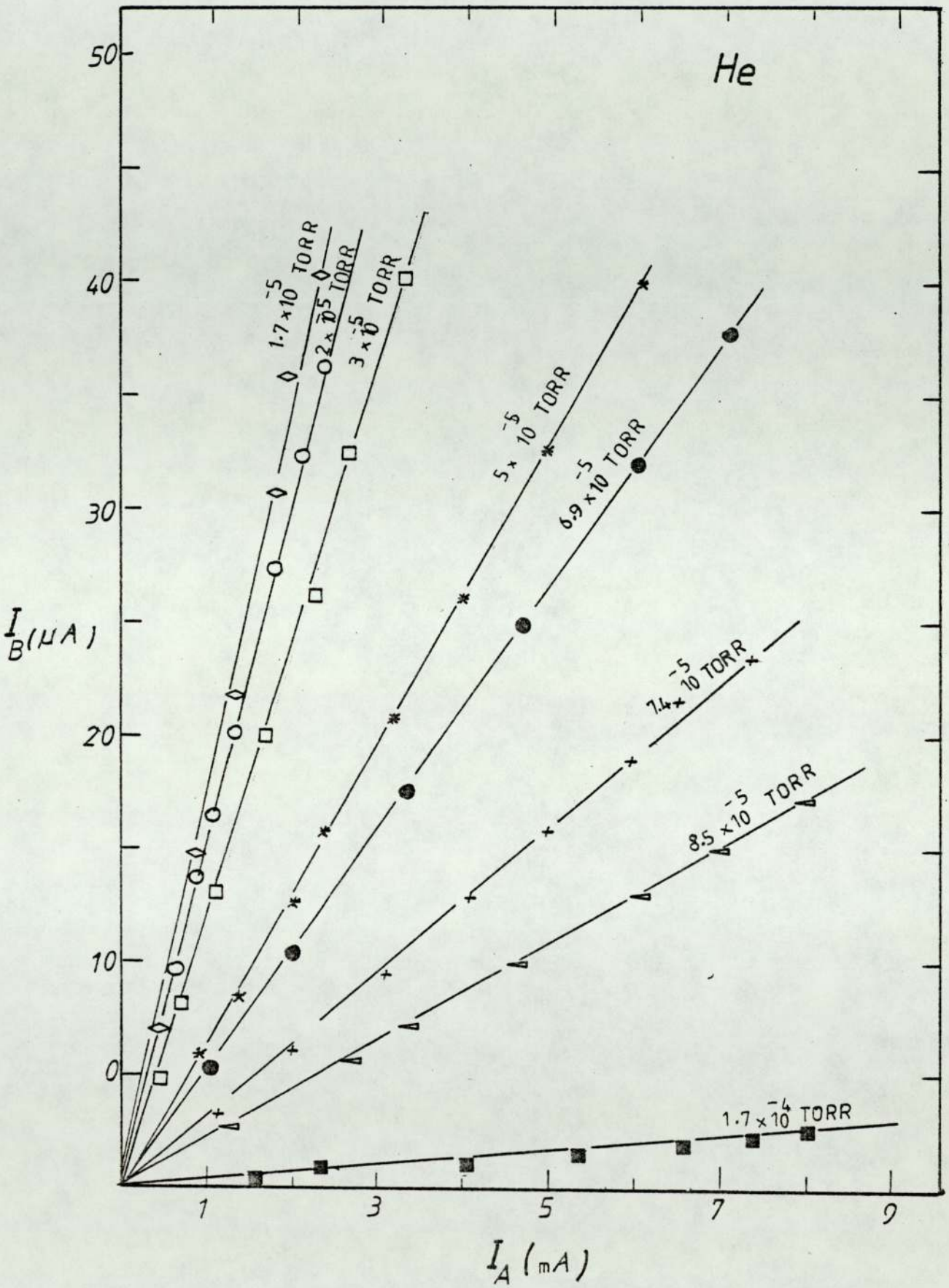

Figure 4.6 Variation of ion beam current, I_B with anode current, I_A using helium.

aperture used in these measurements was 1.5 mm in diameter and was selected to produce optimum performance. With larger apertures a greater fraction of the ions can be extracted but this can result in a reduction in anode current due to the distortion of the electric field through the larger aperture. In addition, use of a larger aperture requires that the chamber pressure must be increased to maintain the same source pressure. On the other hand when very small apertures are used the distortion of the field is eliminated but is not sufficient to compensate for the reduced fraction of ions extracted. It can be seen that the source can be operated from a minimum voltage of about 500 V to 12 kV, but its operation is more stable and more suitable between 1.5 to 10 kV which corresponds to 2×10^{-4} to 2×10^{-5} torr.

However it was quite difficult to operate the source above 10^{-3} torr because electrical breakdown occurs in the chamber whereas at pressures less than 10^{-5} torr, which is at high voltage, it is also extremely difficult to operate the source because breakdown can occur across the insulators.

4.3 Operating modes of the source

The modes of operation for argon, nitrogen and helium have been studied as a function of pressure using two 1.5 mm ion exit apertures. This was done by measuring the variation of anode voltage, V_A, and beam current, I_B, as a function of chamber pressure, p_c, at constant anode currents of 1, 2 and 3 mA. These are shown in figures 4.7 to 4.12 for all three gases. The general shape of these curves are the same for all gases and we can see, for example, with argon in figure 4.7 that as the pressure increases from 5×10^{-6} torr, the anode voltage falls from 12 kV to about 5 kV at 10^{-4} torr. This region has been referred to as the "oscillating mode", Rushton et al[34].

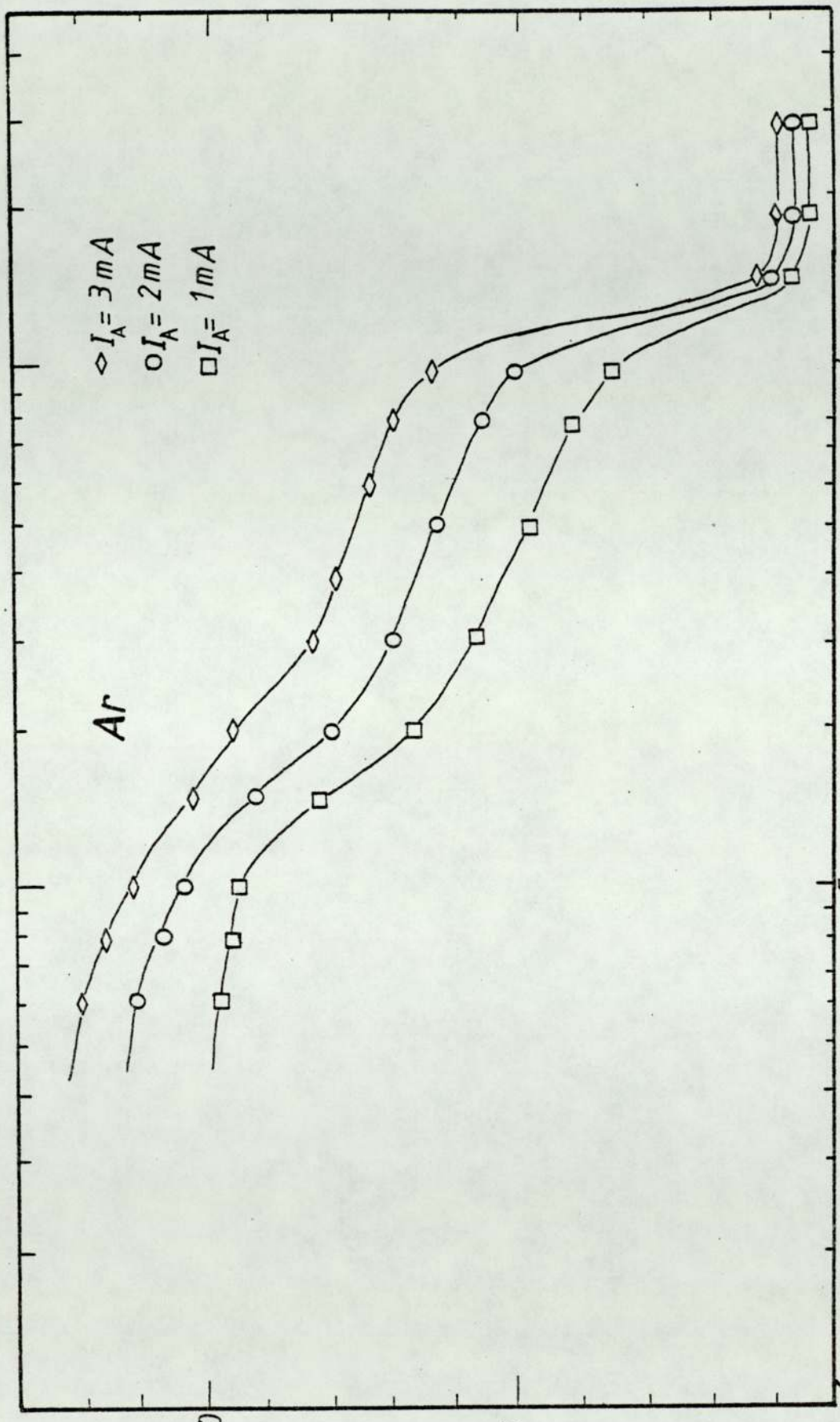

Figure 4.7 Variation of anode voltage, V_A with chamber pressure, p_c using argon.

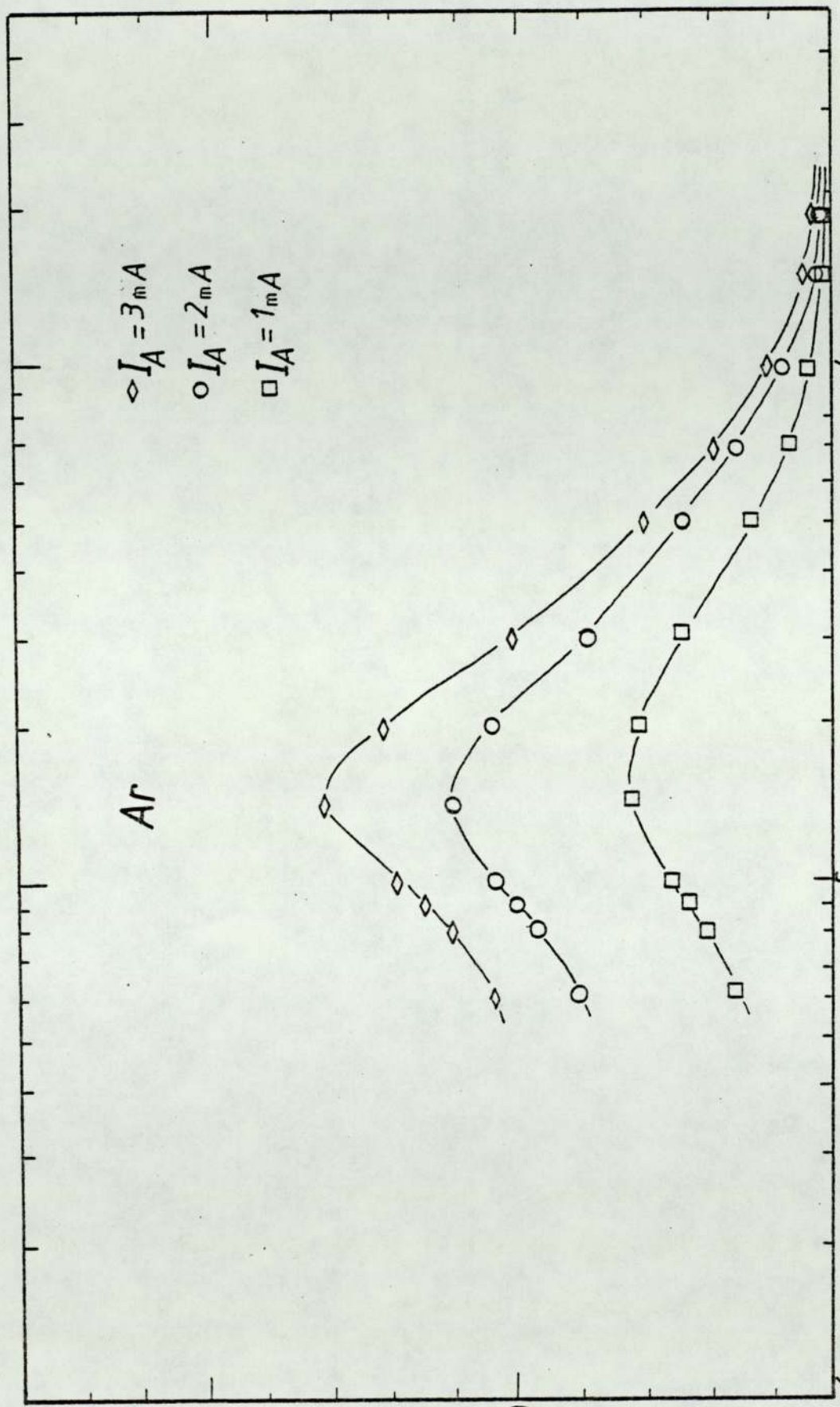

Figure 4.8 Variation of ion beam current, I_B with chamber pressure, p_c, using argon.

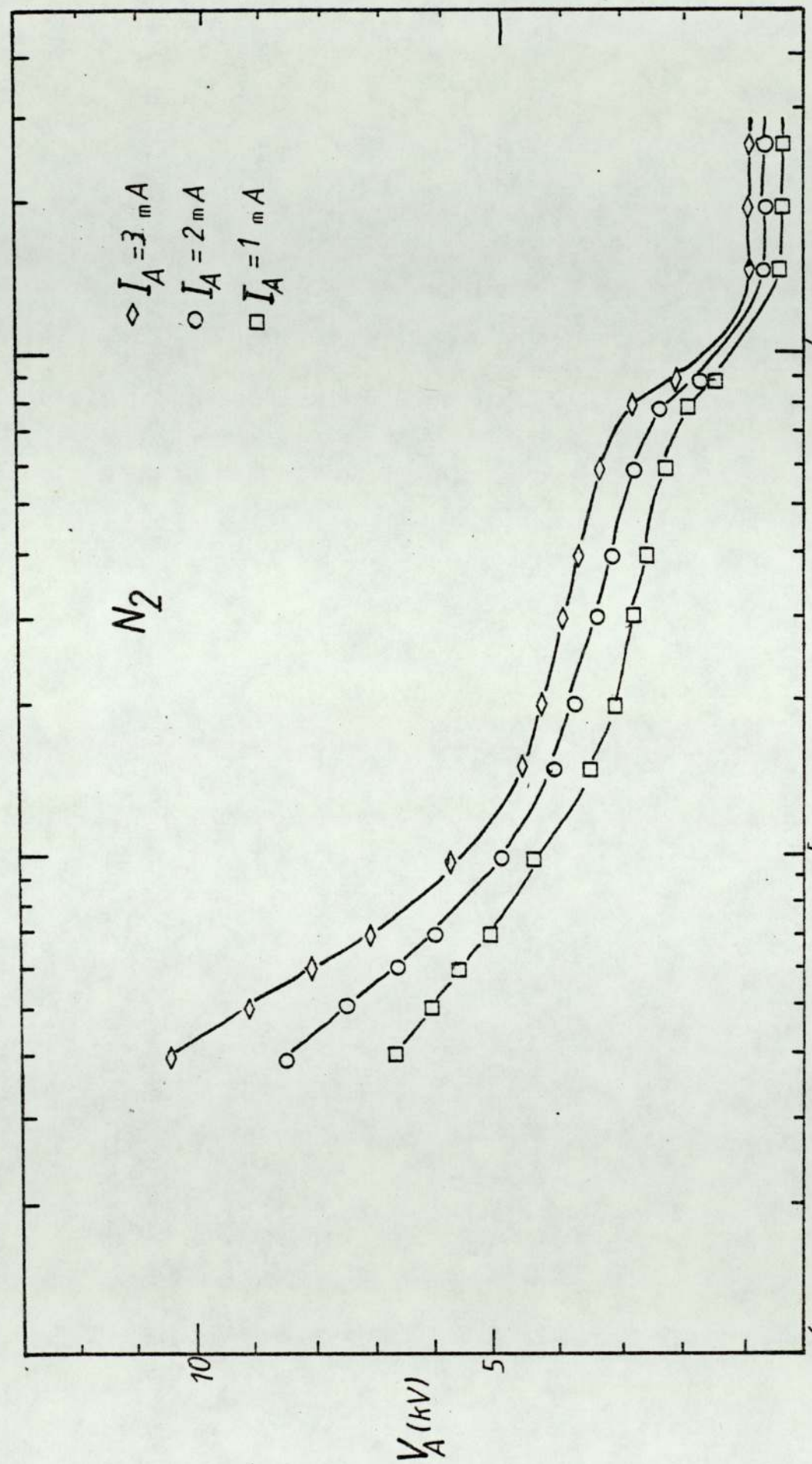

Figure 4.9 Variation of anode voltage, V_A with chamber pressure, p_c using nitrogen.

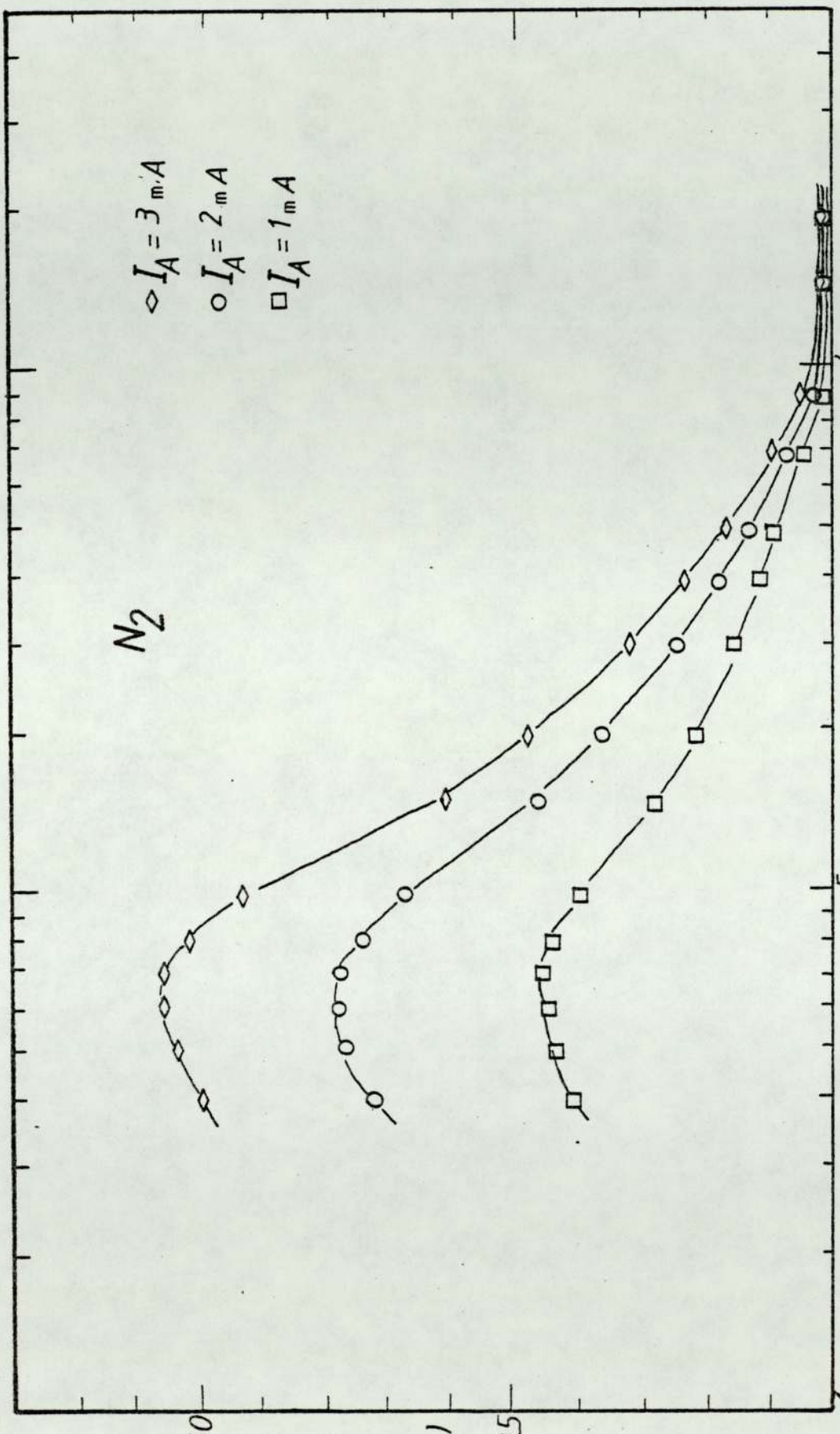

Figure 4.10 Variation of ion beam current, I_B with chamber pressure, p_c using nitrogen.

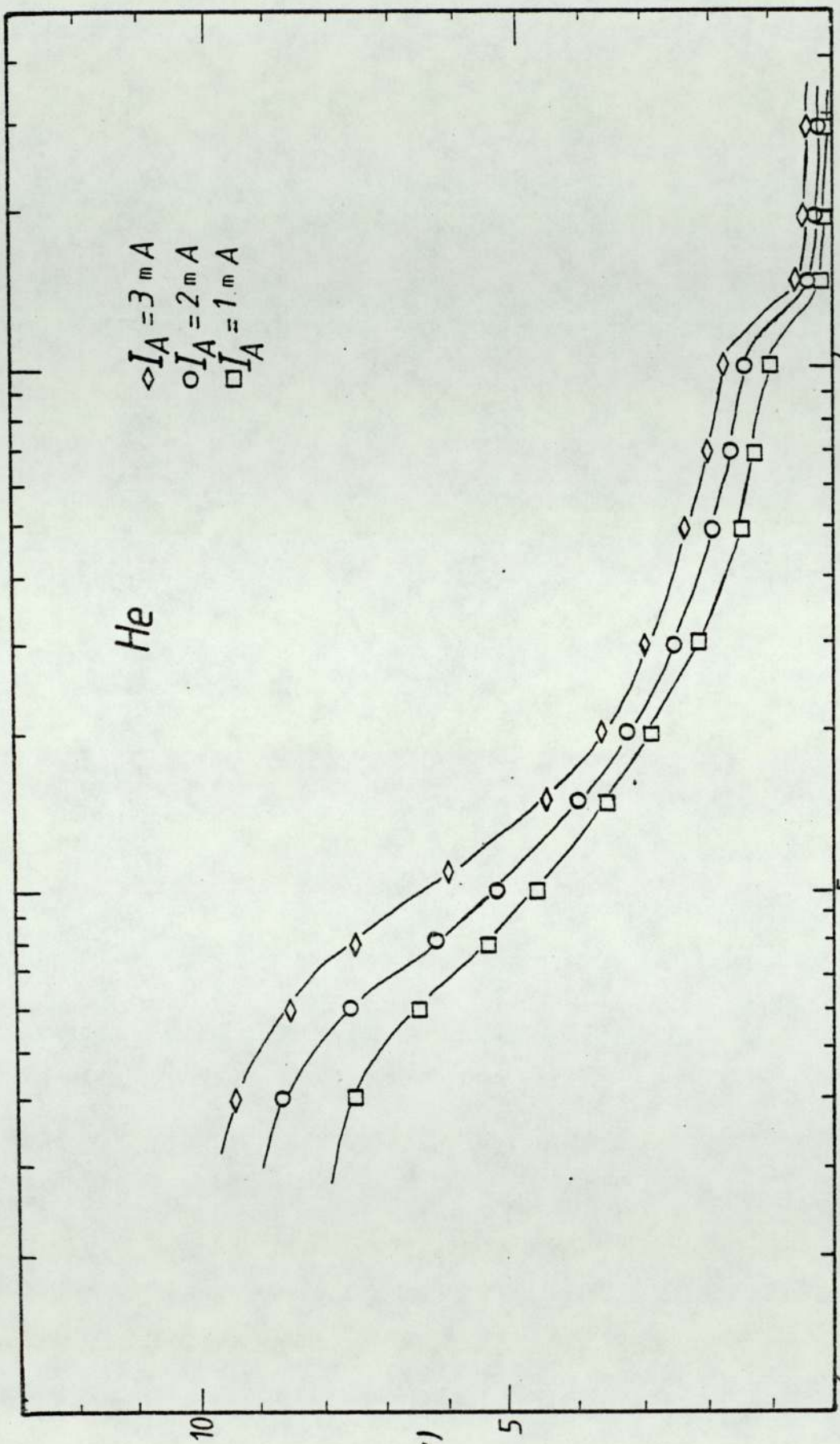

Figure 4.11 Variation of anode voltage, V_A with chamber pressure, p_c using helium.

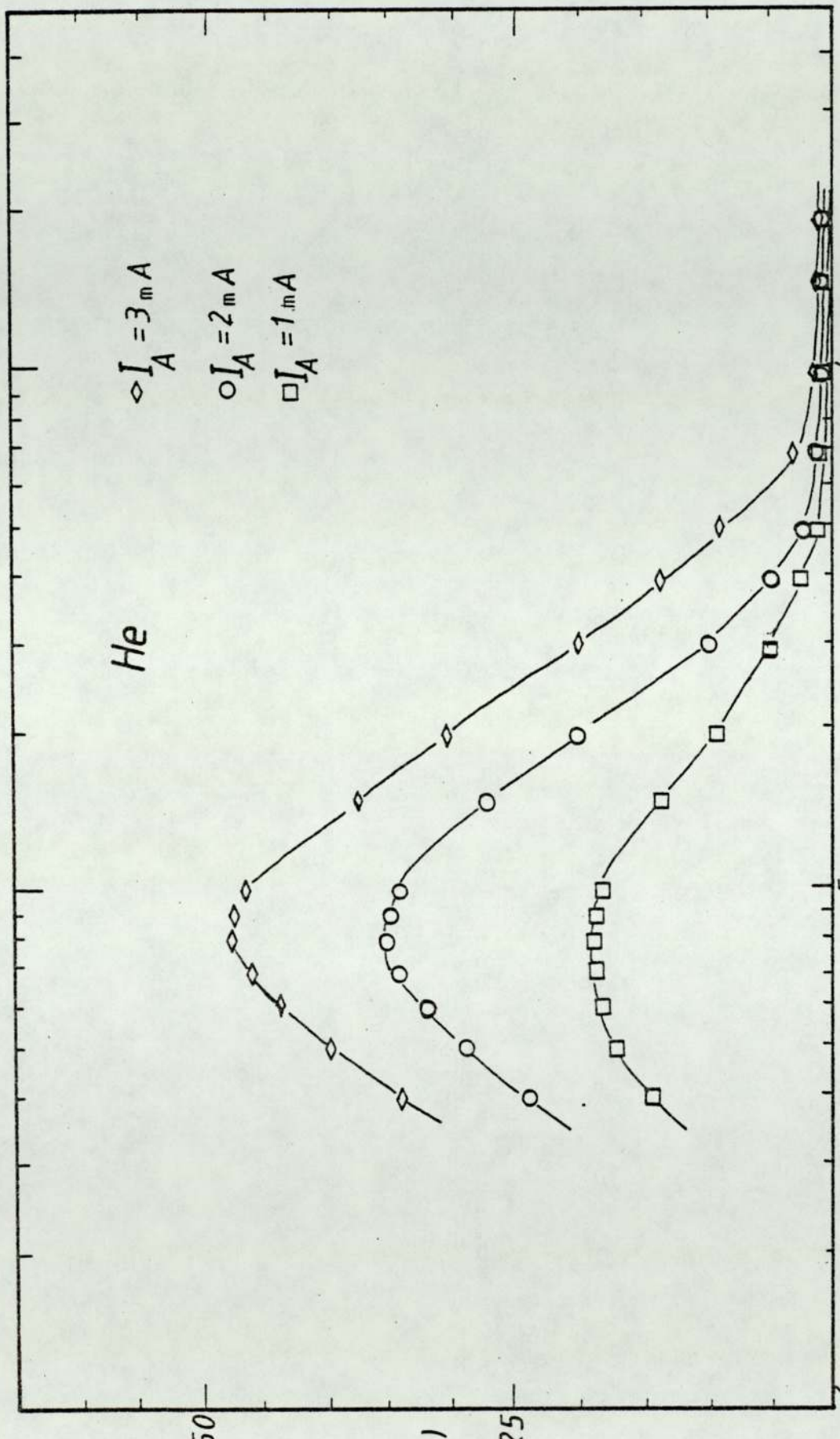

Figure 4.12 Variation of ion beam current, I_B with chamber pressure, p_c using helium

Above 10^{-4} torr, V_A falls very rapidly over a small range of pressures and this region is known as the "transition mode". At even higher pressures the voltage reduces to about 800 V and remains reasonably constant as the pressure increases in the "Glow discharge mode". Figure 4.8 shows the corresponding variation in ion beam current. As the pressure increases from $6x10^{-6}$ torr the ion current increases to a maximum value at about 10^{-5} torr and then rapidly decreases until a pressure 10^{-4} torr and then remains fairly constant and small at about $3x10^{-4}$ torr. The reduction in I_B from the maximum value at very low pressures has not previously been observed. This was presumably due to the fact that no measurements had been possible at these high anode voltages. In the present study this difficulty had been overcome by modifying the length of the insulated region on the H.T. terminal to the anode.

The three distinct regions "oscillation, transition and glow discharge mode" have the same general form as that reported by Khorassany[51], but in his case it appeared that the ion beam current remained constant at the lowest pressures investigated.

It is possible to describe a model of the mechanism occurring inside the source which can explain the modes of operation. In the general glow discharge when the chamber pressure is higher than $2x10^{-4}$ torr, there is no significant contribution to the ionization process from oscillating electrons. In this region the mean free path for electron-molecular collision inside the source is assumed to be very small and thus the electrons will not oscillate significantly around the anode and the ionization process will occur in all regions between the cathode and anode. Thus we will expect to see a general glow discharge spread around the whole volume of the source as shown schematically in figure 4.13a.

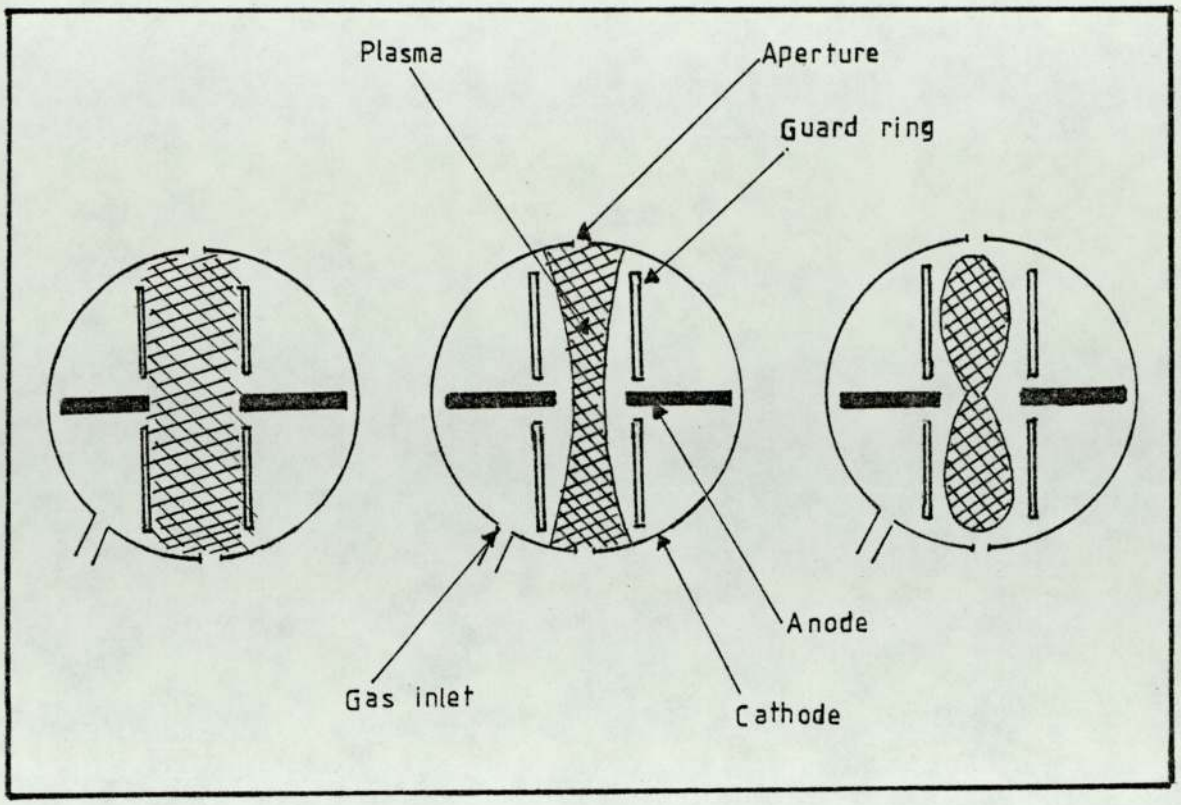

(a) glow mode

(b) transition mode

(c) oscillating mode

Figure 4.13 Schematic diagrams illustrating the three modes of operation.

This explains why the extracted ion beam current is low. On the other hand when the mean free path for the ionization process becomes similar to the source radius, oscillating electrons become significant and the discharge starts to confine itself within the anode as shown in figure 4.13b.

In the transition region as the pressure continues to reduce, the ion current continues to increase as the discharge becomes more confined and, as the mean free path now becomes greater than the radius of the source, the oscillating mode occurs as shown in figure 4.13c. Thus a high degree of ionization occurs resulting in a stable ion beam current. At this stage no satisfactory explanation can be offered for the fairly significant reduction in ion beam current at the lowest operating range of pressure. However, this could be

accounted for by a reduction in the proportion of multicharged ions which is likely to be less at lower pressure. This phenomena is at present a subject of further study in this laboratory.

It is clear that there is no obvious advantage in operating the source at lower pressures as the beam current reduces and the anode voltage increases. Thus it is possible to choose the ideal conditions for operating the source to produce the maximum ion beam current at the optimum pressure.

Observation of the voltage, pressure and ion beam current for a constant anode current shows that the transition mode occurs at different chamber pressures for each gas but it is more important to consider the source pressure and corresponding mean free path for each gas. In the following section an attempt has been made to calculate the mean free path for electron-molecular collisions for all gases, thus substantiating the proposed model to explain the modes of operation.

4.4 Calculation of the mean free path inside the source

In order to calculate the mean free path for electron-molecular collision, it is necessary to find out what is the source pressure for each gas taking into account the measured speed of the diffusion pump, the conductance of the ion exit aperture, the sensitivity of the gauge and the ionization cross-section for each gas.

The mean free path for electron molecular collision, λ_e, for argon, nitrogen and helium is related to the number of molecules per unit volume inside the source, n cm^{-3} and the maximum total collision cross-section, α, of electrons with molecules and is given by:

$$\lambda_e = \frac{1}{n\alpha} \qquad \text{(cm)}$$

n can be calculated from the source pressure, p_s, which can be measured from the chamber pressure, p_c, the conductance of the ion exit aperture, C, and the effective speed of the diffusion pump, S_E, where:

$$\frac{p_s}{p_c} = \frac{S_E+C}{C}$$

where

$$C = \frac{62.5xA}{\sqrt{M}}$$

where A is the area of the two apertures in cm^2

and M is the molecular weight of the particular gas.

The values of α used for all gases are those given by Massey and Burhop[52] at 100 eV which gives the maximum ionisation cross-section.

Table 4.1 shows the values of the total conductance of the two ion exit apertures, the ratios between the source pressure and the chamber pressure, $\frac{p_s}{p_c}$, the transition chamber pressure which are taken from the graphs for the modes of operation, the transition source pressure, p_{ST}, and the values of λ_e for all three gases. It was found that at the transition mode the values of λ_e are 1.53 ± 0.22, 1.65 ± 0.26 and 1.85 ± 0.20 cm for argon, nitrogen and helium respectively. These are in reasonable agreement with each other taking into account the uncertainties in the values of λ_e arising from the random and systematic errors in the speed of the pump, conductance of the aperture and the pressure at the transition mode. Thus the average λ_e of about 1.67 ± 0.23 cm is nearly the same as the radius of the source which is 1.5 cm and this gives good support to the model proposed in the previous section for the modes of operation.

Table 4.1 Calculation of mean free path, λ_e, for different gases

Type of information	Type of gas		
	Argon	Nitrogen	Helium
Speed of the pump at constant volume S_E - l s^{-1}	$90^{\pm}5$	$100^{\pm}6$	$220^{\pm}12$
Conductance of ion exit aperture C - l s^{-1}	$0.33^{\pm}0.02$	$0.42^{\pm}0.02$	$1.09^{\pm}0.02$
Source pressure/chamber pressure p_s/p_c	273	243	202
Chamber transition pressure torr	$1.2^{\pm}0.05$ 10^{-4}	$9.2^{\pm}0.5$ 10^{-5}	$1.4^{\pm}0.05$ 10^{-4}
Chamber transition pressure nitrogen equivalent - torr	8.5×10^{-5}	9.2×10^{-5}	7.7×10^{-4}
Source transition pressure nitrogen equivalent, p_{ST}, torr	2.3×10^{-2}	2.1×10^{-2}	15.7×10^{-2}
Source transition pressure nitrogen equivalent allowing for the gauge position	6.96×10^{-2}	6.1×10^{-2}	4.7×10^{-1}
Mean free path λ_e - cm	$1.53^{\pm}0.22$	$1.65^{\pm}0.26$	$1.85^{\pm}0.20$

4.5 Ion source efficiency

The efficiency, η , of an ion source is also an important criterion to be taken into account. In this study three definitions of η namely η_i, η_p and η_g have been used. The current efficiency, η_i, is the ratio of the ion beam current, I_B, to the anode current, I_A. The power efficiency, η_p, is defined as the ratio of I_B to the input power, i.e. $\eta_p = \frac{I_B}{I_A V_A}$. The third parameter, η_g, is called the gas efficiency which is the ratio between the number of ions extracted from the source per second to the number of the thermal neutrals of the particular gas escaping from the source through the ion exit apertures in the same time.

Figure 4.14 shows the relation between η_i and the chamber pressure for argon at constant anode currents of 1 and 3 mA. It can be seen that η_i increases as the chamber pressure increases to a maximum value of about 30 μA mA^{-1} at a pressure of 1.5×10^{-5} torr before falling to less than 1 μA mA^{-1} at a higher pressure of about 1.5×10^{-4} torr. The current efficiency for nitrogen and helium were also studied and the corresponding curves show the same general shape and are given in figures 4.15 and 4.16.

The maximum value of η_i, was found to be greater for argon than nitrogen and helium. Figure 4.17 shows the variation of η_p against the chamber pressure for argon and the corresponding curves for nitrogen and helium are given in figures 4.18 and 4.19. The general shape of the $\eta_p \rightarrow$ pressure curve is very similar to the $\eta_i \rightarrow$ pressure curve for all gases and the maximum values in each case occur at about the same chamber pressure. However, the maximum value of η_p, is nearly the same for all three gases varying between 4.0 to 4.5 μA $watt^{-1}$ thus if the appropriate pressure is selected, it is possible to operate the source to produce the maximum values of

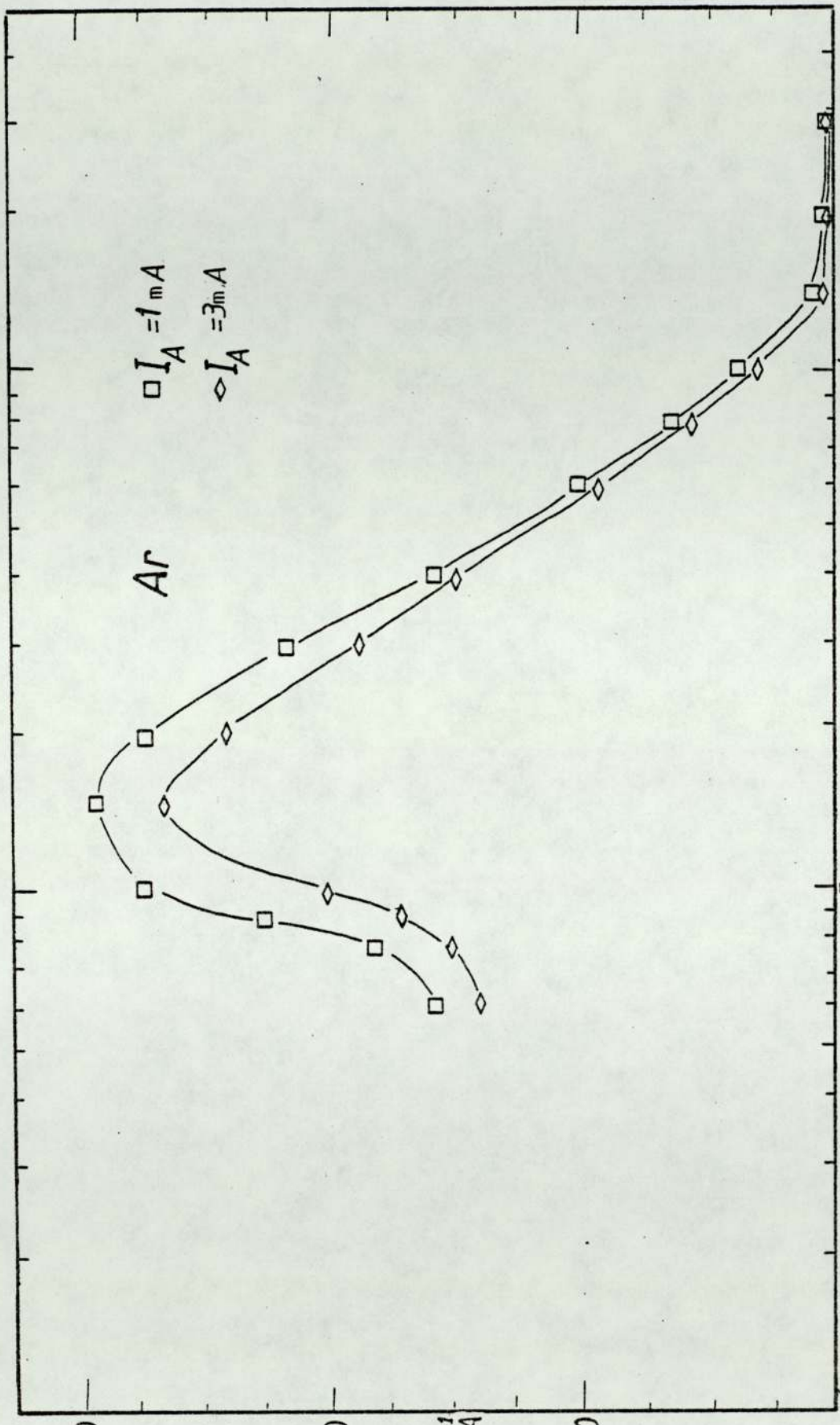

Figure 4.14 Variation of ion beam efficiency, η_i with chamber pressure, p_c using argon

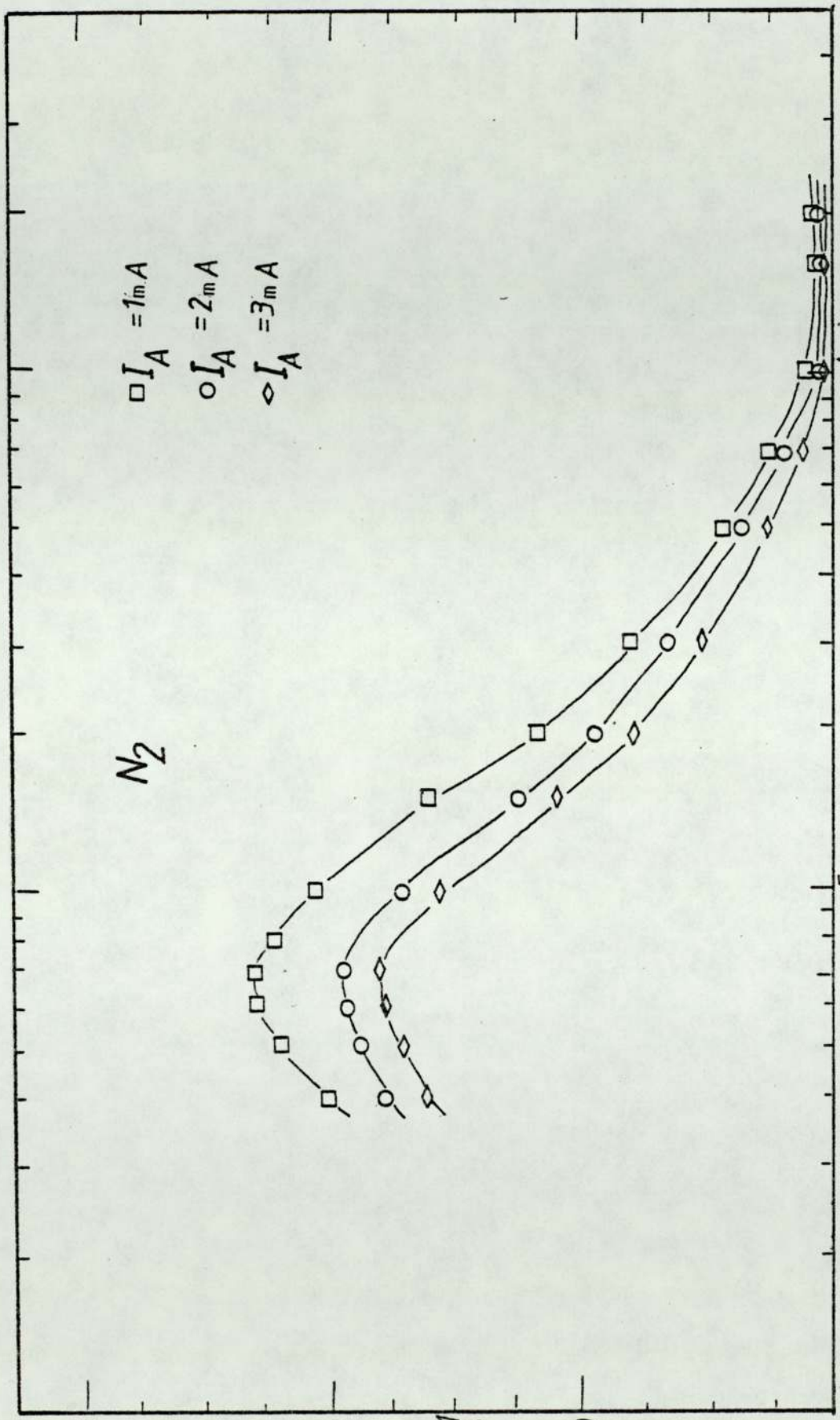

Figure 4.15 Variation of ion beam efficiency, η_i with chamber pressure, p_c using nitrogen

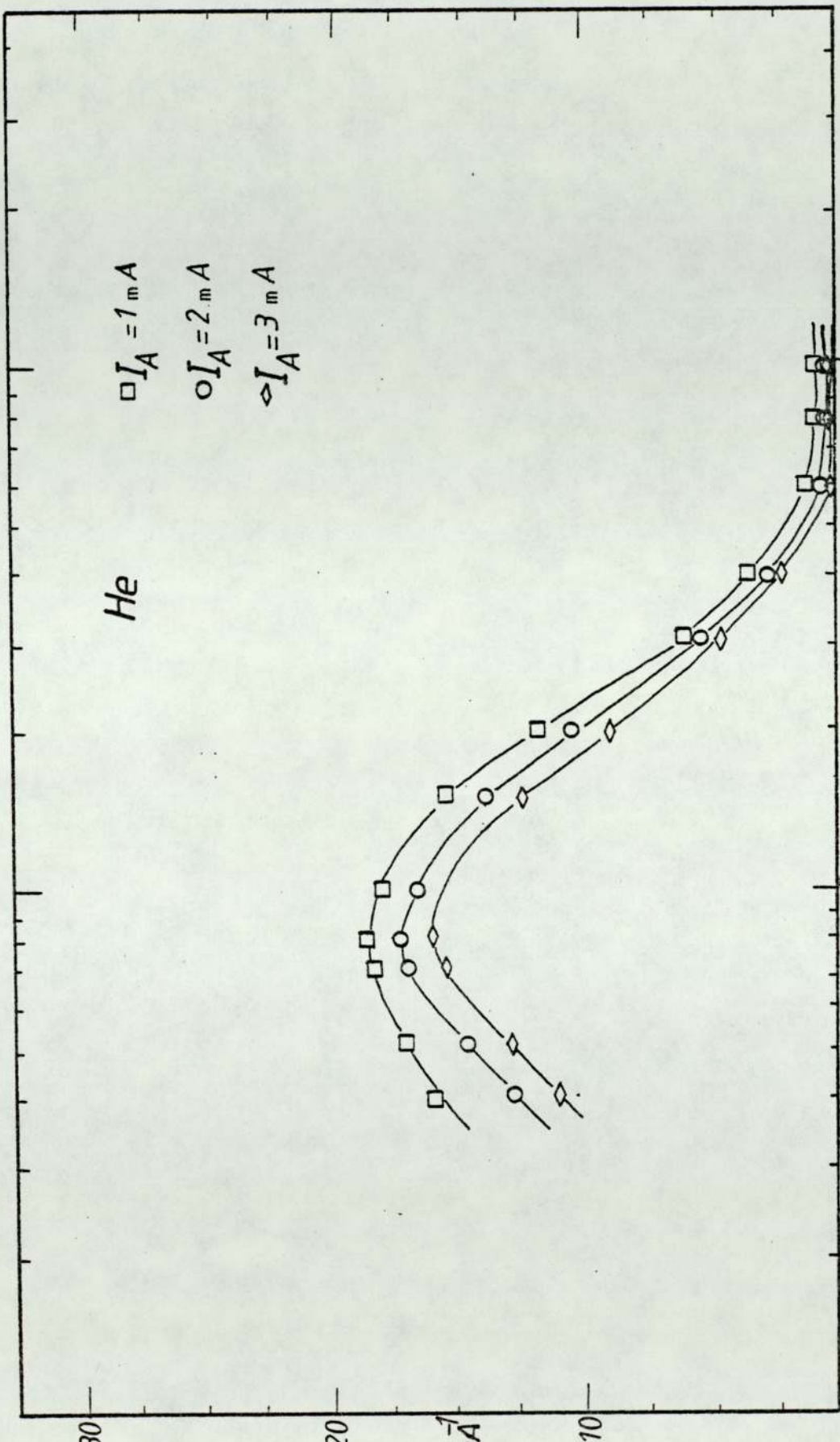

Figure 4.16 Variation of ion beam efficiency, η_i with chamber pressure, p_c using helium

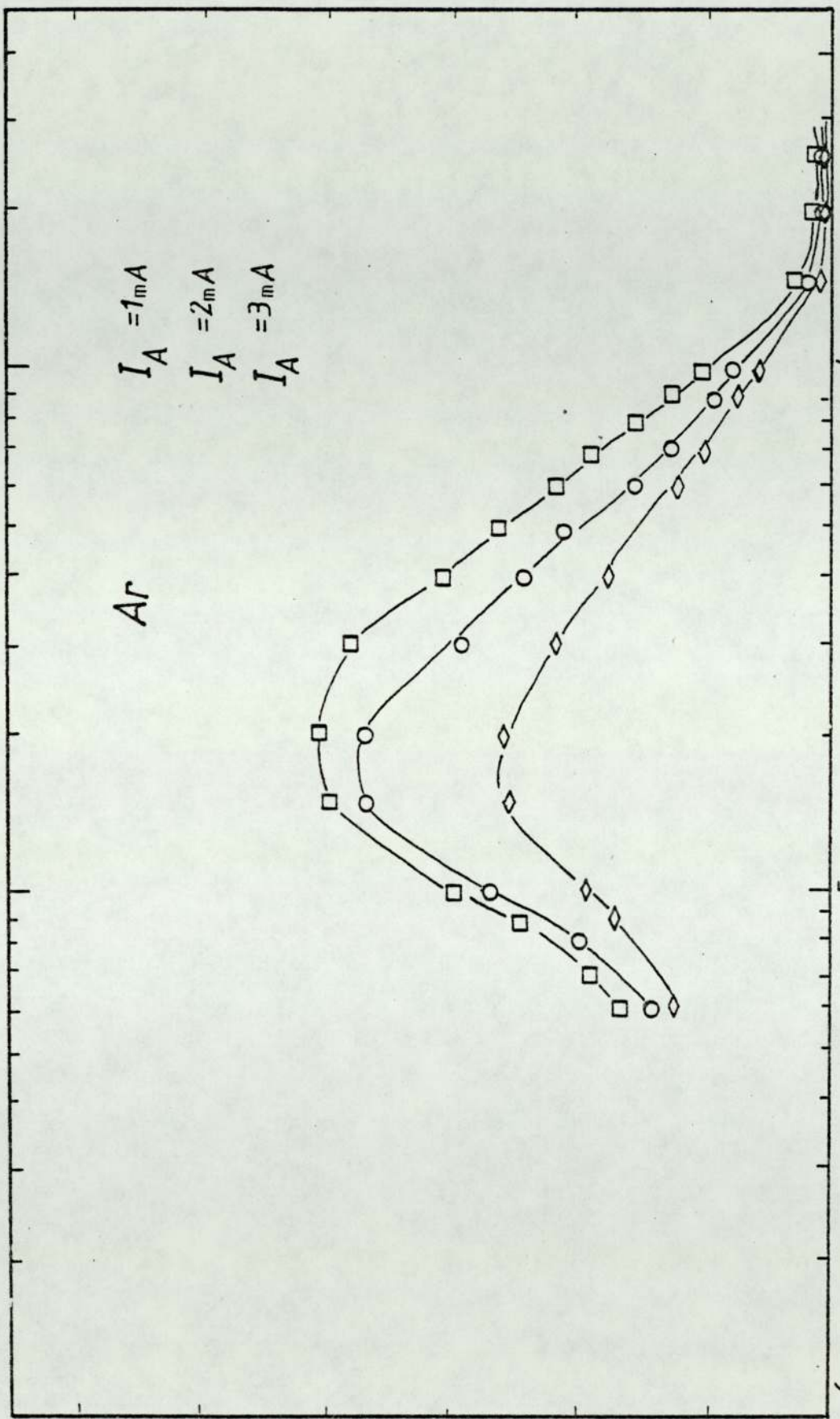

Figure 4.17 Variation of the power efficiency, η_p with the chamber pressure, p_c using argon

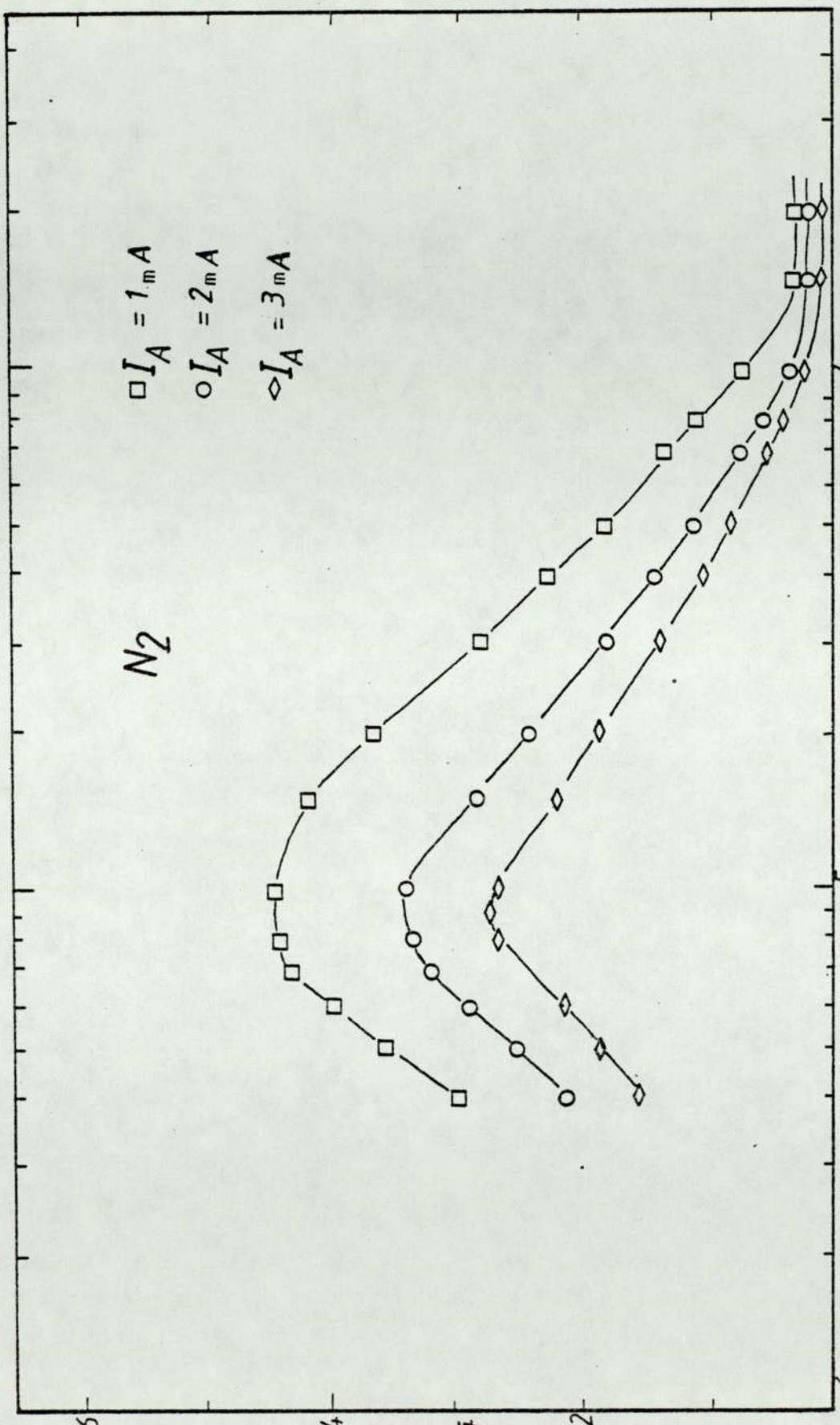

Figure 4.18 Variation of the power efficiency, η_p with the chamber pressure, p_c using nitrogen

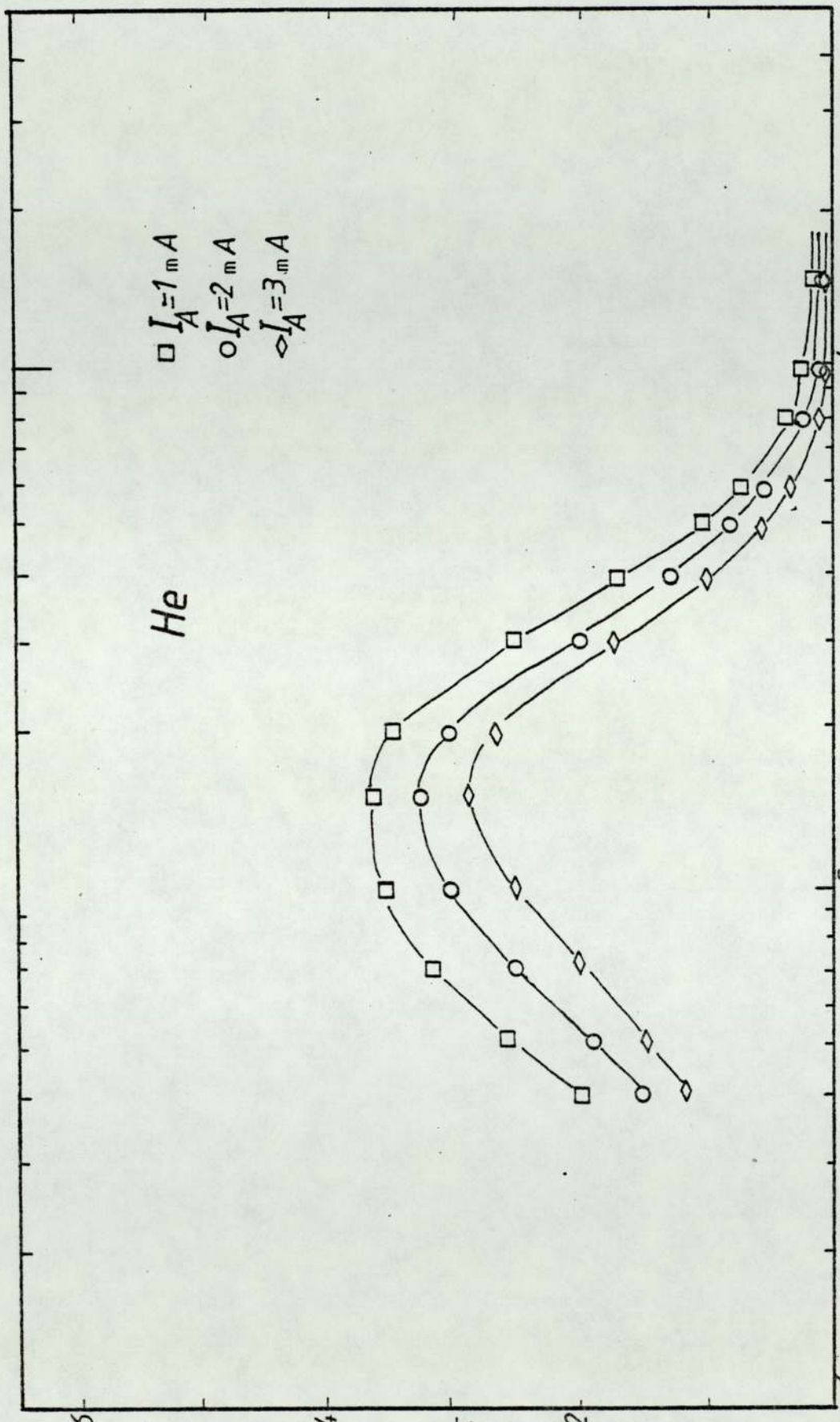

Figure 4.19 Variation of the power efficiency, η_p with the chamber pressure, p_c using helium

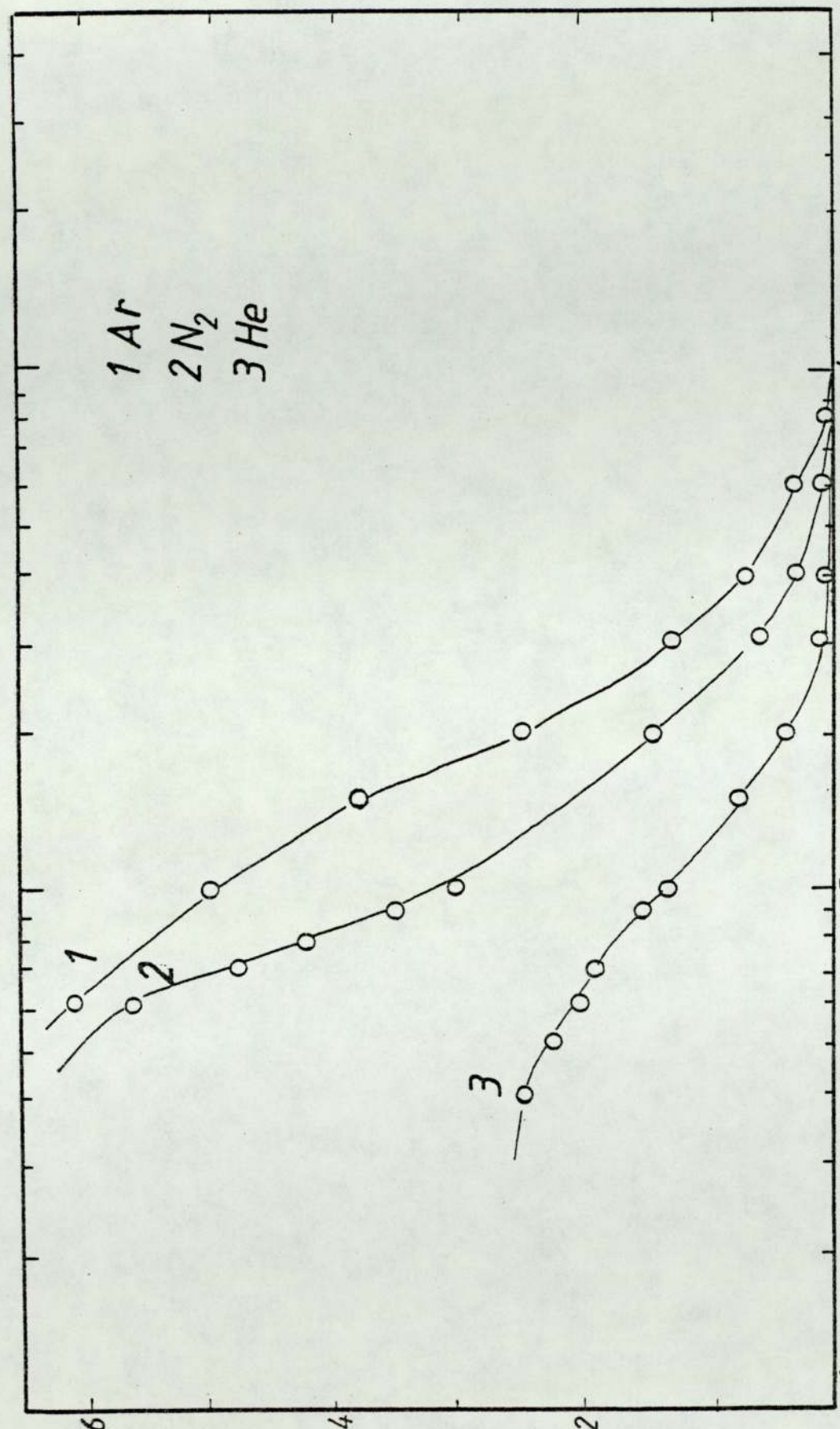

Figure 4.20 Variation of the gas efficiency, η_g with the chamber pressure, p_c using argon, nitrogen and helium

η_i and η_p at the same pressure.

Figure 4.20 shows the variation of η_g as a function of the chamber pressure for argon, nitrogen and helium at an anode current of 3 mA. It can be seen that η_g increases as the pressure decreases and continues to do so to the lowest operational pressure that has been used. The lower values of η_g for nitrogen and helium compared to argon at any given pressure follow the same trend as the corresponding values of η_i and η_p.

It is obvious that η_i and η_p for all gases must increase as the pressure increases from the lowest operating pressure because of the corresponding increase in the measured values of I_B. Similarly η_i and η_p will decrease at still higher pressures giving rise to a particular operating pressure at the optimum beam and power efficiency. On the other hand it was observed that when η_i and η_p increase as the pressure increases the gas efficiency decreases with increase in pressure. This can be accounted for by the fact that the ions decrease less than the decrease in the number of thermal neutrals when the pressure changes from 1.5×10^{-5} to 6×10^{-6} torr, resulting in a decrease in η_g.

CHAPTER 5

THE NUMBER, ORIGIN AND ENERGY OF ELECTRONS PRODUCED BY THE SOURCE

5.1 Introduction

In the earlier development work of the cylindrical ion source in this laboratory, it was observed that it is possible to ion etch insulating materials. It was believed that there must be some electrons in the ion beam which are able to neutralize the build up of the charge on the non-conducting surface. In a later paper, Ghander and Fitch[45] used a focusing system to improve the performance of this source for etching and they showed that the etching rate of a copper film could be increased when they used a focusing electrode which was about -3.5 kV, with respect to the cathode. However, it was found that under these conditions it was apparently not possible to etch an insulating material such as glass. They claimed that this was due to the suppression of electrons by the negative focusing electrode. Only when the focusing voltage was reduced to zero was it possible to observe any etching. However, their publication shows that the etched surface of glass is very smooth and the shielded region is by comparison very rough. It is quite possible that this rough appearance could be some contamination and the smooth "etched" surface had not been etched at all. The claim that the surface has been smoothed could only be justified if they had shown a micrograph of the glass surface prior to etching. This claim has not been confirmed in the present study after examination of a similar specimen of glass in the S.E.M. which was obviously so smooth that no surface structure could be observed at all and was certainly as smooth as that of the micrograph given

by Ghander and Fitch.

A more typical etched specimen of glass was shown by Navez[53] which shows rather characteristic grooves on the surface. However, it had become apparent as early as 1971 that insulating materials could be etched, for example, in the case of an acrilonitrile butadiene styrene (ABS) plastic specimen (Fitch and Rushton)[44]. It was suggested by Dhariwal and Fitch[49] in 1977 and Franks[54] in 1978 that there were possibly energetic neutrals present in the beam which were capable of etching the non-conducting material. Furthermore, Franks used a spherical ion source and proposed that these energetic neutrals were produced from the edge of the cathode aperture. It seems important to determine whether there are electrons in the beam or electrons surrounding the beam and to find out the origin and energy of these electrons, their location and significance in their contribution to the etching process and experiments performed with this aim in view are described in the rest of this Chapter.

5.2 Detection and measurement of the electrons

Any measurements of the electrons in the beam are dependent upon the ability to extract the electrons from the beam and two possible methods were considered, namely, a magnetic and electrostatic system.

5.2.1 The magnetic analyzer

Before the analysis using a magnetic system was undertaken it was important to study the influence of the magnetic fields upon the performance of the source. Rushton et al[33] have studied the effect of the magnetic field on the cylindrical source and they found that the major effect upon the performance of the oscillator was when the magnetic field was along the Z axis which is along the axis of the cylinder.

Using the same analysis as Rushton[55] for the spherical source we see that the forces, F, on the electron due to a magnetic field, B, in the direction x, y, and z for velocities V_x, V_y and V_z are given by the following equations:

$$F_z = e(B_x \Lambda V_y)$$
$$F_y = e(B_x \Lambda V_z)$$
$$F_x = e(B_y \Lambda V_z)$$
$$F_z' = e(B_y \Lambda V_x)$$
$$F_y' = e(B_z \Lambda V_x)$$
$$F_x' = e(B_z \Lambda V_y)$$

In the case of the spherical source $V_y >> V_x$ and V_z, thus the greatest values of F will be F_z and F_x'. Hence we would expect the greatest perturbation of the source to be due to any field directed in the (x-z) plane. This was demonstrated by noting the change in anode current as a function of magnetic field using a small horseshoe permanent magnet calibrated with a Hall probe and placed at various distances from the centre of the source. Figure (5.1) shows the variation of B, as a function of distance from the magnet and figure 5.2, shows the corresponding variation of anode current I_A with B for V_A = 5 kV and $p_c = 1.5 \times 10^{-5}$ Torr.

It is interesting to note at about 0.1 mT there is a maximum value of I_A as found by Rushton for the cylindrical source and it was believed to be an optimum condition when the applied magnetic field nearly cancels the residual earth's field. In order to deflect the electron from the beam it was necessary to construct a small electromagnet such that its main component of the field is at right angles to the beam. Of course, this situation produces the strongest stray field in the most undesirable direction, that is in the x-z plane of the source. The electromagnet was constructed from a coil

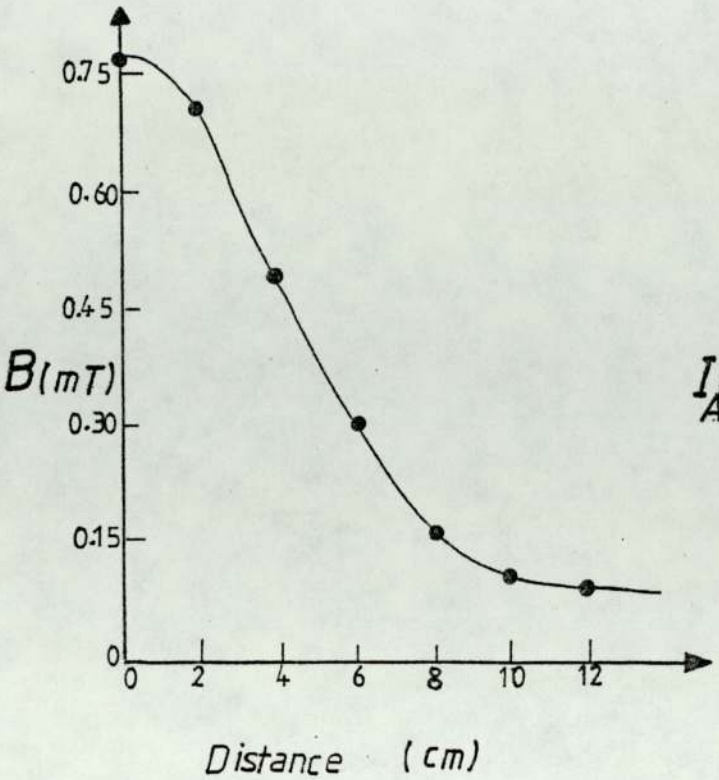

Figure 5.1 The variation of magnetic field with distance from polepiece.

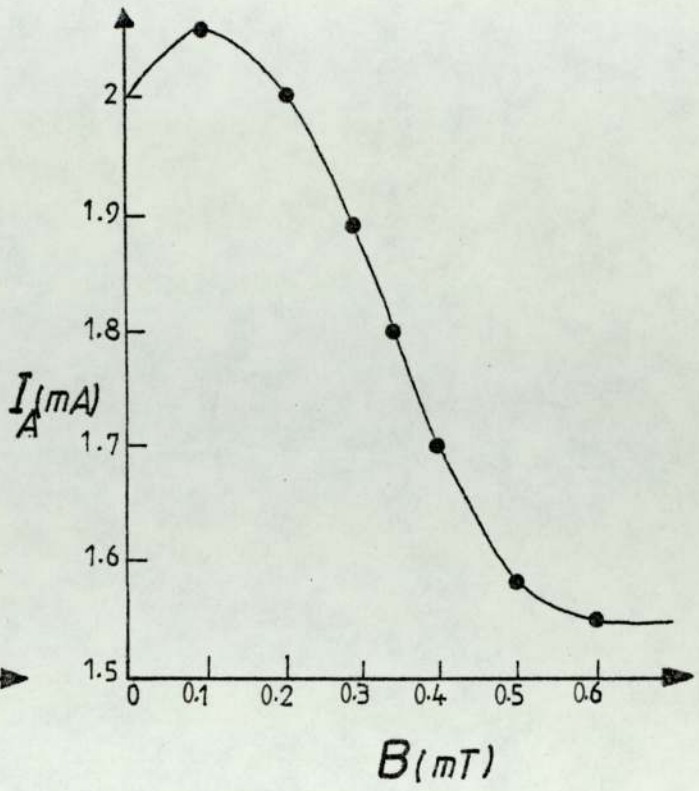

Figure 5.2 The variation of anode current with magnetic field

by winding 100 turns per centimetre of 0.75 mm diameter copper wire and the coil was fitted on to soft iron and the calibration of magnet is shown in figure 5.3. A small plate was positioned at an angle to the beam in order to collect any deflected electrons. It was assumed that the electron would have an energy less than 100 eV and in order to deflect the electron through a suitable radius of about 2 cm and using the equation

$$B^2 = \frac{2m\ V}{r^2 e}$$

this gives a value of B to be about 2.2 mT. Of course this magnetic field of 2.2 mT would have a negligible effect on the ions on account of their heavier mass and greater energy.

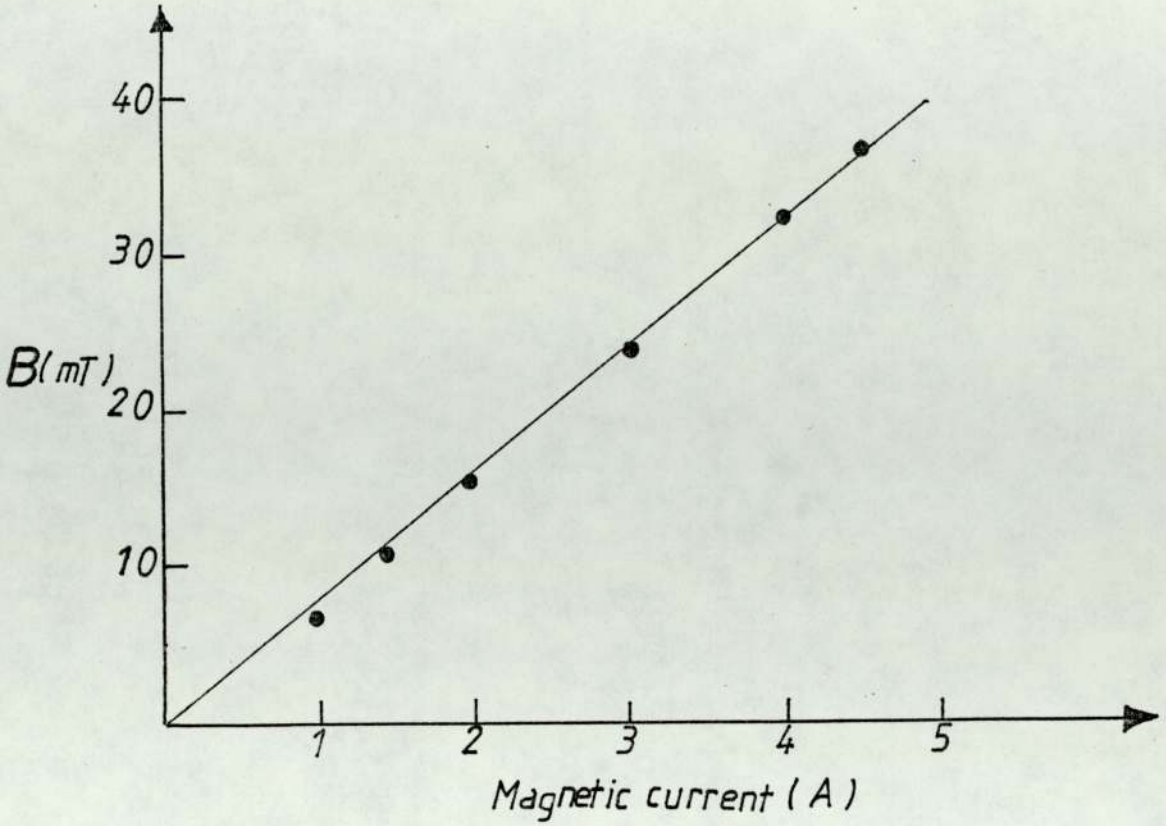

Figure 5.3 Calibration curve of the electromagnet.

The complete arrangement is shown schematically in figure 5.4. Using this arrangement with a field of about 2.2 mT, this produced a stray field about in x-z plane of a few mT which caused a deterioration in performance of the source. This was satisfactorily overcome by introducing a μ-metal shield as shown in figure 5.4, containing a small aperture for the ion beam and this reduced the stray field to a negligible value.

Attempts were made to detect an electron current on the collector for various magnetic fields and at the same time to note any change occurring in the current in the Faraday cup. One such example is shown in figure 5.5 which shows that over the range of applied magnetic fields from zero to 20 mT that the Faraday cup current remains constant and only a very small and constant electron current of about 0.4 μA was observed. It was also found that this situation remained virtually the same for different source conditions and various positions and orientations of the electron

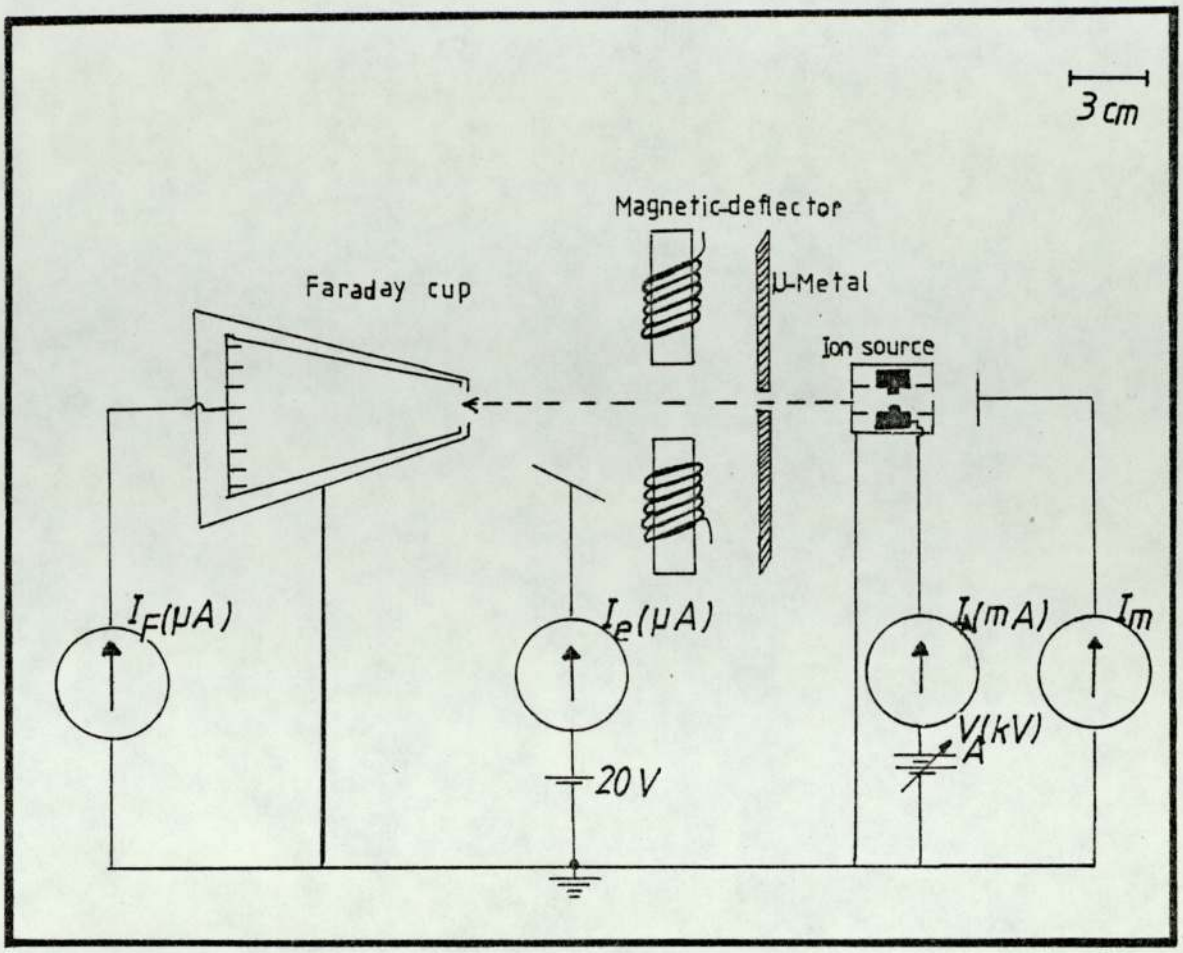

Figure 5.4 Schematic diagram of the analyzer showing the source, μ-metal shield, magnet and ion and electron collectors.

collector plate and including the addition of a 20 V on the collector plate. These experiments show that had there been electrons emitted in the general direction of the ion beam such that they were able to penetrate the aperture in the shield plate, then it may be expected that a current would be observed on the collector plate. If, on the other hand, it can be assumed that this was not the case and there were secondary electrons produced from the source aperture with no fixed orientation then this could explain why it was not possible to observe any significant electron current to the plate. In this case, the magnetic deflector would only deflect a

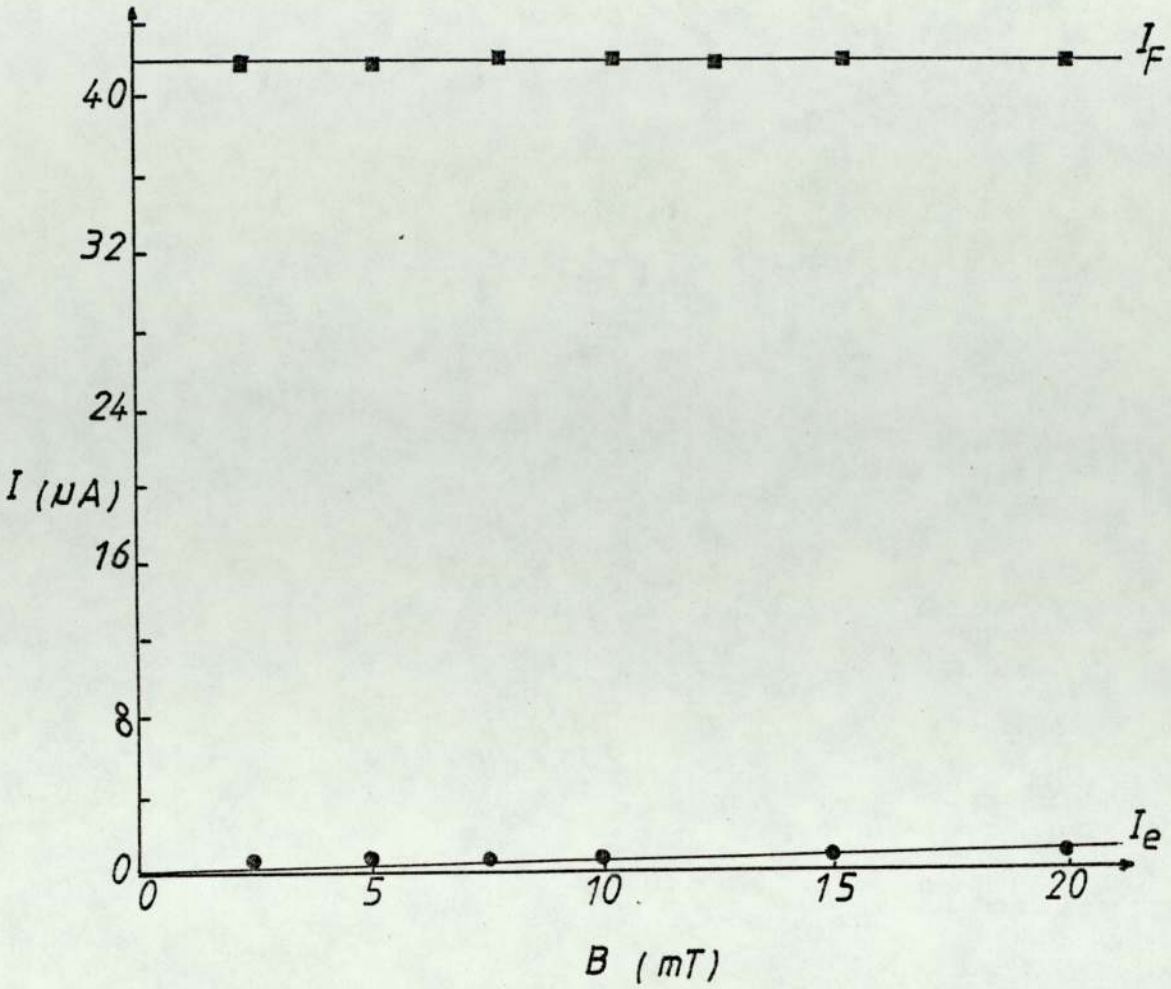

Figure 5.5 Ion beam current and electron current as a function of magnetic field.

small fraction of these electrons in the required direction to the electron collector plate. Thus an alternative system using an electrostatic deflector was likely to be more suitable.

5.2.2 The electrostatic analyzer

For the measurement of the electrons, it was required to design a device capable of separating and detecting them. Preliminary experiments were attempted which simply depended on a positive electrode placed close to the source aperture which was able to collect the electrons and allow the beam to pass through to the collector. This electrode was made from a small plate with a variable diameter aperture and even with rings of different sizes, it was found that this electrode could intercept the beam and

collect some low energy ions. In order to overcome this effect, the apertures were enlarged and in this case, the electrode also acted as a focusing device which was able to focus the low energy ions and at the same time accelerate the electrons passing through them. Therefore this technique was not adequate to provide the required information and an electrostatic analyzer was ultimately selected for this measurement.

The electrostatic analyzer is shown schematically in figure 5.6 and consists essentially of the two parallel plates P_1 and P_2, P_1 being connected to a positive voltage and thus acting as a collector of negative charge and P_2 was earthed and thus negative with respect to P_1 to collect any positive charge. The same Faraday cup as used in the previous measurements was used to measure the ion beam. The positive potential to P_1 was variable between 0 and 5 kV and the currents I_e and I_i to P_1 and P_2 respectively were measured with two digital meters.

In order to investigate the ability of this analyzer to deflect the negative and positive charges, the two parallel plates were coated with a thin layer of fluorescent material which was prepared in this laboratory by mixing solutions of barium nitrate and potassium silicate at a certain concentration before mixing with a suitable quantity of phosphor. With the source operated at V_A = 5 kV and I_A = 2 mA, a small illuminated spot appeared on the positive plate P_1 when the deflecting voltage was about 100 volts while no spot appeared on the other plate. However, when the positive voltage was increased to about 3 kV, then a large illuminated spot was clearly seen on P_2 and in this case the small spot on P_1 moved back along the length of the plate. This qualitative analysis showed that the analyzer was adequate to separate the negative and positive charges. In order to confirm

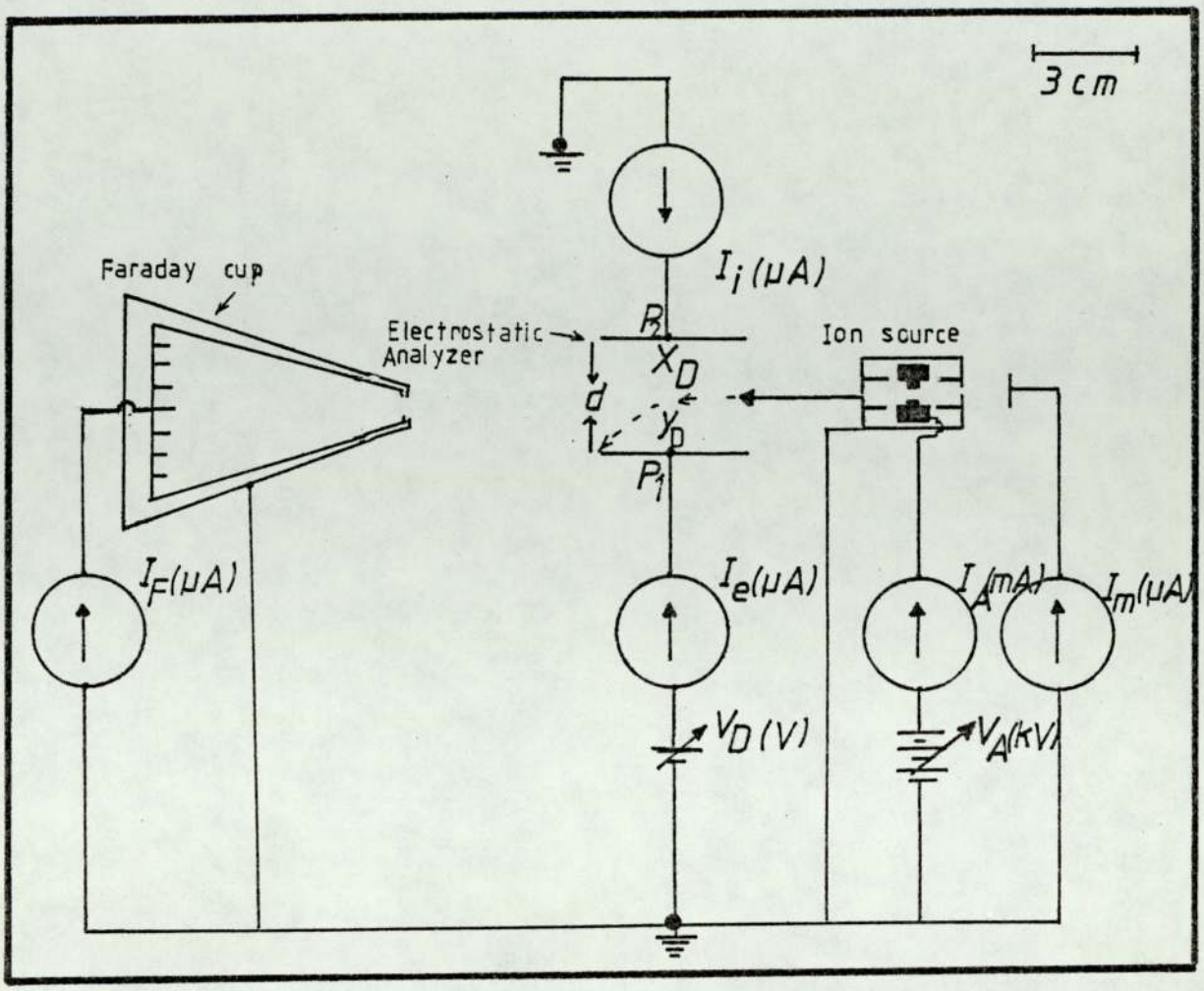

Figure 5.6. The complete arrangement of the electrostatic analyzer.

this, it was decided to calculate the deflection, y_D, of the ions and electrons using the equation given by Klemperer[56] for the deflection of a charged particle in an electrostatic field where:

$$y_D = \frac{X_D^2}{2d} \cdot \frac{V_D}{V_{ch}}$$

and X_D is the length of the deflector, d is the distance between two parallel plates, V_D is the deflecting voltage and V_{ch} is the accelerating voltage of the charged particle. In the present analyzer X_D was 3.5 cm and d selected to be 3 cm to avoid any interception of the undeflected beam. The two plates P_1 and P_2 were placed 2 cm away from the source to prevent electrical breakdown

between them and the source body. Assuming the field is homogeneous and neglecting any end effects, with V_{ch} = 140V then y_D = 1.5 cm. when V_D is about 100 volts. Of course this voltage has negligible effect on the ions with energies of about 4 keV. If V_D is increased for example to 3kV, then the ions are deflected about 1.5 cm. An experiment was then performed to demonstrate the deflection of the ions and electrons with the source operated at V_A = 5 kV and I_A = 2 mA. Figure 5.7 shows the three currents to the Faraday cup, I_F, and to the plates I_e and I_i. It was shown that the I_e increased rapidly with increasing V_D and saturated at a deflecting voltage of about 200 volts before V_D reached 2 kV when it again saturated at V_D = 3 kV. The figure 5.7 also shows that the I_i was small until V_D = 2 kV then increased to reach a saturated current at 3 kV.

The Faraday cup current I_F remained nearly constant for V_D up to 1 kV and decreased very rapidly to reach a small value at about 3 kV. Thus figure 5.7 shows that at a low deflecting voltage, the electrons were deflected whereas the ions were not and this explains why I_F remained constant at this voltage. When the deflecting voltage increased from about 2 kV to 3 kV, there was an increase in I_i due to the collection of the ions and production of secondary electrons which were attracted to the positive potential of the plate P_1 and resulted in an increase in I_e. At the same time I_F decreased and reached a residual value of I_F of less than 1 μA. This residual current was probably due to the escape of secondary electrons produced by energetic neutral particles which will be discussed in the next Chapter.

The results show that if V_D is operated at less than about 200 volts then I_e is only due to the collection of electrons from the beam as the other secondary effects can be neglected. Figure 5.8

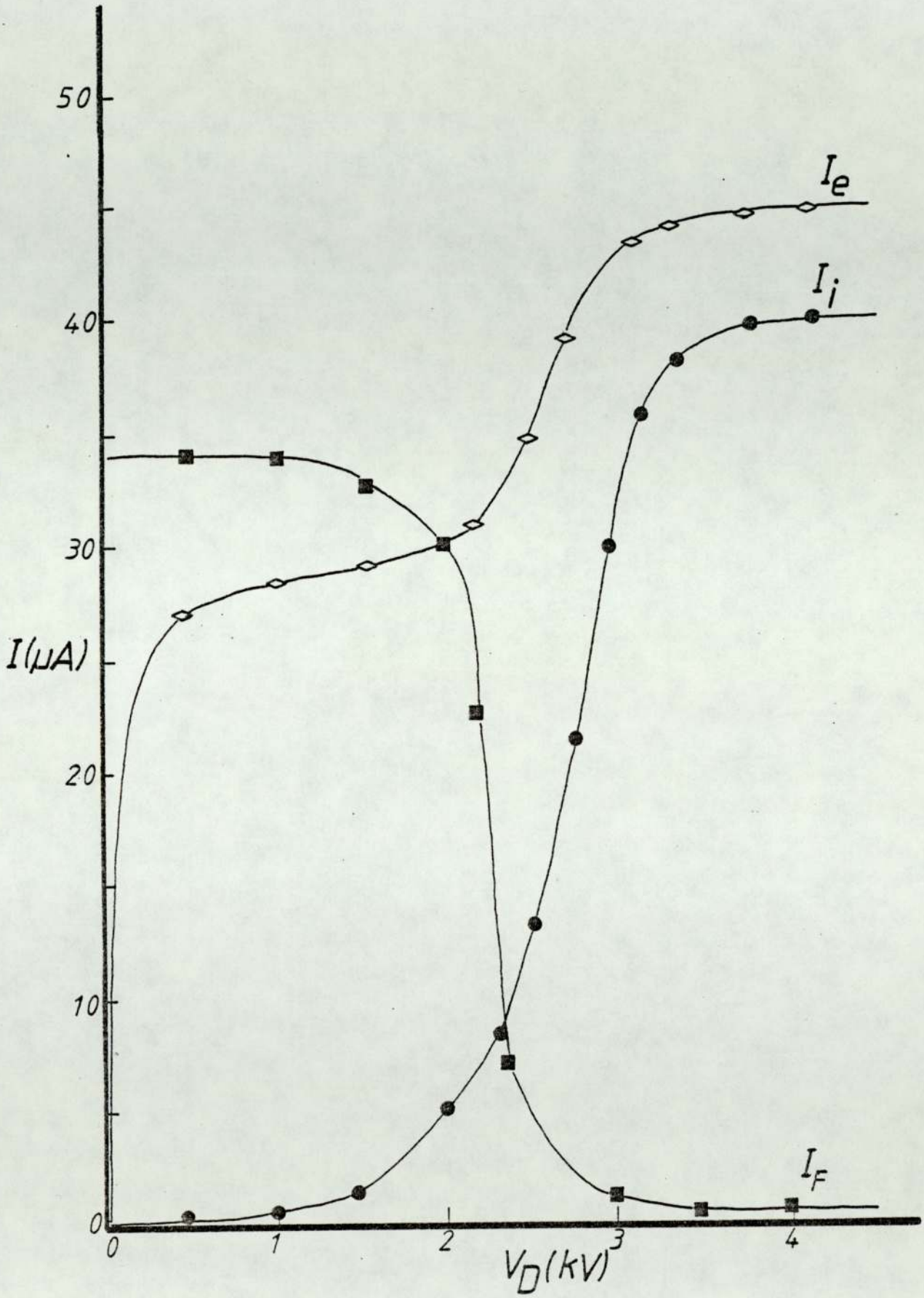

Figure 5.7 Variation of electron current, I_e, ion current, I_i and Faraday current, I_F as a function of deflecting voltage, V_D.

shows I_e and I_F as a function of V_D up to 200 volts for the source operating at V_A = 5 kV and I_A = 2 mA. It can be seen that I_e increased by only a very small amount up to 50 volt and then increases to a saturated value of I_e about 20 μA when V_D = 100 volt, whereas I_F is constant at about 32 μA.

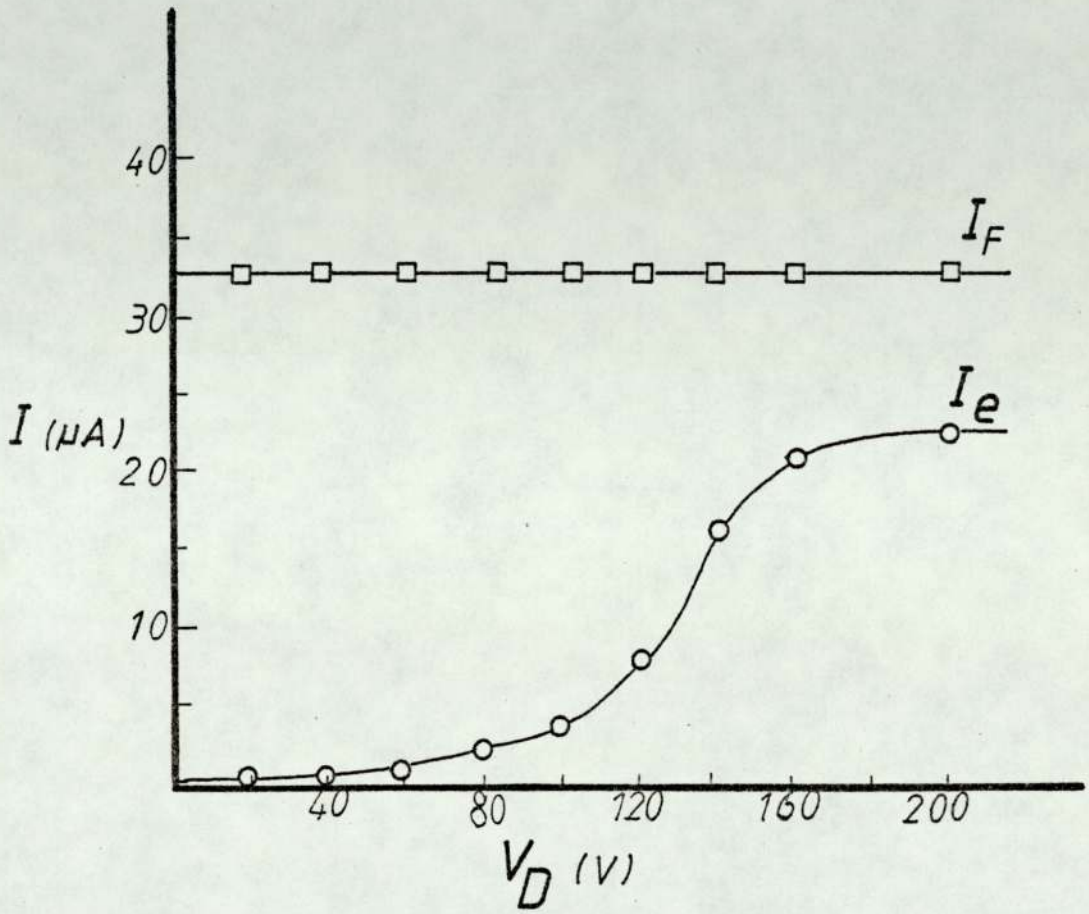

Figure 5.8 Variation of I_e and I_F as a function of V_D.

Figure 5.9 shows the variation of I_e with V_D for I_A = 2 mA for different pressures and thus different beam currents. These curves show that I_e varies with I_F and Table 5.1 shows that the ratio $\frac{I_F}{I_e}$ is approximately constant. It also shows that I_e saturated at about the same deflecting voltage for each case implying that the electron energy is approximately constant.

This analysis clearly shows that, a significant electron current can be extracted from the beam at low voltage, thus implying that they are low energy electrons. Furthermore, it is significant

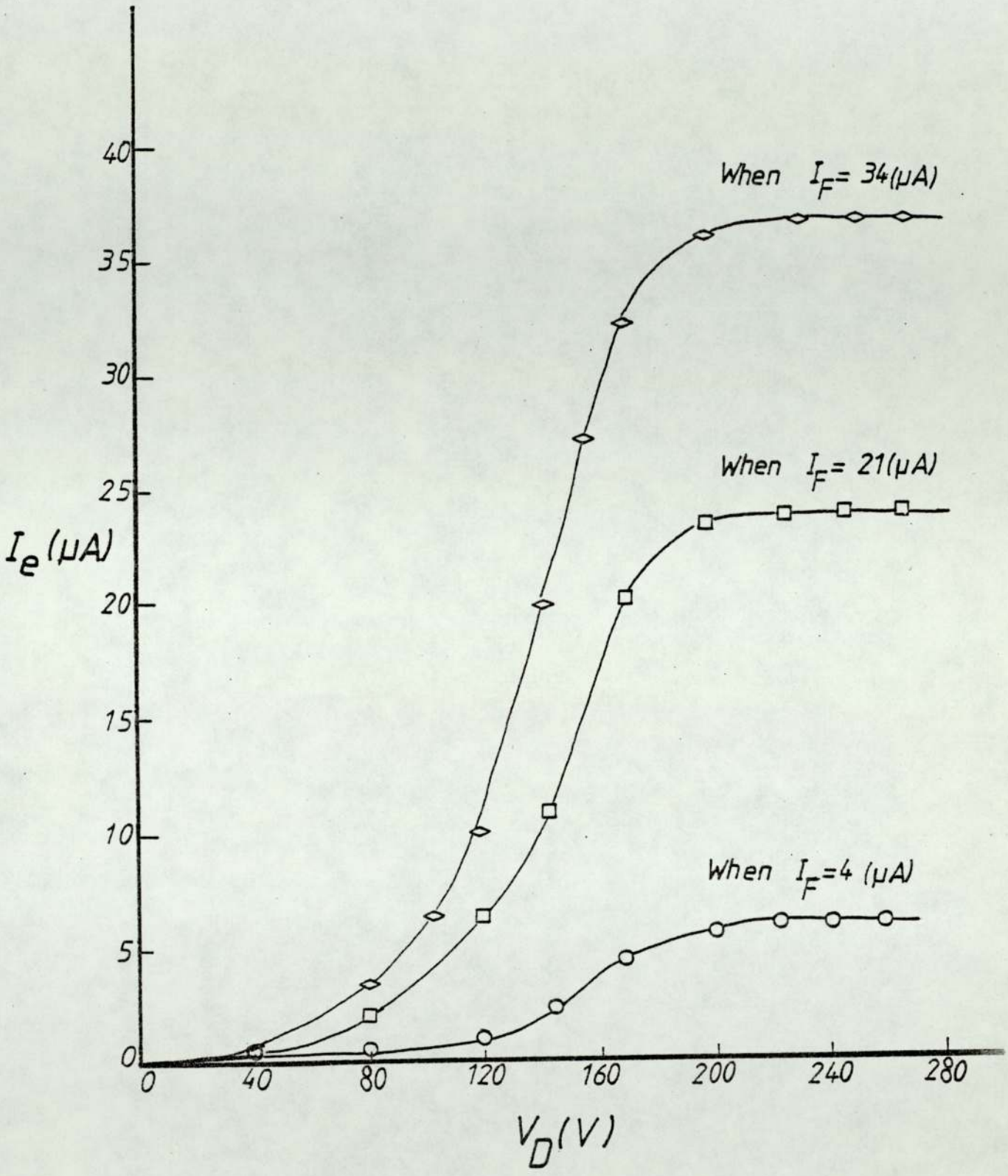

Figure 5.9 . Variation of electron current, I_e as a function of deflecting voltage, V_D for different chamber pressure.

Table 5.1 Different conditions of source operation and the ratio of $\frac{I_F}{I_e}$

p_c torr	V_A kV	I_F (μA)	I_e (μA)	$\frac{I_F}{I_e}$
2×10^{-5}	7	34	37	0.85
6×10^{-5}	5	21	24	0.80
1.2×10^{-5}	3	4	6	0.60

to note that when these electrons are extracted, there is no noticeable change in the beam current as measured by the Faraday cup. Thus it seems that these electrons are in a region surrounding the beam and unlikely to contribute to any effect when using this source for etching non-conducting material. In the following sections this will be clearly demonstrated when accounts are given of the attempts to determine the origin and energy of these electrons.

5.3 Origin of the electrons

Following the work described in the previous section, it was thought likely that these electrons were being produced by secondary electron emission from ion bombardment of the edge of the cathode aperture. Experiments were performed to demonstrate this by taking advantage of the variation of secondary electron yield, γ, with different materials. In order to achieve this it is necessary to maintain I_F and V_A constant to ensure that the same number of ions of the same energy are striking the cathode aperture. The source is normally used with aluminium cathodes because of the high

secondary yield and this will be compared with stainless steel which has a lower secondary yield.

The electron current, I_e, as a function of the deflecting voltage V_D, is shown in figure 5.10a using argon gas and figure 5.10b using helium gas with the plates 1 cm from the source aperture. All the measurements referring to the figures 5.10a and b are taken with V_A = 5 kV and I_F = 15 μA. These results clearly show that I_e is higher for aluminium than stainless steel but for both materials I_e is less for helium than with argon due to the lower secondary yield for helium.

Figure 5.11 shows the same characteristics using argon but with plates and at varying distances from the source aperture. These curves show that the collection efficiency of electrons is greater when the source is closer to the plates and showing that these electrons have been emitted in random directions. These experiments clearly demonstrated that these low energy electrons originate from the cathode aperture.

5.4 Measurement of the electron energy

If the analysis of the previous section is correct then these electrons should be of low energy typically in the range of 0.1 to 20 eV. Thus an attempt was made to measure the energy of the electrons taking into account not only the low energy but the fact that these were emitted from the cathode aperture in random direction. For this particular measurement an analyzer was constructed and tested with an electron beam of know energy before being applied to this particular problem.

5.4.1 Design and testing of the electron analyzer

The retarding field analyzer is shown schematically in figure 5.12 and consists essentially of two parallel grids g_1 and g_2 of

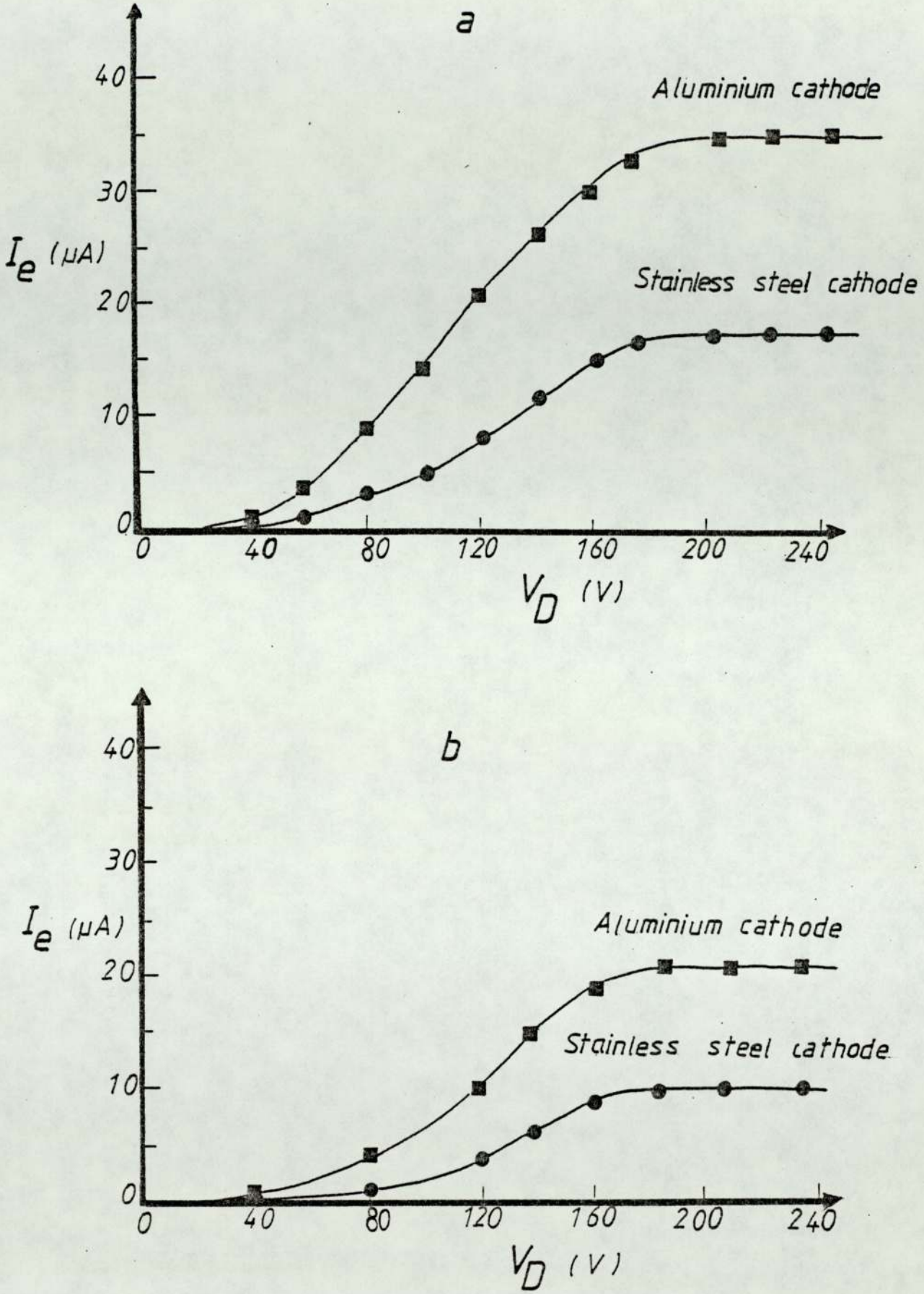

Figure 5.10 Variation of electron current, I_e with deflecting voltage V_D for aluminium and stainless steel cathodes using (a) argon and (b) helium.

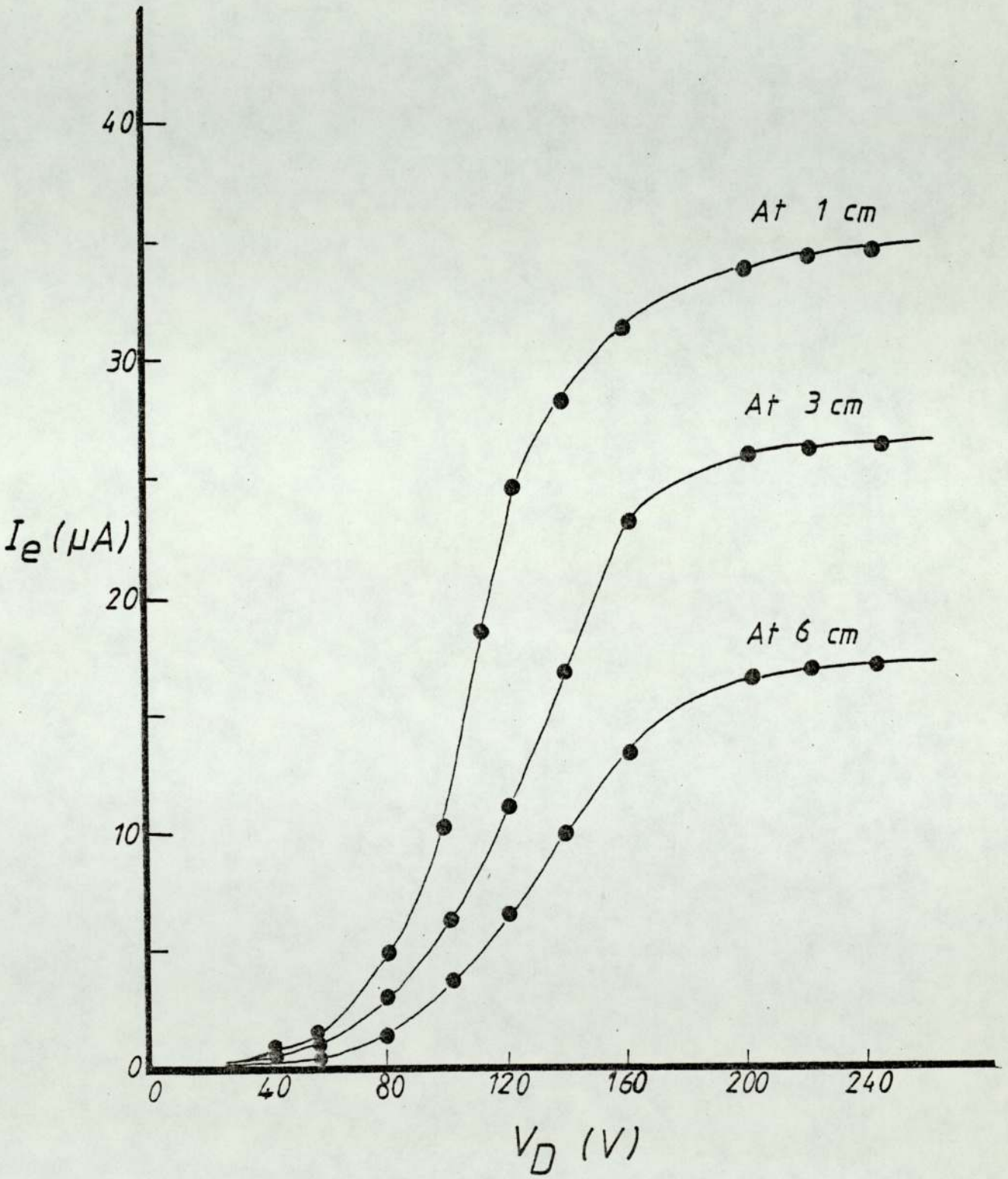

Figure 5.11 Variation of electron current, I_e with deflecting voltage V_D, for different distances from the source aperture using argon.

rectangular shape (38x38 mm) and containing 35 tungsten wires of diameter 0.35 mm. These wires were spaced 1 mm apart and thus the grids have a transparency of about 60%, g_1 being used as the retarding grid and g_2 as the accelerating grid. A small nickel plate, C, was used to record the electron current, I_e. In these measurements the two power supplies used for the retarding voltage V_1 and the accelerating voltage V_2 could provide up to 200 volts positive with respect to earth.

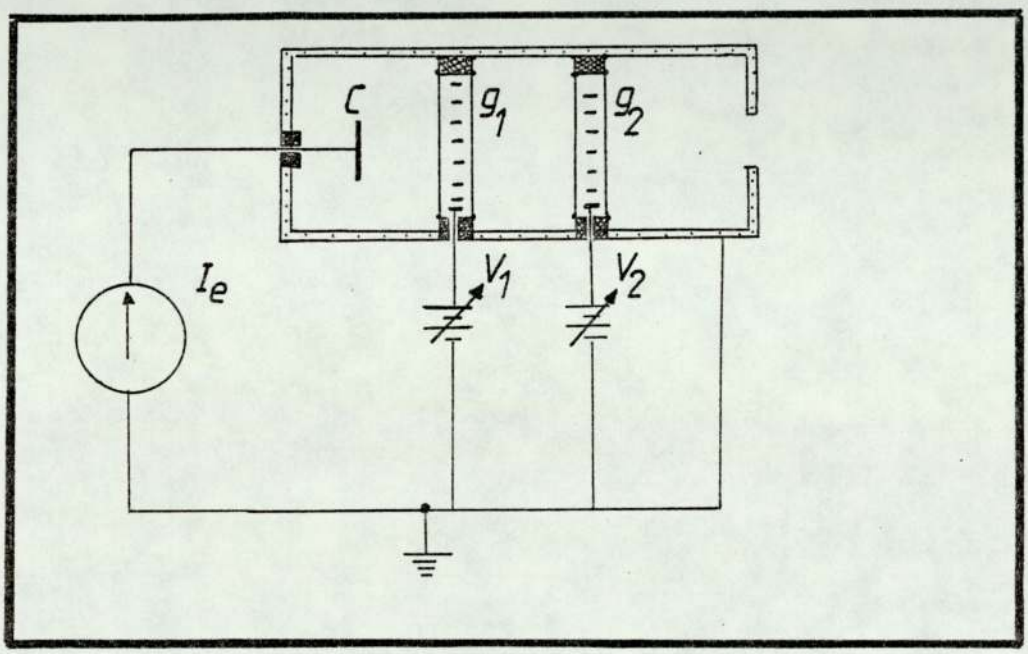

Figure 5.12 Schematic diagram of the retarding field analyzer.

The grids and the collector were fixed inside but isolated from an earthed small box which acts as a screen and minimises the collection of the stray electrons present in the vacuum chamber. Assuming the electrons start with zero energy and enter into the electrostatic field produced by V_2 then they gain a maximum kinetic energy $E = eV_2$ and the electron can be repelled by V_1, thus the derivative of I_e with respect to V_1, $\frac{\partial I_e}{\partial V_1}$ gives the energy distribution of the electrons.

In this work and before the analysis was undertaken for measuring the energy distribution of the electrons emitted from the cathode aperture, it was important to examine the efficiency of this analyzer, this could be confirmed by measuring the energy distribution of thermionically emitted electrons accelerated through a known potential. Figure 5.13 shows the complete arrangement of the filament and the analyzer. The thermionic electrons were

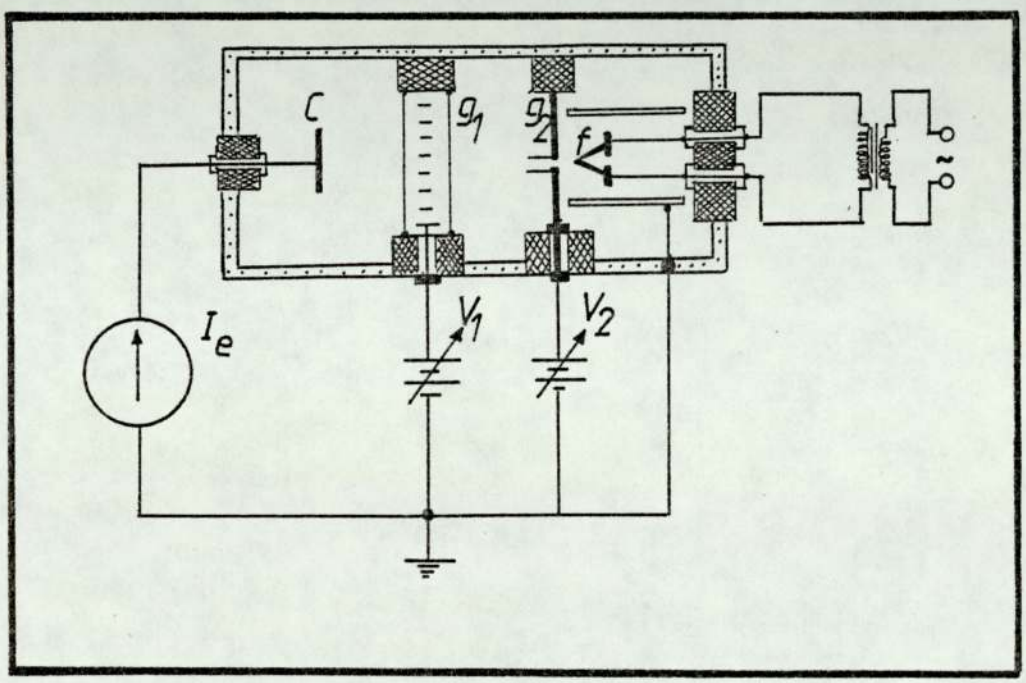

Figure 5.13 Schematic diagram of the complete arrangement of the filament and the analyzer.

emitted from a hair pin tungsten filament which was surrounded by a small cylinder at earth potential to collimate the electrons. The grid, g_2, was in fact made as a plate with a hole 3 mm in diameter to allow the electrons to enter into the retarding field. An improvement was made to the collimation of the electron by fitting a 2 mm length of tube to the hole in g_2. The complete arrangement was placed into the vacuum chamber at pressure about 10^{-5} Torr and the filament was heated by an A.C. supply via an isolating

transformer. Thus in this situation if the electrons transmitted through g_2 are assumed to be in a direction normal to the plane of g_1, then all the electrons will pass through g_2 with energy e V_2 and when V_1 is equal to V_2 the retarding field will be zero and I_e will be maximum, whereas with $V_1 = 0$, the retarding field would be equal and opposite to the accelerating field and I_e will be zero as shown in figure 5.14a. Thus in this situation the true retarding voltage, $V_R = V_1 - V_2$.

In practice it is obvious that the collimation will be far from

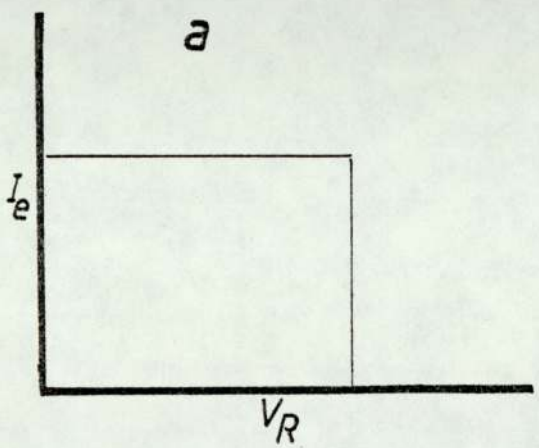

Figure 5.14a Ideal $I_B \rightarrow V_R$ characteristics

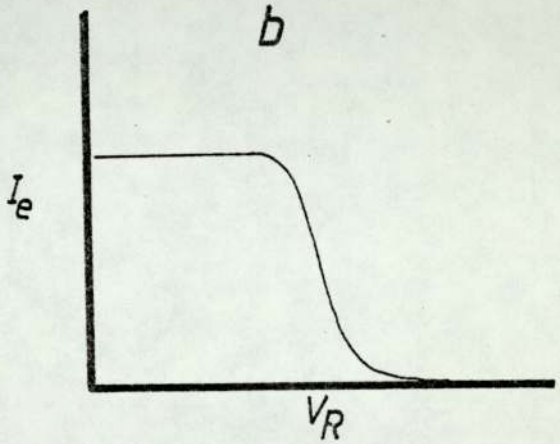

Figure 5.14b Practical $I_B \rightarrow V_R$ characteristics

perfect and thus I_e will reduce before V_1 has become zero and V_R maximum as shown in the figure 5.14b.

Figure 5.15a shows the variation of I_e with V_R and figure 5.15b shows the corresponding values of $\frac{\partial I_e}{\partial V_R}$ which is the energy distribution N(E) against E. It can be seen that I_e reached a maximum value at $V_1 = 90$ V and I_e remains constant until about $V_1 = 50$ V then I_e decreases rapidly and reaches zero at $V_1 = 0$. This shows that the electrons have an energy of about 70 eV with a spread of $\pm$ 10 volt which could be expected with this simple design of the analyzer.

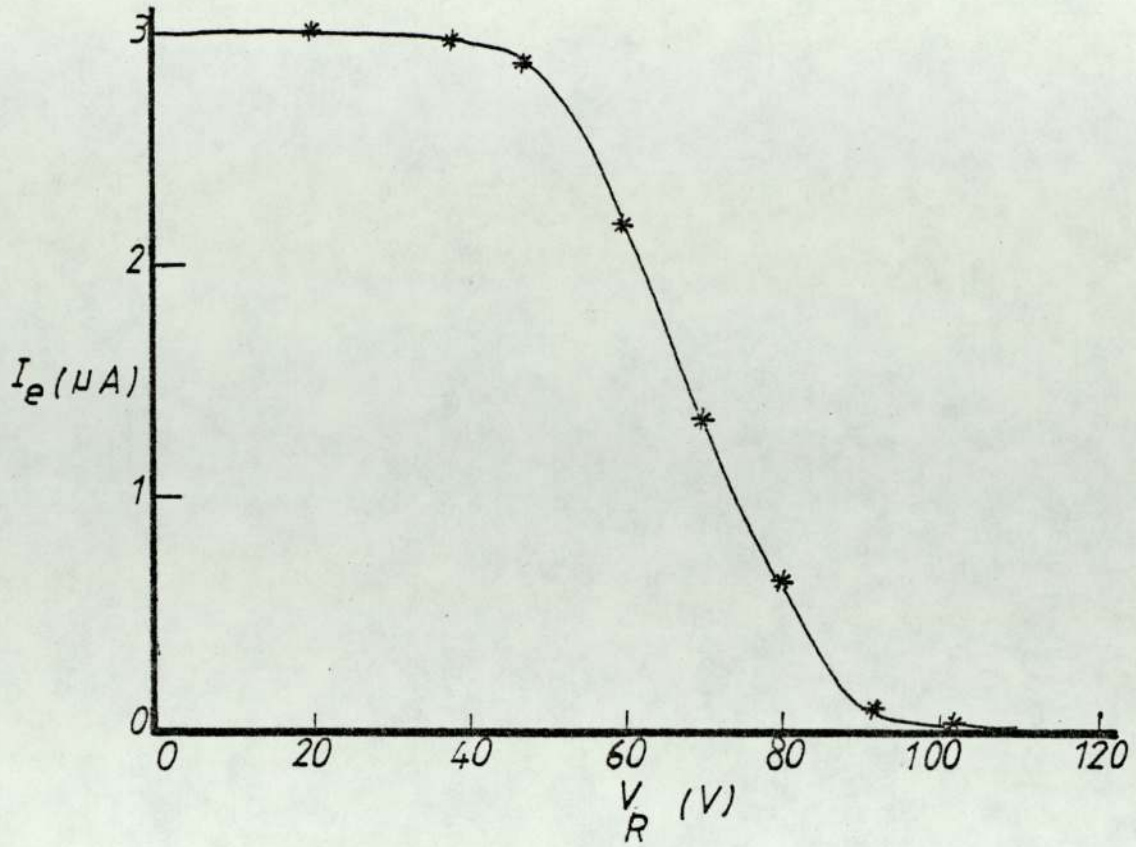

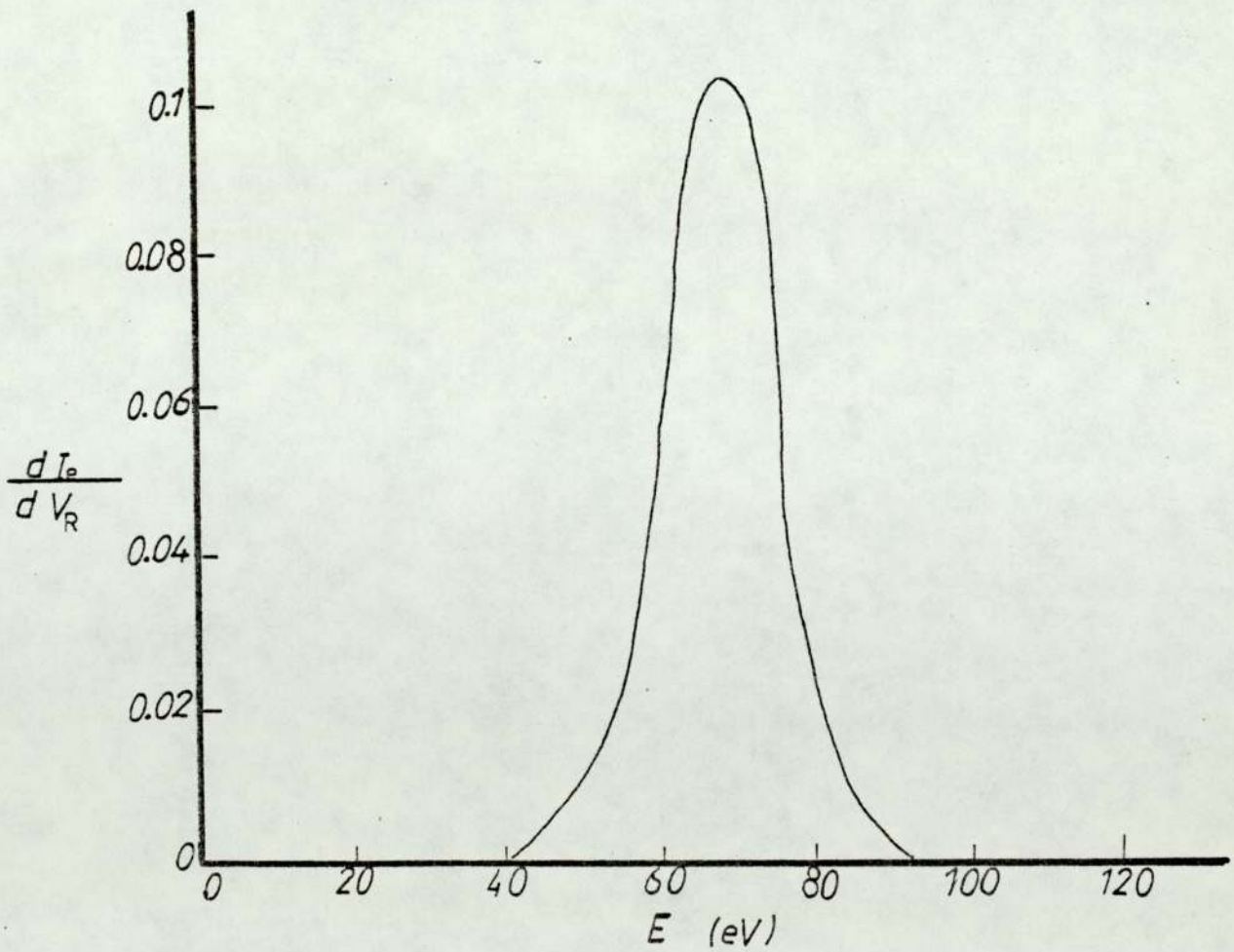

Figure 5.15 (a) Collector current, I_e against retarding voltage, V_R,
(b) energy spectrum for electron beam of known energy.

5.4.2 Energy distribution of the electrons

Figure 5.16 shows the schematic diagram of the analyzer and the ion source and because the electrons are emitted from the cathode in random direction and also originate from the aperture, the analyzer was placed at an inclination to the ion beam to increase the

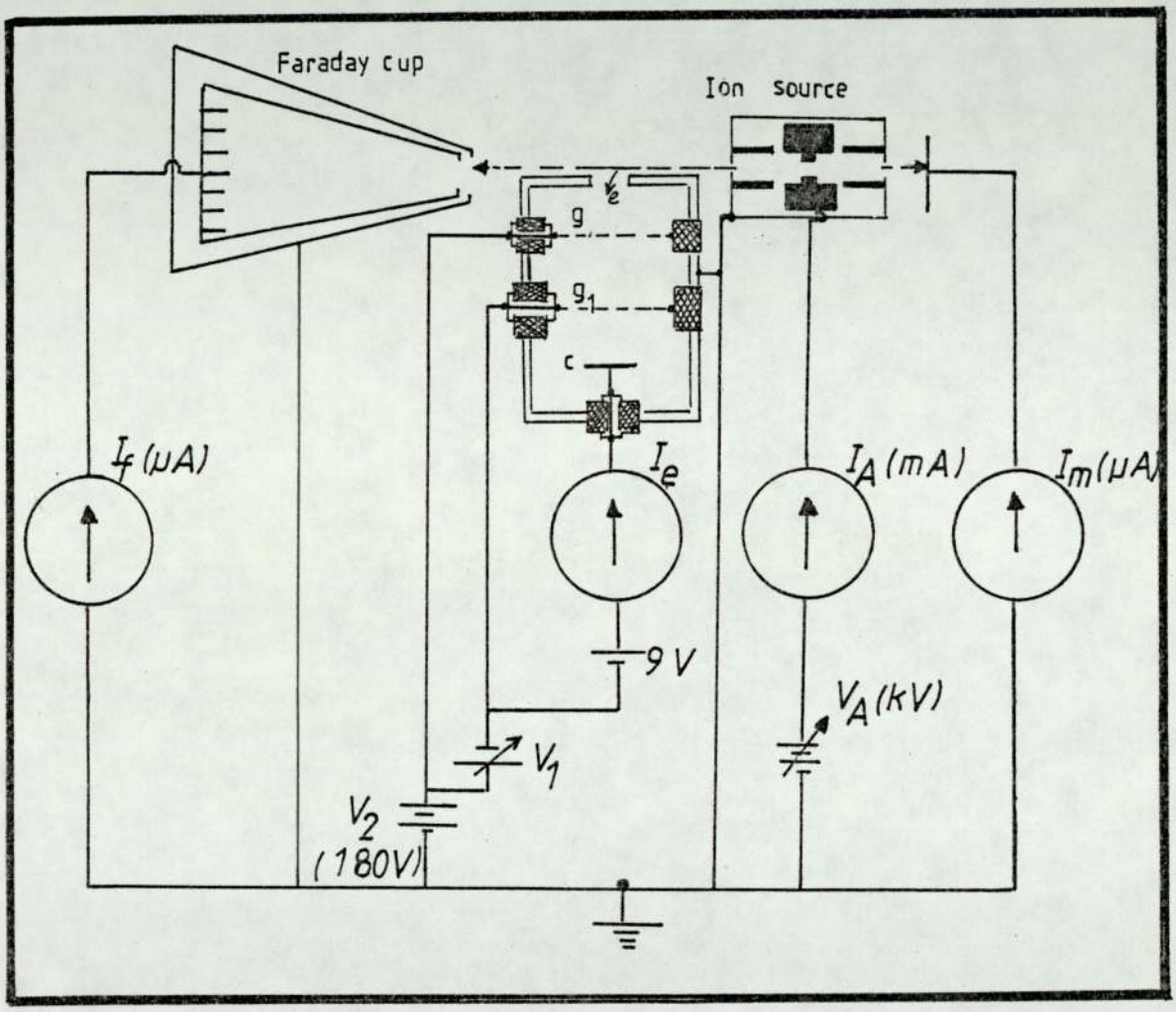

Figure 5.16 Schematic diagram of the electron energy analyzer.

possibility of the electrons entering the aperture of the analyzer.

In order to make $V_R = V_1$, then the figure 5.16 shows that V_1 was made variable with respect to V_2 and not earthed as in the previous case. Similarly it can be seen from the figure the electron collector was held at a small positive potential of 9 V with

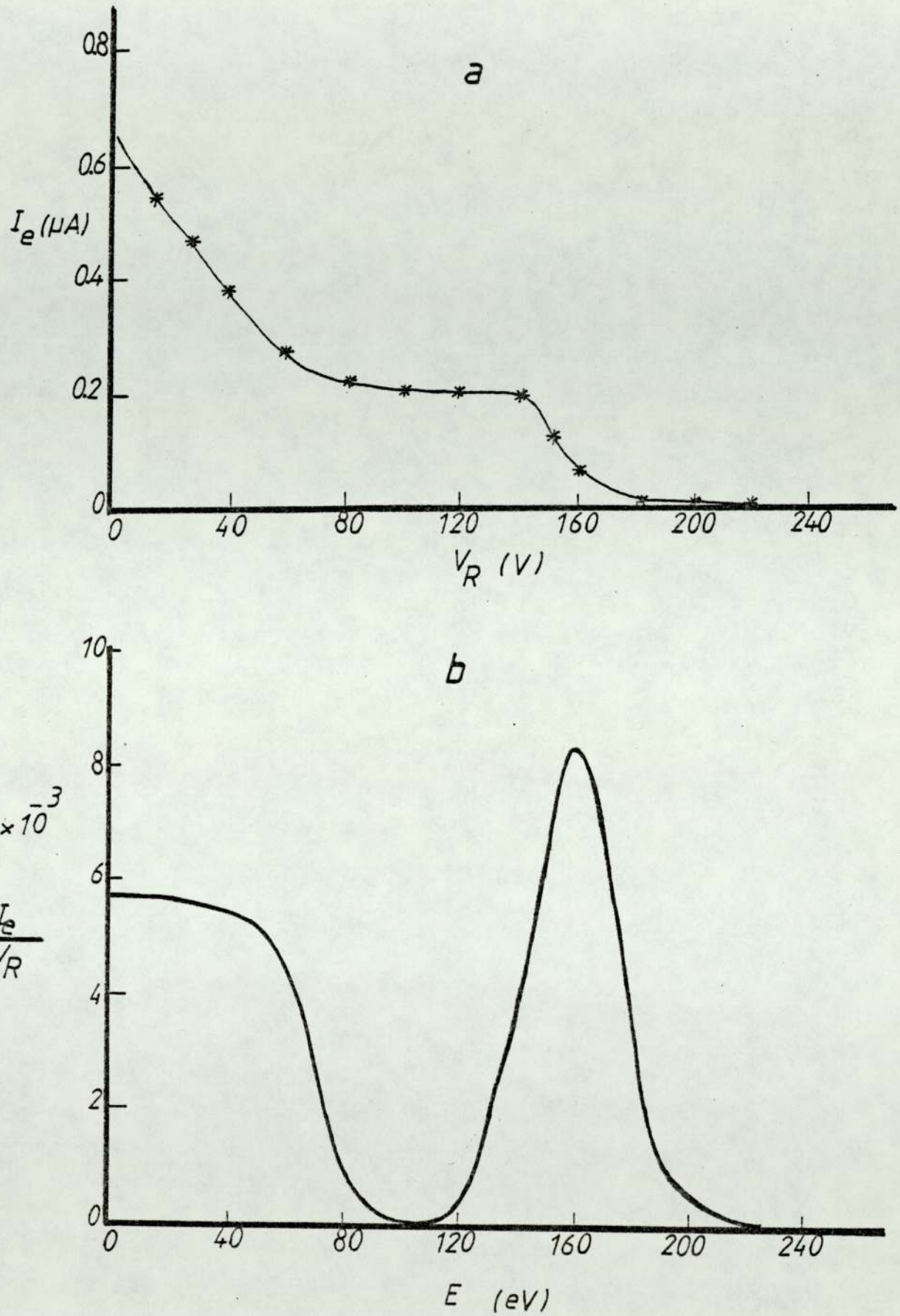

Figure 5.17 (a) The characteristics of $I_e \longrightarrow V_R$

(b) The energy spectrum using argon

respect to V_1 to reduce the emission of secondary electrons. In this arrangement V_2 was selected to be +180 volts in order to attract the maximum number of electrons from the aperture. Now when $V_1 = 0$ then g_1 and g_2 are at the same potential then $V_R = 0$ and I_e reaches maximum whereas $V_1 = -180V$ then $V_R = -180$ V and I_e reached zero if the electrons are emitted with negligible small energy.

Figure 5.17a shows the variation of I_e with V_R which is negative with respect to V_2. It can be seen that there is a slow decrease in I_e as V_R increases from zero to 140 V after which I_e decreases rapidly to zero when V_R is about 180 volts. Figure 5.17b shows the corresponding energy spectrum. The most notable feature is a high energy peak at about 160 volts with a spread of $\pm$20 V and a low energy background which is probably due to the collection of the stray low energy electrons.

However, there is no evidence for the existence of any electrons of energy greater than that due to the original accelerating voltage of 180V. These results support the previous assumption that the electrons collected by the plates are low energy secondary electrons produced at the cathode aperture. Of course, if there were any electrons trapped in the emerging ion beam then it would not be possible to detect these in this kind of analyzer but there was no evidence of this when the magnetic analyzer was used. Thus it has been shown that these low energy electrons do not contribute to the total beam current as measured by the Faraday cup and therefore do not have any significant important in the application of this source.

It will be shown in the next Chapter that the successful application of this source to insulating materials can be explained much better by the formation of energetic neutrals in the beam.

CHAPTER 6

THE NUMBER, DISTRIBUTION AND ENERGY OF THE FAST NEUTRALS PRODUCED BY THE SOURCE

6.1 Introduction

It has already been discussed in Chapter 2 that this source can be used for etching non-conducting materials as well as conductors. This was believed to be due to the presence of the fast neutrals in the beam. Of course in this respect the term "fast neutrals" is meant to imply that the particle will have energy sufficient to cause sputtering and will be at least in excess of 100 eV and more likely several keV. Thus in this Chapter all discussions refer to fast neutrals and not the slow thermal neutrals discussed previously in Chapter 4 when the gas efficiency of the source was being calculated.

It should be clear from Chapter 2 that the only studies outside this laboratory relating to the production of the fast neutrals by this source have been done by Franks[54] but he gave no information in this publication regarding how these results were obtained. Thus it was considered essential that to obtain an overall analysis of the behaviour of the source it was necessary to determine the numbers and the energy of the fast neutrals produced for various gases. In section 2, experiments will be described concerning the number of fast neutrals produced and in section 3 experiments will be described in which the energy of the neutrals has been determined by two methods, one a direct method involving a retarding field energy analyzer and the other, an indirect method involving measurement of relative sputtering yields for ions and neutrals.

6.2 Measurement of the number and distribution of fast neutrals

6.2.1 Ion deflection system

The measurement of the neutrals depends upon the ability to separate the charged particles, ions and electrons, from the total beam and thus leaving only the neutral particles. A deflection system has been developed to deflect the charged particles and to collect the uncharged particles. This system consists essentially of two parts, namely the electrostatic analyser and different collectors. The electrostatic analyzer is shown schematically in figure 6.1 and consists of two stainless steel plates, p_1 and p_2, which were used

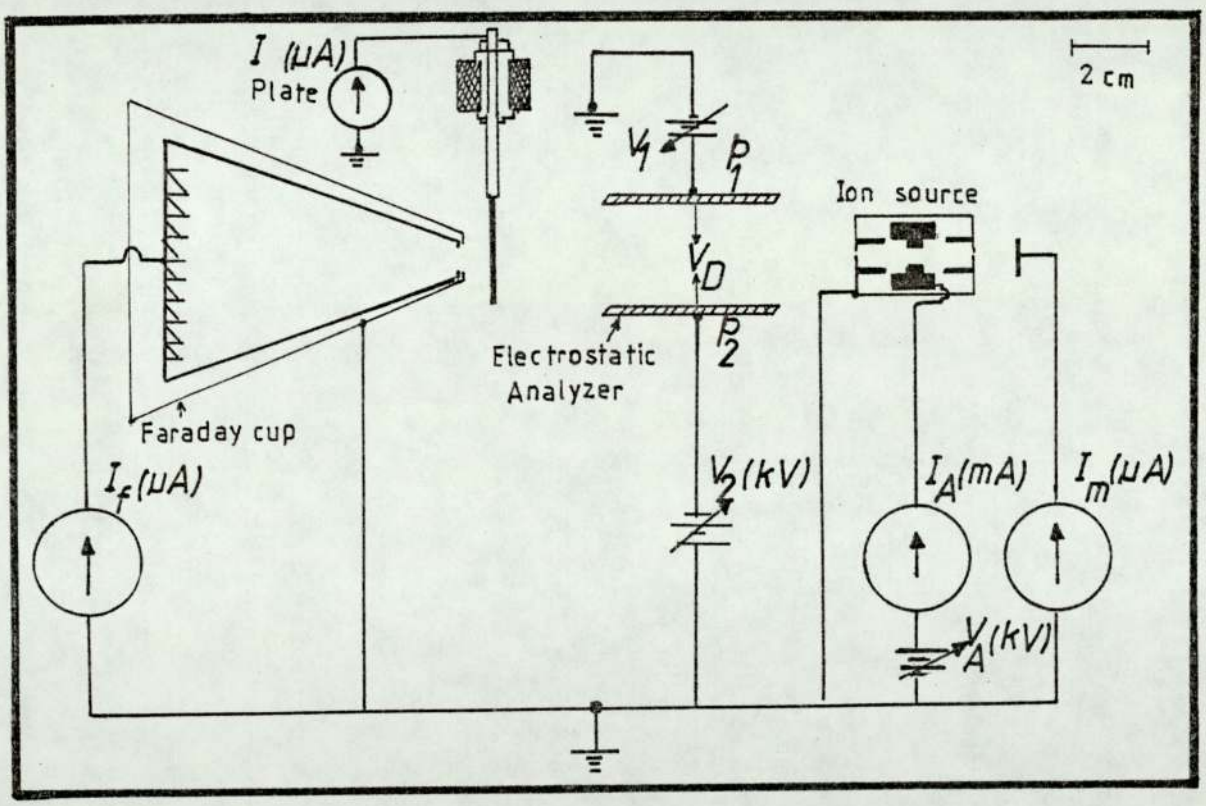

Figure 6.1 Schematic diagram of the electrostatic analyzer.

when it was required to deflect the charged particles. The collectors used were a Faraday cup and a flat plate to detect the positive ions and the neutrals respectively. The analyzer was designed to deflect the emerging ions and low secondary electrons

in an electrostatic field and collect them by P_1 and P_2. The potential, V_D, between P_1 and P_2 can be produced by applying voltages V_1 and V_2 to the two plates P_1 and P_2 by negative and positive polarity power supplies, which were able to provide up to $\pm$ 5 kV. The two deflector plates made from nickel sheet 4 cm in length and 3 cm apart, were about 2 cm away from the source to prevent electrical breakdown between the earthed source body and the plates. The analyzer uses the same principle of operation as discussed previously in Chapter 5.

Figure 6.2 shows the three arrangements of the analyzer and the source to measure the ions and neutrals. In figure 6.2a, using the Faraday collector with $V_D = 0$, the current I_1, indicates the number of ions, assuming there was no escape of secondary electrons. In figure 6.2b, using the flat plate collector with $V_D = 0$, the current I_2 indicates the ion current together with the current equal to the secondary electrons produced by the fast neutrals and ions bombarding the collector plate. Similarly with the arrangement as in Figure 6.2c with $V_D = V_A$, the collector current, I_3, is equivalent to the secondary electrons produced by only the fast neutrals. Thus the three currents I_1, I_2 and I_3 can be represented by the following equations, assuming that all the ions are singly charged and that the secondary electron coefficient is the same for ions and neutrals of the same energy:

$$I_1 = n_+ e \qquad \ldots\ldots\ldots V_D = 0$$

$$I_2 = (n_+ + \gamma n_+ + \gamma n_o)e \qquad \ldots\ldots\ldots V_D = 0$$

$$I_3 = \gamma n_o e \qquad \ldots\ldots\ldots V_D = V_A$$

Where n_+ is the number of ions arriving per second, n_o is the number of fast neutrals per second, e is electron charge and γ is the secondary electron yield for ions and neutrals. The solution of these three equations gives:

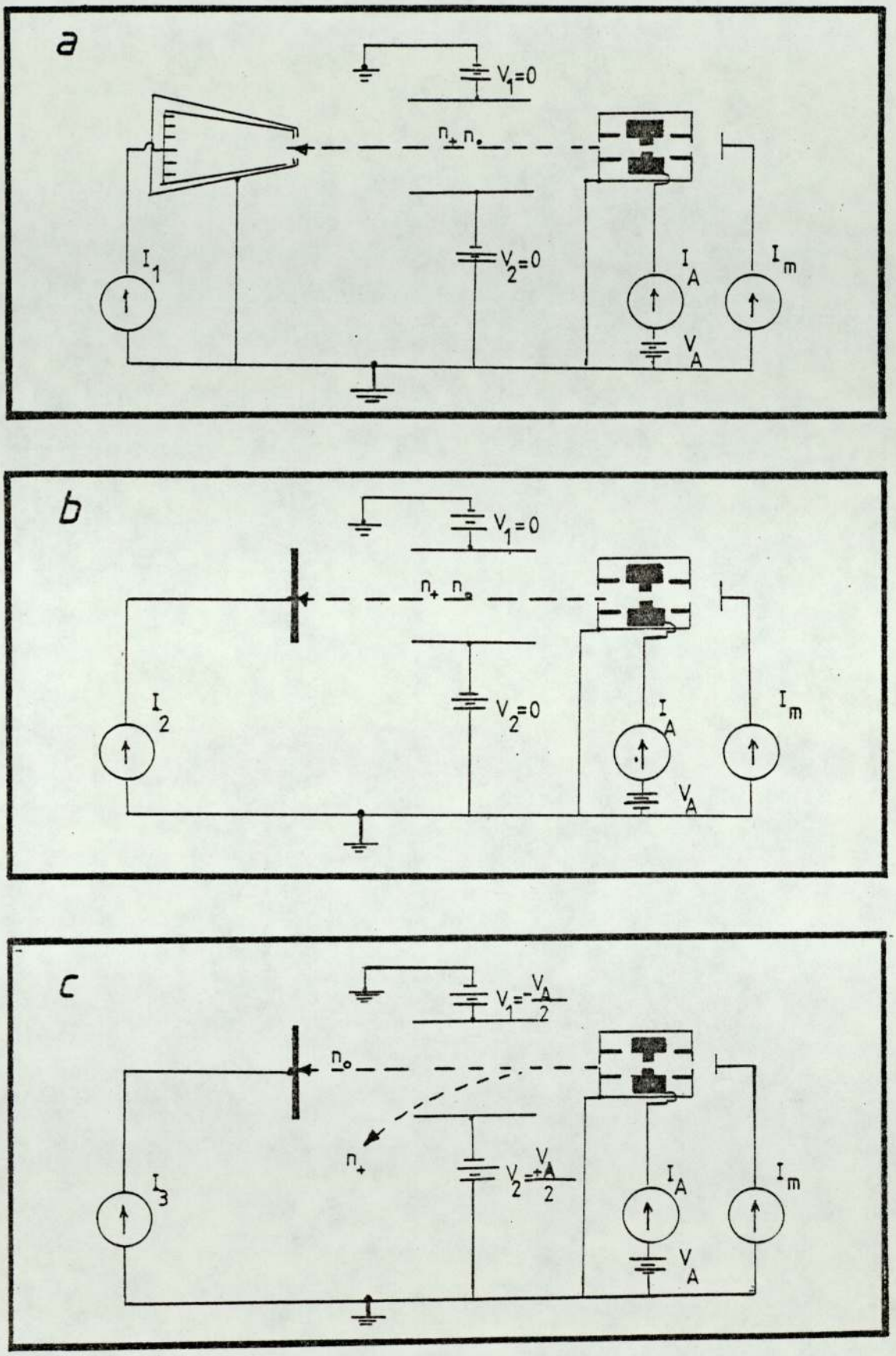

Figure 6.2 Schematic diagram of the ion source and the analyser showing the three arrangements.

$$n_+ = \frac{I_1}{e} \quad , \quad n_o = \frac{I_1 I_3}{(I_2 - I_1 - I_3)e}$$

and hence the percentage of neutrals, N_o, and the percentage of ions, N_+, in the total beam and the value of γ are given by:

$$N_o = \frac{n_o}{n_o + n_+} = \frac{I_3}{I_2 - I_1} \% \qquad \ldots\ldots (6.1)$$

$$N_+ = \frac{n_+}{n_o + n_+} = \frac{I_2 - I_1 - I_3}{I_2 - I_1} \% \qquad \ldots\ldots (6.2)$$

$$\gamma = \frac{I_2 - I_1 - I_3}{I_1} \qquad \ldots\ldots (6.3)$$

Thus the measurement of I_1, I_2 and I_3 enables us to find N_o, N_+ and γ. The value of I_1 was measured by the Faraday cup which represents stage one. I_2 and I_3 are measured by the plate when the deflected voltage $V_D = 0$ and $V_D = V_A$ respectively and represents stage two. This implies that the measurements taken at stage one were not taken under the identical conditions of stage two, with the consequence that large experimental errors could be present as it was necessary to admit air into the vacuum system to insert the flat plate collector to change from stage one to stage two.

Thus the system was modified to overcome these difficulties in which all measurements could be taken under the same experimental conditions. In the new arrangement, the flat plate collector was attached to an electrically isolated bar which was able to slide vertically from the top of the vacuum chamber through a "WILSON seal". The position of the plate was adjusted to give the required position and distance away from the source and thus could be achieved without any disturbance of the pressure and the

experimental conditions. In this new arrangement it was found possible to record I_1, I_2 and I_3 in less than one minute and thus it could be reasonably assumed that the conditions were the same for all three measurements.

6.2.2 Variation of the percentage of the neutrals for different gases

Table 6.1 gives the values of I_1, I_2 and I_3 and the corresponding values of N_o and γ for argon for I_A = 1, 2 and 3 mA for various values of V_A and P_c. Figure 6.3 shows the variation of N_o with the anode voltage V_A, at constant anode current I_A = 1, 2 and 3 mA using argon gas. It was observed that the percentage of fast neutrals increases from about 25 to 85 as the anode voltage decreases from about 9 kV to 2.0 kV as the corresponding pressure increased from 10^{-6} to 10^{-4} Torr. It was also found that the percentage of the neutrals at higher pressures and lower anode voltage reached about 85% and remained reasonably constant with further increase of pressure.

This is much more acceptable than previously found by Fitch et al[42] as their curves indicated that on extrapolation to higher pressures more than 100% of neutrals would be produced which is clearly an impossible situation. The uncertainty in these experiments was very much less than found by Fitch et al[42] due to the maintenance of the experimental conditions throughout the measurements. Of course, when the values of N_+ were calculated over the same range of pressure then the exact reverse situation occurs in which the percentage of ions increases as the pressure decreases and anode voltage increases. These experiments were also performed for helium and nitrogen and the results given in figure 6.4 and 6.5 show the very similar trends to that observed for argon.

However, the same value of N_o for each gas did not occur at the same anode voltage. For example, with I_A = 2 mA, N_o = 50% occurs at

Table 6.1 shows N_o and γ for argon at I = 1, 2 and 3 mA

Pressure ($\times 10^{-5}$ Torr)	V_A (kV)	I_1 (μA)	I_2 (μA)	I_3 (μA)	N_o %	γ
1.2	9	15.5	35	4.5	22	0.96
1.3	8.5	15.8	35.4	4.8	24	0.93
1.5	8	16.2	36	5.2	26	0.9
1.8	7	15.6	35.2	5.6	28	0.89
2.6	6	14.6	33.4	6.6	35	0.81
4	5.5	14.4	33.4	7.2	43	0.80
5.2	5	13.3	30.9	0.8	51	0.66
6.8	4.5	10.1	22.4	8.1	65	0.41
8.2	4	6.1	17	7.8	71	0.51
10	3.5	5	14.8	7.3	75	0.5
11	3	2.8	10.8	6.2	77	0.64
12	2.5	1.7	7.6	4.5	77	0.67
1.5	9	27.4	55.6	7.8	27	0.74
1.6	8.5	31.4	63.1	8.6	27	0.71
1.8	7.5	31.2	60.8	9.2	31	0.65
2	7	28.9	58.4	10.2	34	0.66
6	6	28.0	54.4	11.6	44	0.55
8	5.5	24.8	47.4	11.4	51	0.45
9.4	5	18.2	40.6	12.5	55	0.43
10	4.5	13.2	30.2	12	70	0.5
11	4	8.4	23.3	11	76	0.38
12	3.5	7.4	18.4	9	81	0.27
13	3	3.2	11.2	6.4	82	0.21
3.2	8	53.4	121	23.7	35	0.8
6.8	7	38.3	88.5	20.6	41	0.77
7	6	31.9	69	18	48	0.60
10	5	23.5	41.8	13.2	70	0.39
12	4.5	16.5	33.8	12.6	85	0.2
13	4	13.3	26.2	11.2	86	0.15
14	3.5	7.4	18.4	9	87	0.11
15	3	5.4	11.9	5.5	89	0.11

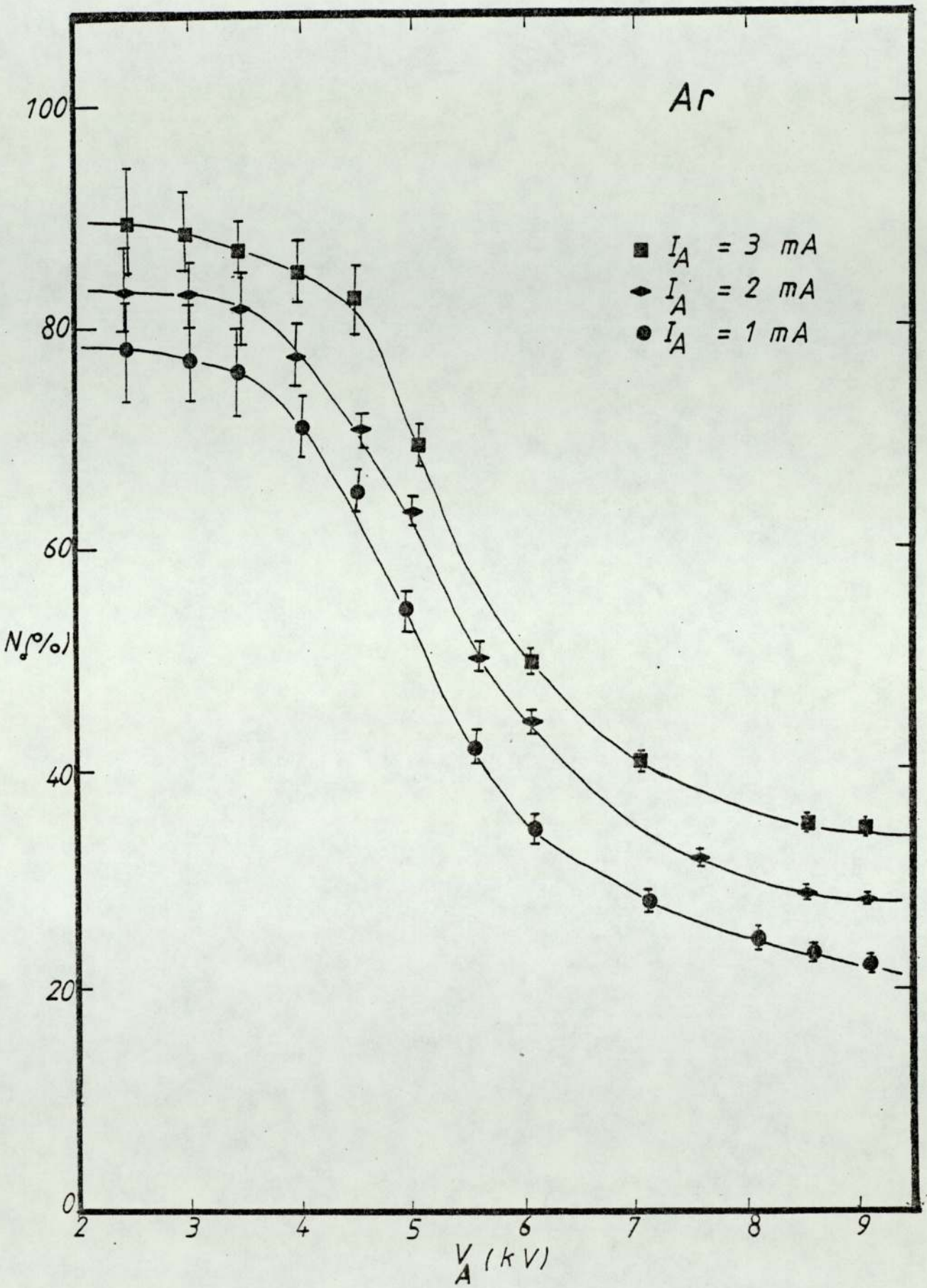

Figure 6.3 Variation of percentage of fast neutrals, N_o with anode voltage, V_A using argon.

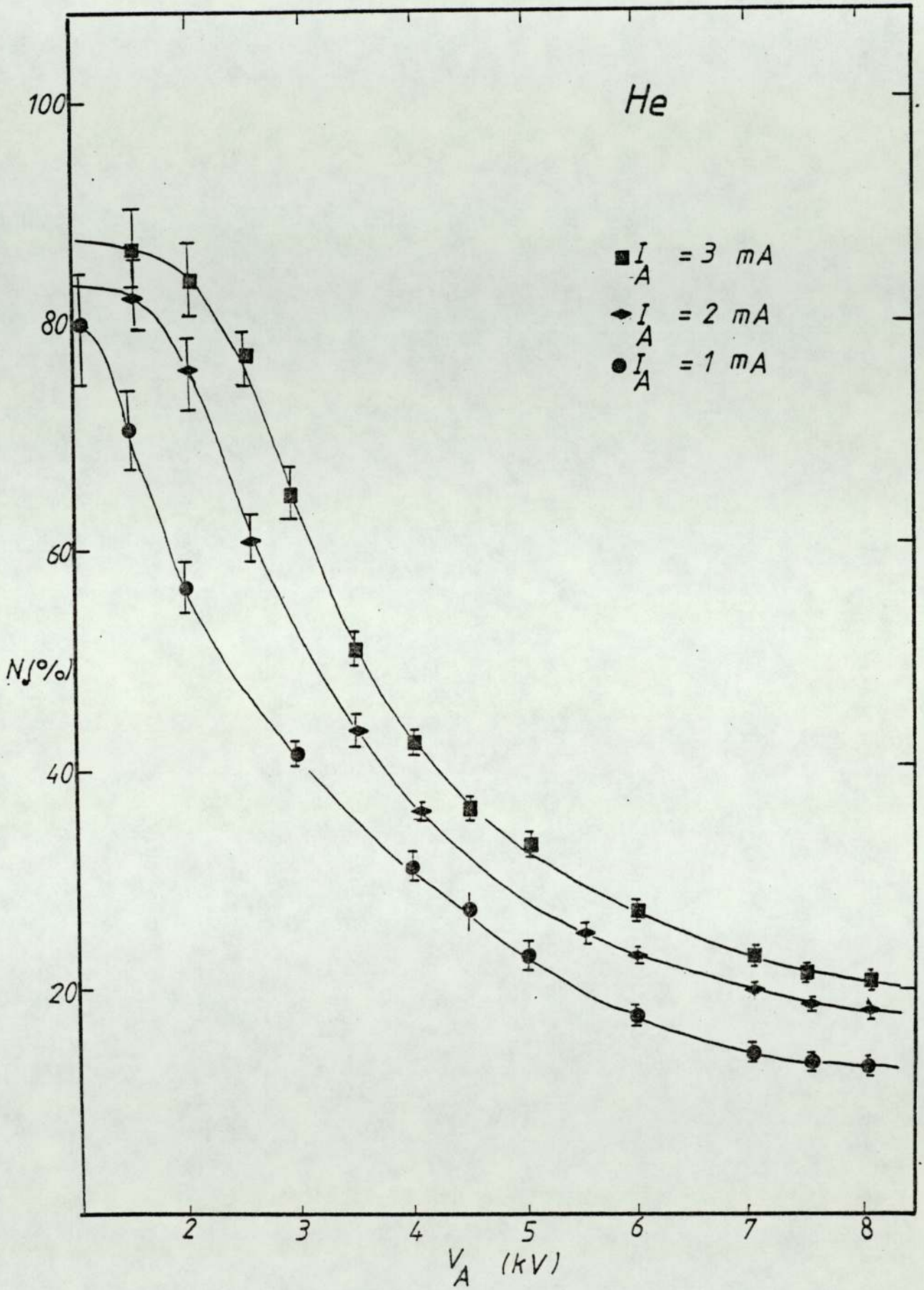

Figure 6.4 Variation of percentage of fast neutrals, N_o with anode voltage, V_A using helium.

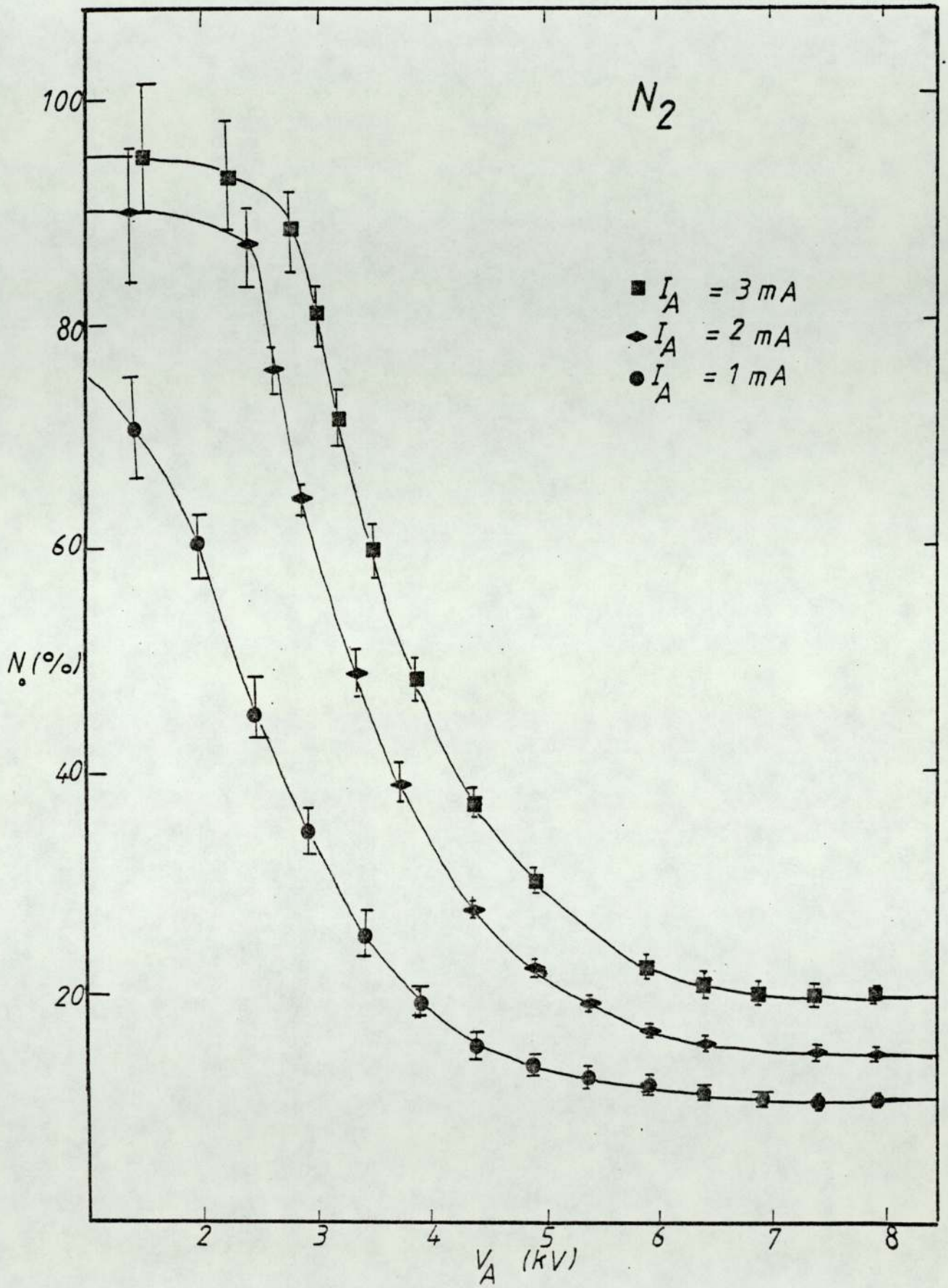

Figure 6.5 Variation of percentage of fast neutrals N_o, with anode voltage V_A, using nitrogen.

V_A = 5.5, 3.1 and 3.5 kV for argon, helium and nitrogen respectively but this is not surprising taking account of the discussion in Chapter 4 on the modes of operation for these gases in which the transition occurs at different source pressures. It should be noted on the figures 6.3 to 6.5 that error bars are included which have been estimated from equation 6.1 and it is clear that the error bars are considerably greater at higher pressures. This is due entirely to the fact that at higher pressure the measured current is very much smaller as the source is operating in the most inefficient mode.

Figure 6.6a, b and c shows the variation of the γ with V_A for I_A = 1, 2 and 3 mA using argon. These figures show that the γ increases from about 0.2 to 0.8 when V_A increases from 2 to 9 kV and does not change significantly with I_A. It can again be seen that the uncertainties in γ are greater at higher pressures as was found with N_o. The variation of γ for helium and nitrogen at I_A = 2 mA are given in 6.7a and b and show that γ varies from about 0.2 to 1.0 and 0.2 to 1.1 for helium and nitrogen respectively, as the ion energy increased from about 1 to 7 keV.

The values of γ for all three gases, argon, helium and nitrogen, are in reasonable agreement with that found in literature, for example Carter and Colligon[57] and do give some confidence to the interpretation of the measurements made to determine the percentage of neutrals. Of course it would be unreasonable to attempt to make any more precise comparison with other published work because this is only really possible when secondary electron yields are measured in ultra vacuum conditions.

6.2.3 Calculation of the percentage of neutrals in terms of a charge exchange process

An attempt has been made in this section to explain the previous

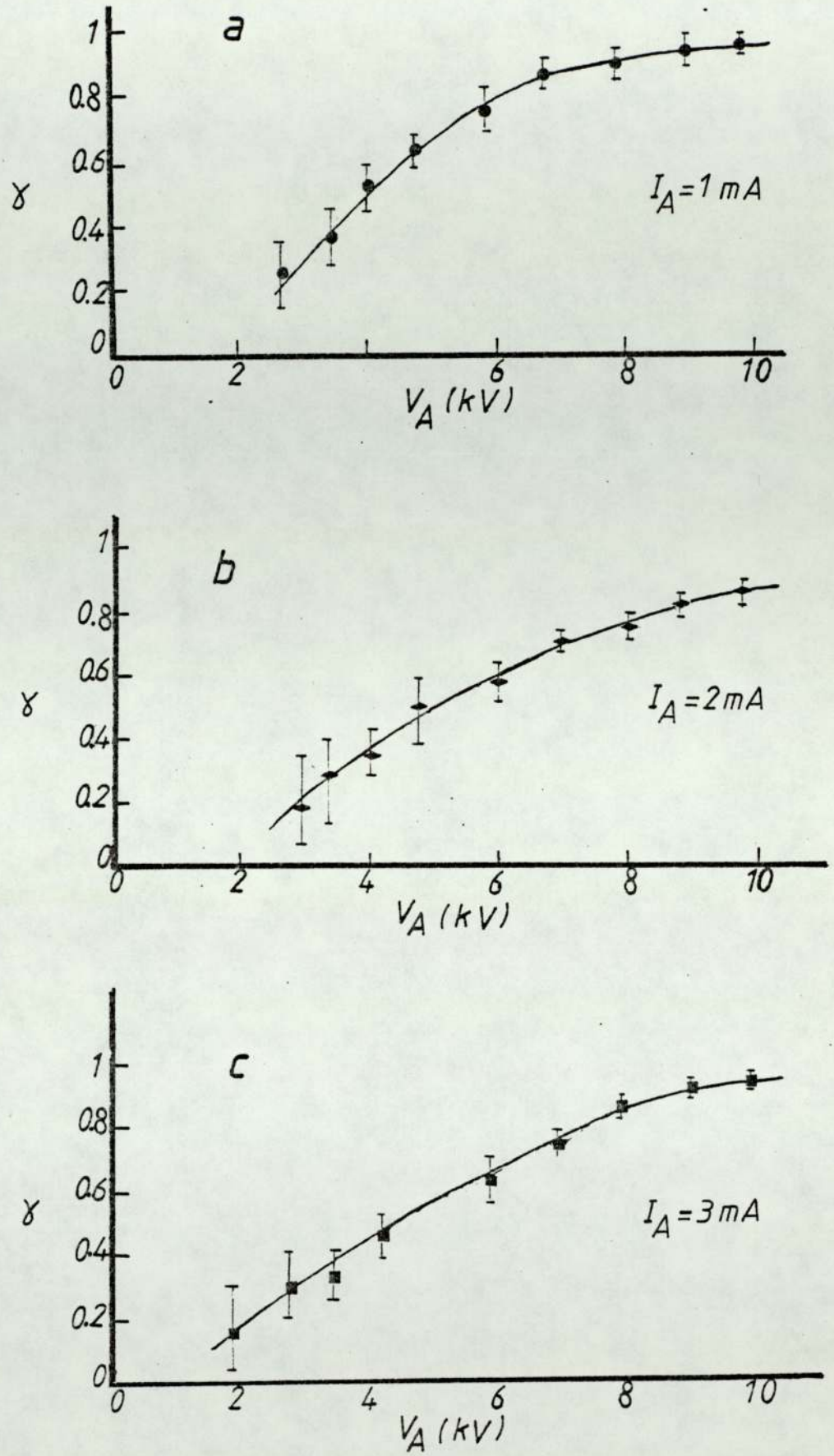

Figure 6.6 Variation of secondary electron coefficient γ, with anode voltage using argon at (a) I_A = 1 mA, (b) I_A = 2 mA and (c) I_A = 3 mA.

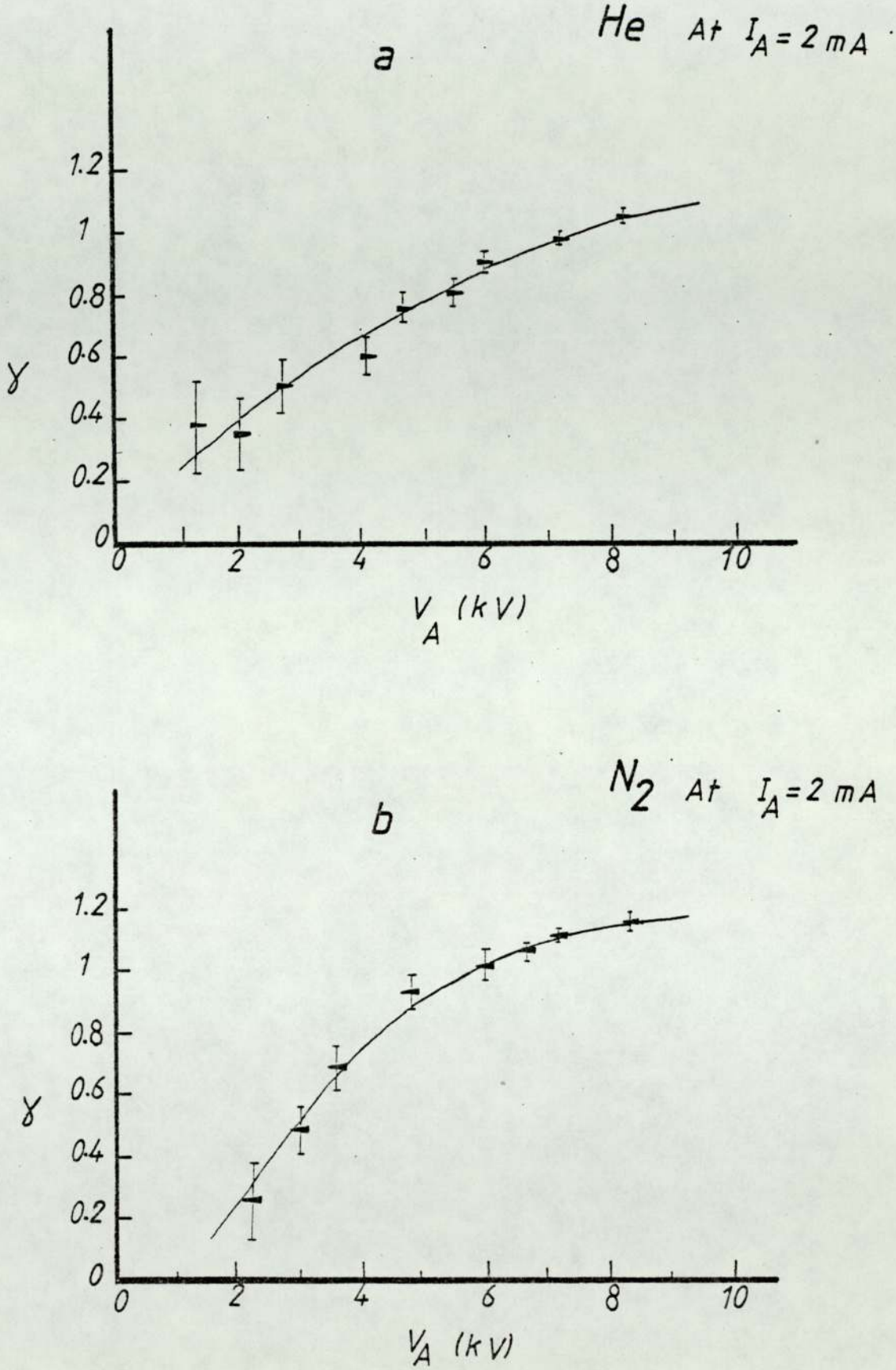

Figure 6.7 Variation of secondary electron coefficient, γ with anode voltage V_A, at constant I_A, using (a) helium and (b) nitrogen.

results of the variation of the percentage of the fast neutrals as a function of pressure inside the source. Previous observations and measurements included in this Chapter suggest that the energy of the ions and the fast neutrals are the same. Thus the most likely process occurring is a symmetrical resonance charge exchange process in which a fast ion (A_F^+) collides with a slow neutral (A_S^o) to produce a fast neutral (A_F^o) and a slow ion (A_o^+) which can be represented by the equation:

$$A_F^+ + A_S^o \rightarrow A^+{}_S + A^o{}_F$$

The cross section, σ, for this reaction is given by Salsborn[58] as

$$\sigma^{\frac{1}{2}} = (a-b)\ln V$$

Where a and b are constants and V is the velocity of the ions which of course depends on the mass and energy of the ions. Figure 6.8 shows the variation of $\sigma^{\frac{1}{2}}$ with V for helium and argon as given by Rapp and Frances[59] but unfortunately, this does not include the values for nitrogen. Thus at a given impact velocity σ can be determined and the probability of charge exchange process N, is given by:

$$N = \bar{l}n\sigma$$

Where $\bar{l}$ is the average path length of the ions and n is the gas density. Therefore N can be calculated when σ, l and n are known.

The values of n can be calculated in terms of the source pressure taking into account the sensitivity and position of the pressure gauge and the speed of the diffusion pump for each gas as discussed in Chapter 4. The values of σ were estimated from figure 6.8 for

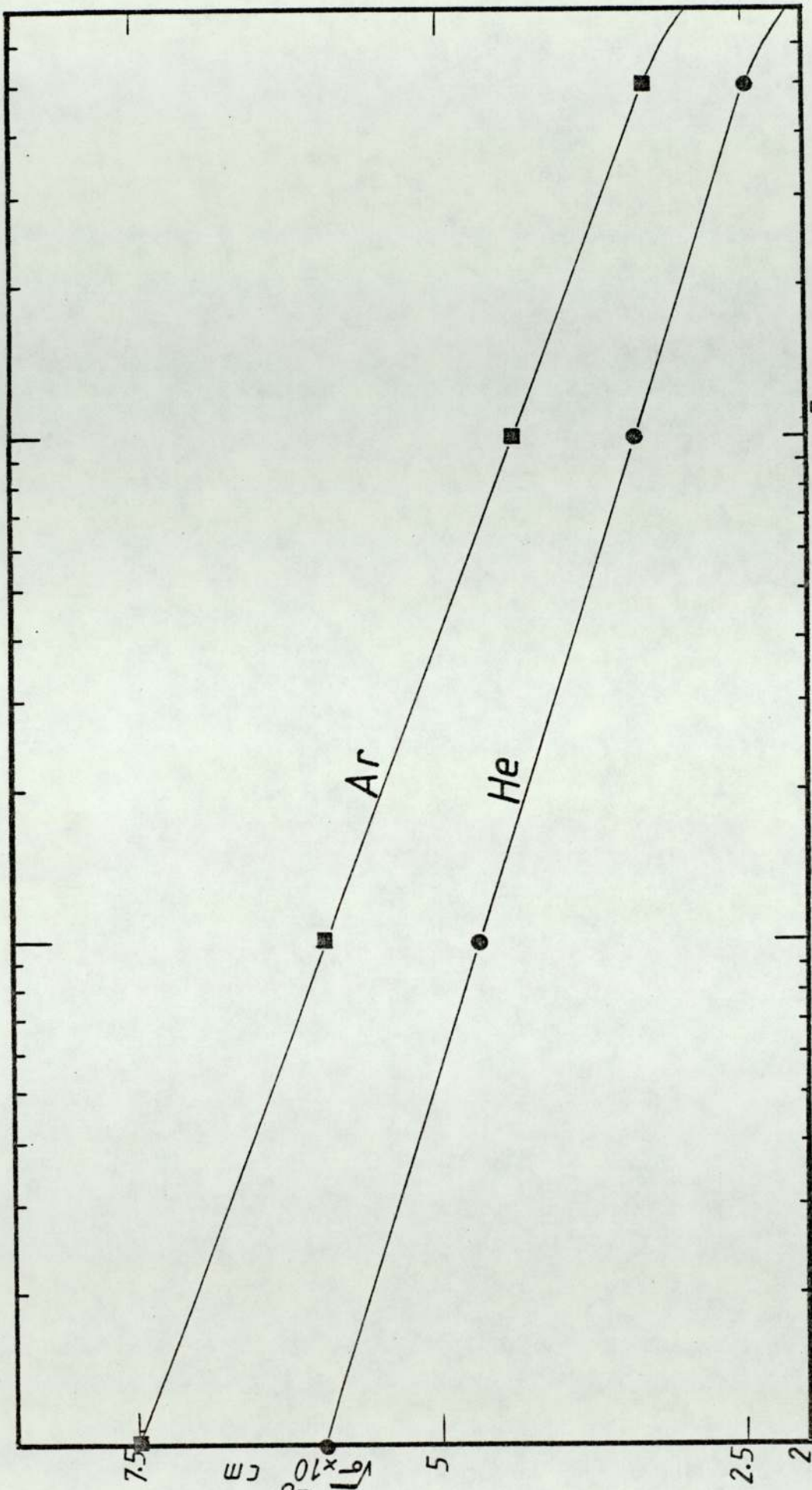

Figure 6.8 Symmetrical resonance charge transfer cross section against voltage as given by Rapp and Francis for helium and argon.

various values of velocity which were calculated from the energy of the ions which were assumed to be 0.75 V_A as given by Khorassany[41]. It is only possible to make an estimate of $\bar{l}$ and was taken to be about 3 mm which was inferred from the observation of the visible discharge seen in the cylindrical ion source and taking into account that the effective radius of the spherical source is 1.5 cm. The values of N are expressed as a percentage for argon and helium when I_A = 1 mA and are given in Table 6.2 which include the calculated values of gas density and the experimental values of N_o. Calculation for N_o for both gases as a function of V_A are given in figure 6.9 and the experimental values of N_o are plotted against the theoretical values of N_o as shown in figure 6.10.

Taking into account the number of uncertainties in both the experimental measurements and theoretical calculations, including such things as, the assumptions about γ for ions and neutrals, the charge exchange and the ion path length, the agreement between the theoretical and experimental values of N_o is quite encouraging. Of course, in figure 6.10 the plot of N_o theoretical against N_o experimental should have been a straight line of slope 45°. The major discrepancies from this are at high pressure when N_o theoretical exceeds 100%. This is clearly an impossible situation and must be the main reason for this disagreement between theory and experiment. It is unlikely that the values of the molecular density are in error and σ does not change much within the energy range concerned and therefore one could suggest that the original assumption that $\bar{l}$ is constant is incorrect. At high pressures when the plasma sheath moves towards the cathode wall the mean free path decreases and hence $\bar{l}$ is reduced. Such a correction would reduce N_o theoretical and it would only require a change of $\bar{l}$ from 3 to say 2 mm to reduce N_o theoretical to less than 100%.

Table 6.2 Shows the values of N_o for argon and helium at I_A = 1 mA

	Pressure (10^{-5} Torr)	Source pressure (10^{-2} Torr	V_A (kV)	E (keV)	Velocity (10^{-7} cms^{-1})	No.of mols 10^{16}mol cm^{-3}	σ 10^{-16} cm^2	N_o (th) %	N_o (exp) %
Argon	1.8	1.1	7	5.25	1.58	.35	16.4	17	26
	2.6	1.5	6	4.5	1.46	.49	16.8	25	35
	4	2.4	5.5	4.12	1.40	0.77	17	39	43
	5.2	2.9	5	3.75	1.34	.96	17.3	49	51
	6.8	4.1	4.5	3.35	1.26	1.35	17.65	70	65
	8.2	4.67	4	3	1.2	1.5	17.9	80	71
	9.6	5.6	3.5	2.6	1.1	1.8	18.4	99	75
	11	6.36	3	2.25	1.03	2.1	18.9	119	77
	12	6.94	2.5	1.8	.924	2.3	20.18	139	79
Helium	1.3	4.3	6	4.5	4.6	1.4	6.5	27	17
	2.2	4.7	5	3.75	4.2	1.5	6.76	30	23
	1.5	5	4.5	3.35	4.0	1.66	6.89	34	28
	1.7	5.72	4	3	3.75	1.88	7.15	40	30
	2.2	7.4	3	2.25	3.25	2.42	7.84	54	40
	3.2	10.7	2	1.5	2.65	2.72	8.26	86	57
	4.5	15.1	1.5	1.1	2.3	4.9	8.7	127	70

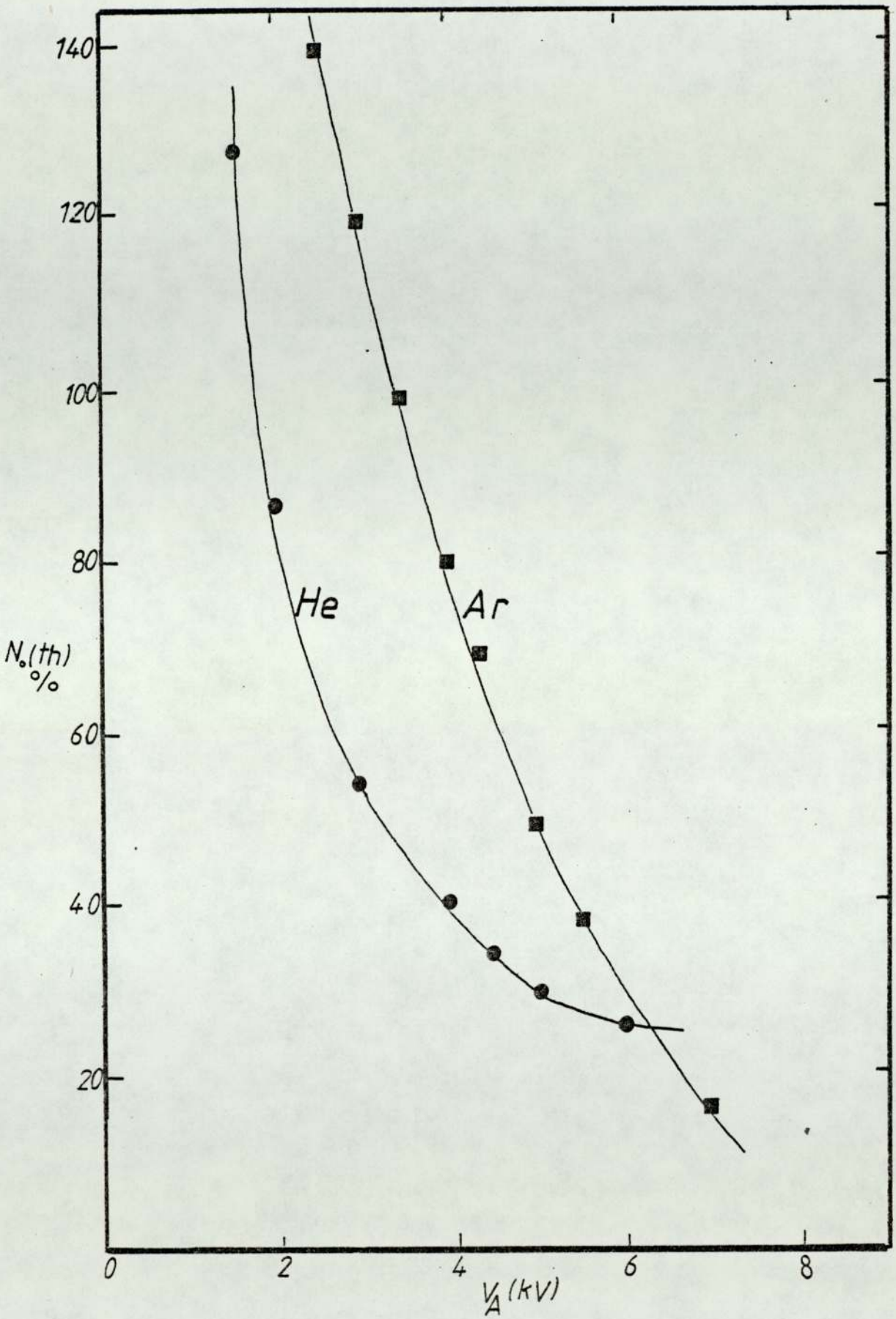

Figure 6.9 Calculated percentage of fast neutrals N_o(th) as a function of anode voltage, V_A for argon and helium.

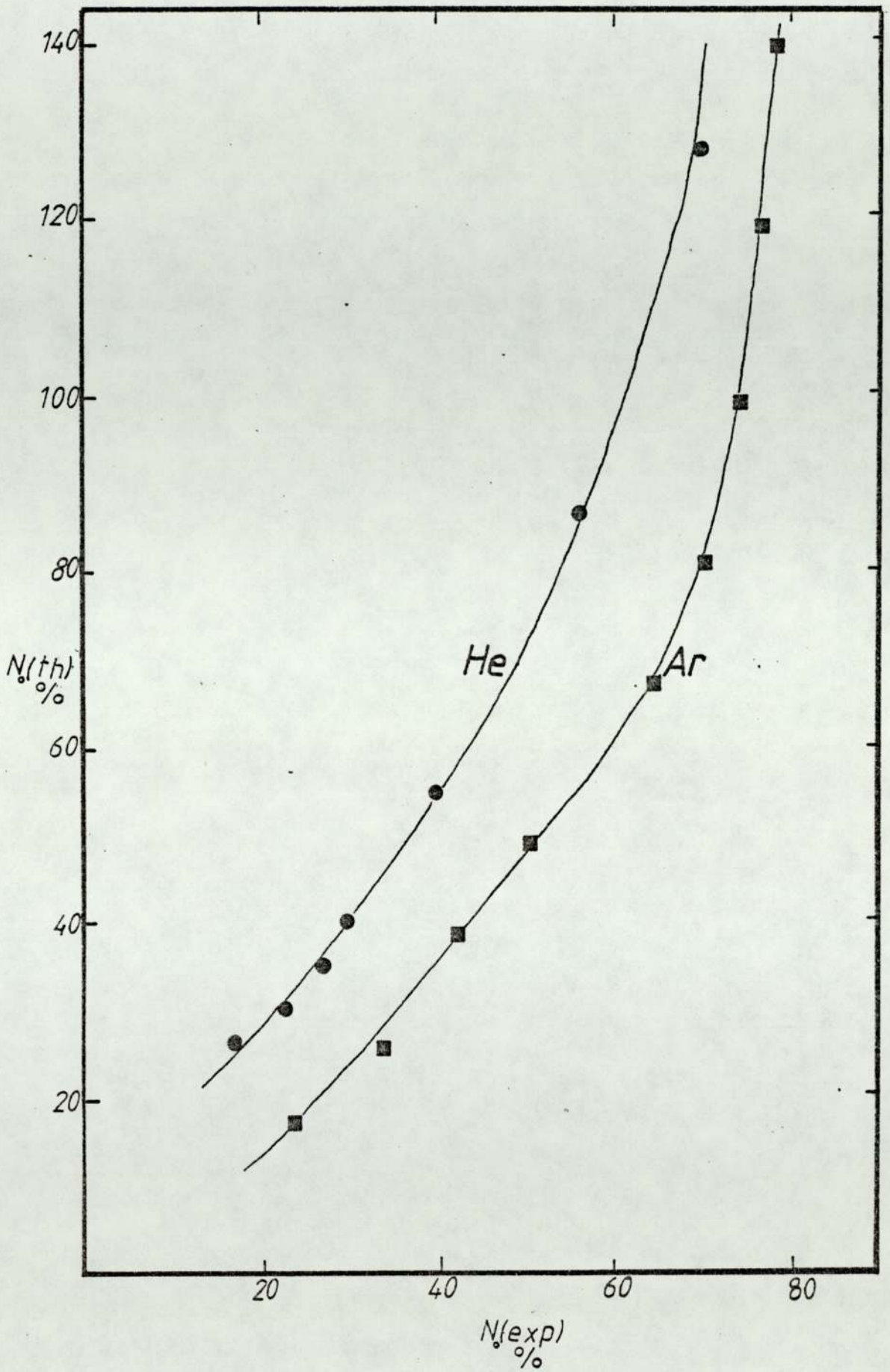

Figure 6.10 The calculated percentage of fast neutrals, N_o(th) against the experimental percentage N_o(exp) for argon and helium.

Of course, allowance should also be taken into account for the possibility of a similar charge exchange occurring outside the source before the ions enter the Faraday cup. Measurements have been taken to show how the Faraday cup current decreases with distance of the Faraday cup from the source aperture and values for argon are shown in figure 6.11. It can be seen that the current reduces slowly with increasing distance and, for example, with $P_c = 6 \times 10^{-5}$ Torr the current decreases by 12% for a distance of 10 cm. The probability of charge exchange taking place at 6×10^{-5} Torr over 10 cm. is about 8.5%. This agreement is quite reasonable particularly as there will be some additional reduction in the Faraday cup current due to the divergence of the beam and the consequent loss of low energy ions.

The corresponding theoretical and experimental value of N_o inside the source are 54% and 44% respectively and thus it can be confidently stated that the fast neutrals are mainly produced by a charge exchange process inside the source.

6.2.4 Investigation of the distribution of neutrals

It has been seen in the previous section how the percentage of neutrals was measured for the total beam and how they are produced from a charge exchange process inside the source. A further experiment was performed to estimate the distribution of neutrals within the emerging beam, using a small probe which could be scanned across the beam. The probe consisted of an aluminium strip, 1 mm wide and 50 mm long, and was connected to the insulated rod which could be moved vertically in the vacuum chamber. The position of the probe was adjusted in order to make it normal to the direction of the beam and it was able to detect the current at different distances from the centre of the beam with $V_D = 0$ and $V_D = V_A$ giving probe currents of I' and I'' respectively.

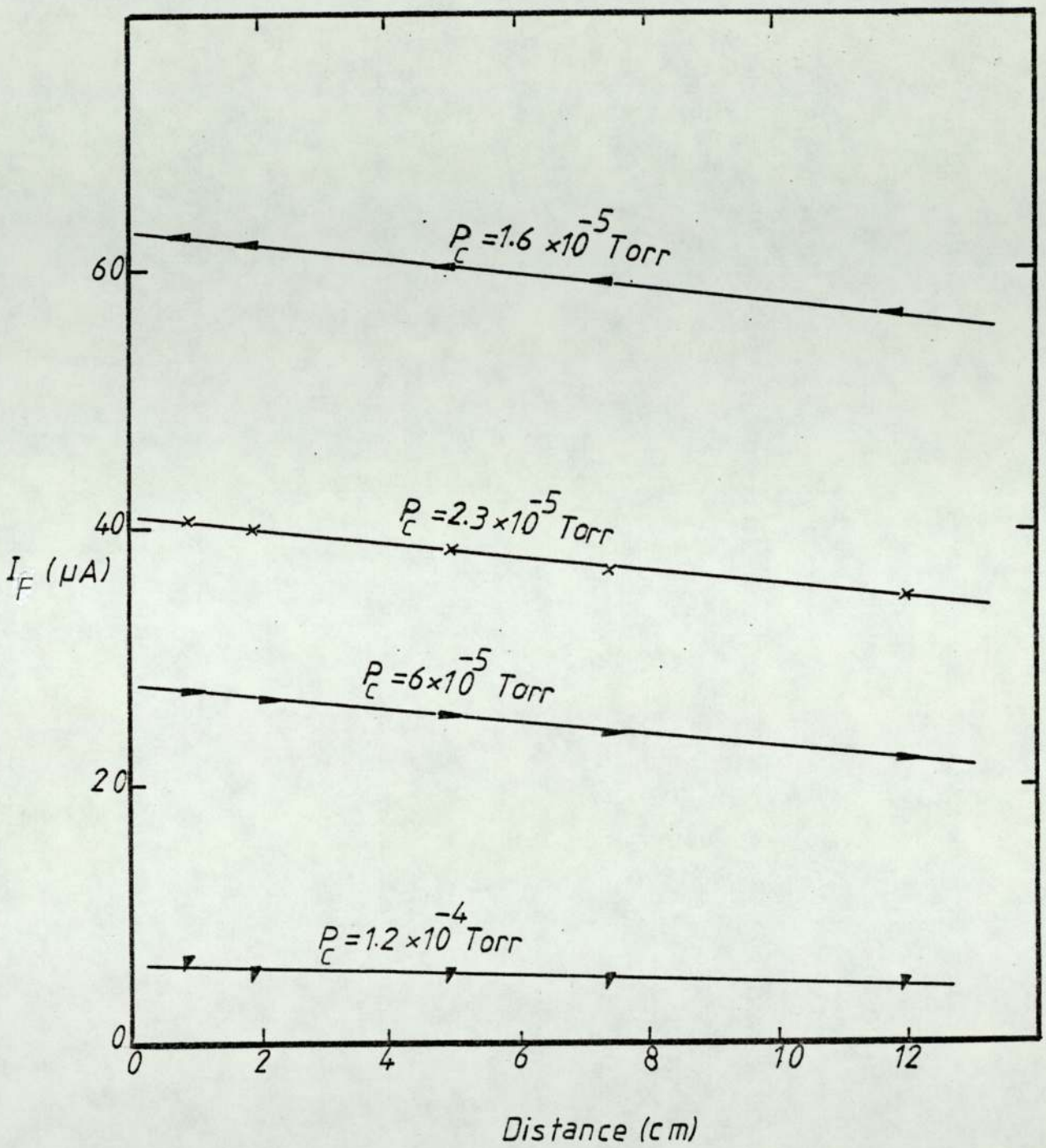

Figure 6.11 The variation of Faraday current, I_F against the distance from the source for argon.

Hence $I' \propto n_+ + \gamma (n_+ + n_o)$

and $I'' \propto \gamma n_o$

Thus $(I' - I'') \propto n_+ + \gamma n_+$

and therefore $$\frac{n_o}{n_+} \propto \frac{I''}{I'-I''}$$

Thus measurements of I' and I'' make it possible to estimate the distribution of the fast neutral within the beam.

The probe was fixed at 9 cm from the source and using argon, I' and I'' were recorded as the probe was scanned across the beam and the results for I_A = 2 mA are shown for V_A = 7, 4 and 3 kV in figures 6.12a, b and c respectively. The corresponding ratios of $\frac{n_o}{n_+}$ are shown in figure 6.13a, b and c.

These curves show, as expected, that as the voltage decreases and hence the pressure increases, n_o/n_+ increases. In addition it should be noted that there is clear evidence that the neutral density is higher in the centre of the beam and perhaps more important, the total divergence of the neutrals appears to be less than the ions. This is consistent with arguments presented in the previous section as it is known[41] that most of the ions at the edge of the beam are of low energy and thus the neutral density will be less as the charge exchange cross-section will be less at these lower ion energies.

The above ideas can be compared with those reported in a very recent paper by Franks[47]. He states that the output of this source is complex and contains ions, "stable" neutrals and excited neutrals, although surprisingly he makes no mention of excited ions. In addition, although no details of his measuring techniques were

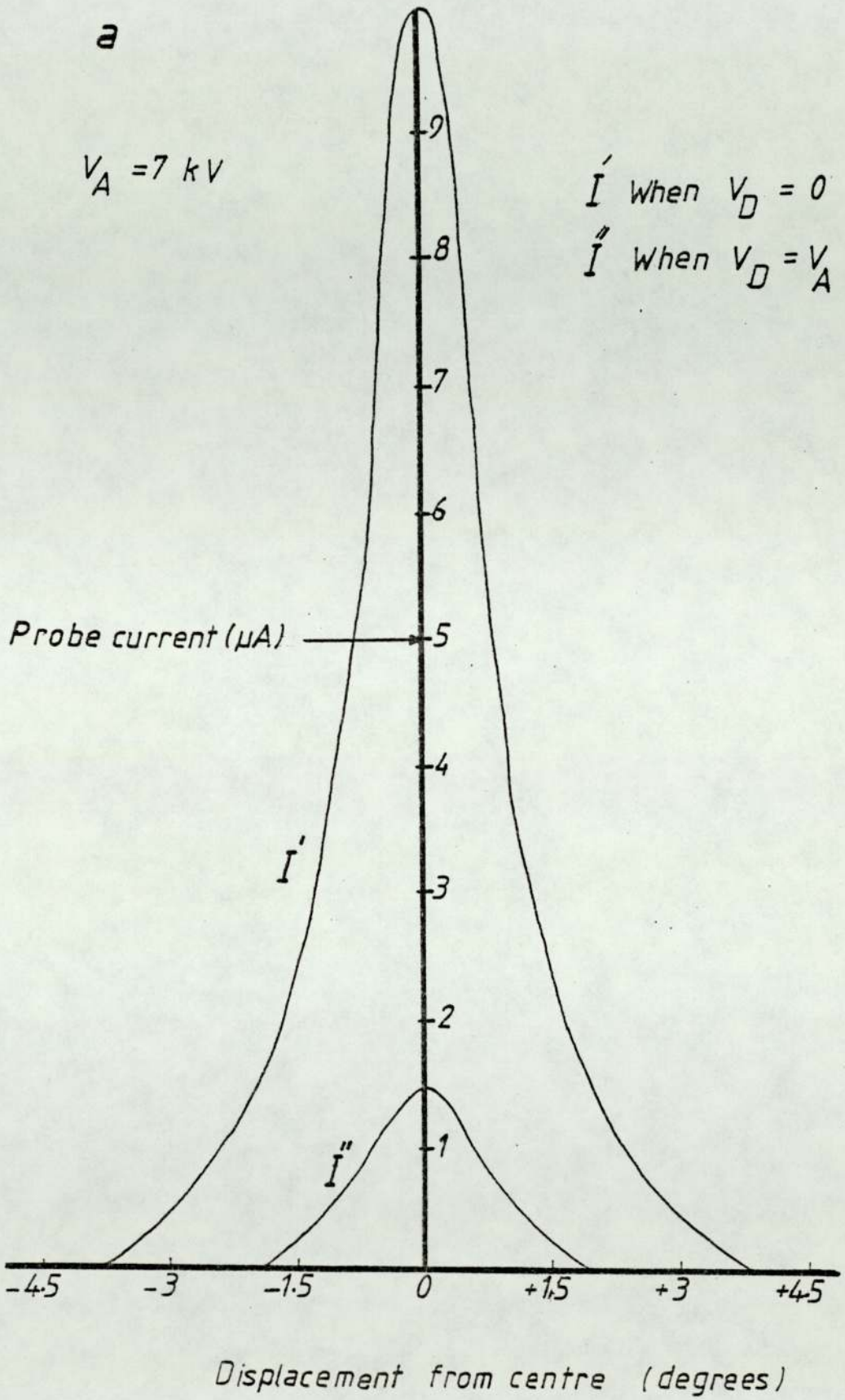

Figure 6.12a Probe current, I', and I'' against the displacement from centre for anode voltage 7 kV.

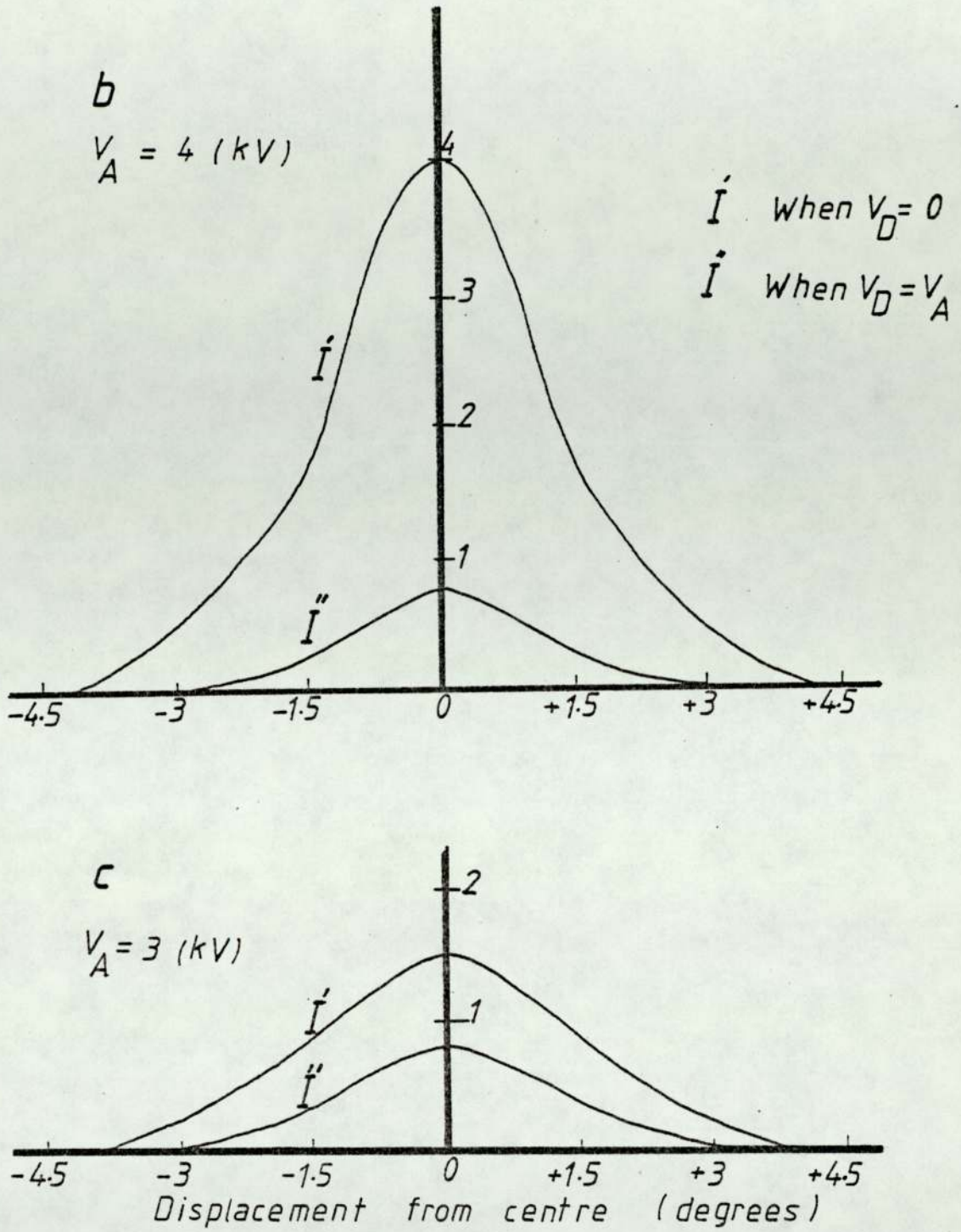

Figure 6.12 Probe current, $\acute{I}$ and $\acute{\acute{I}}$ against the displacement from the centre for anode voltage (b) 4 kV and (c) 3 kV.

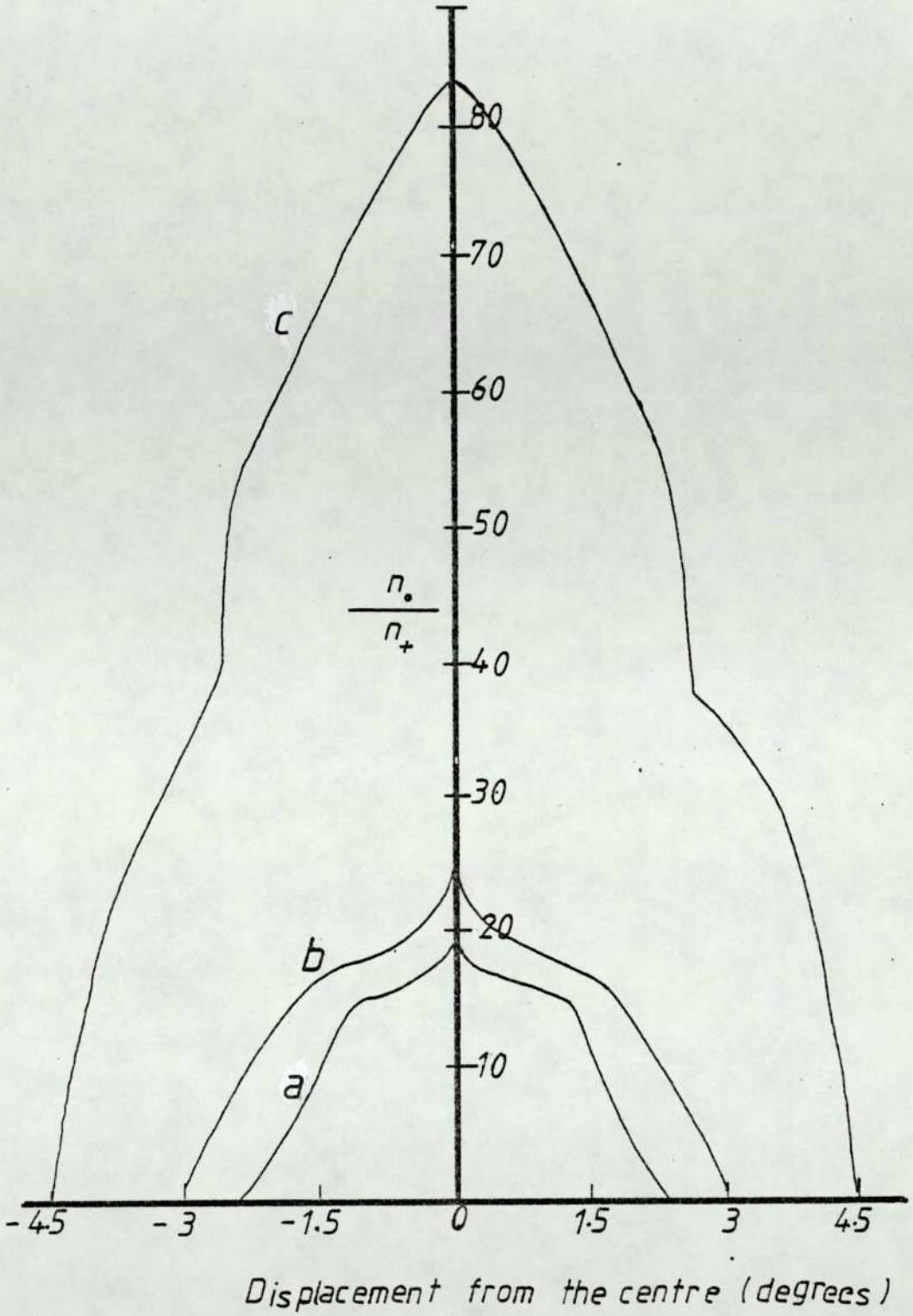

Figure 6.13 The distribution of fast neutrals in the beam at different anode voltages (a) 7kV, (b) 4kV and (c) 3kV.

given, he found that the neutral/ion ratio first decreased and then increased with increasing distance from the source aperture. This is not in agreement with present work as the Faraday cup current decreased linearly and slowly with increasing distance. However, he does state that the beam consists of a core of stable neutrals of low divergence which is surrounded by a more divergent ion beam which is in agreement with the experimental results given in this section.

6.3 Measurement of the energy of the fast neutrals

The aim of the work described in this section is to report the attempts to measure the energy of the fast neutrals. This was done in two ways, firstly, in a direct method using a crossed-beam technique in which the neutrals were ionized by an electron beam and the resulting ions were then analyzed. In the second method, the energy was inferred from a comparison of the sputtering yields for ions and neutrals.

6.3.1 Direct method using a crossed beam technique

This technique depends on the possibility of ionization of the neutrals and then the ability to measure the ion energy using a retarding field analyzer. Figure 6.14 shows the complete arrangement for this technique which consists essentially of the ion source, the electrostatic deflector, electron gun fixed inside the ionization chamber and the retarding field analyser including the Faraday Cup. The electrostatic deflector used in this measurement was similar to that described previously in section 6.2. The electron gun consists of a hair-pin tungsten filament which was surrounded by a small cylindrical screen at earth potential. The filament was heated by an A.C. supply via an isolating transformer and the electrons were accelerated through a 3 mm hole in the centre of the

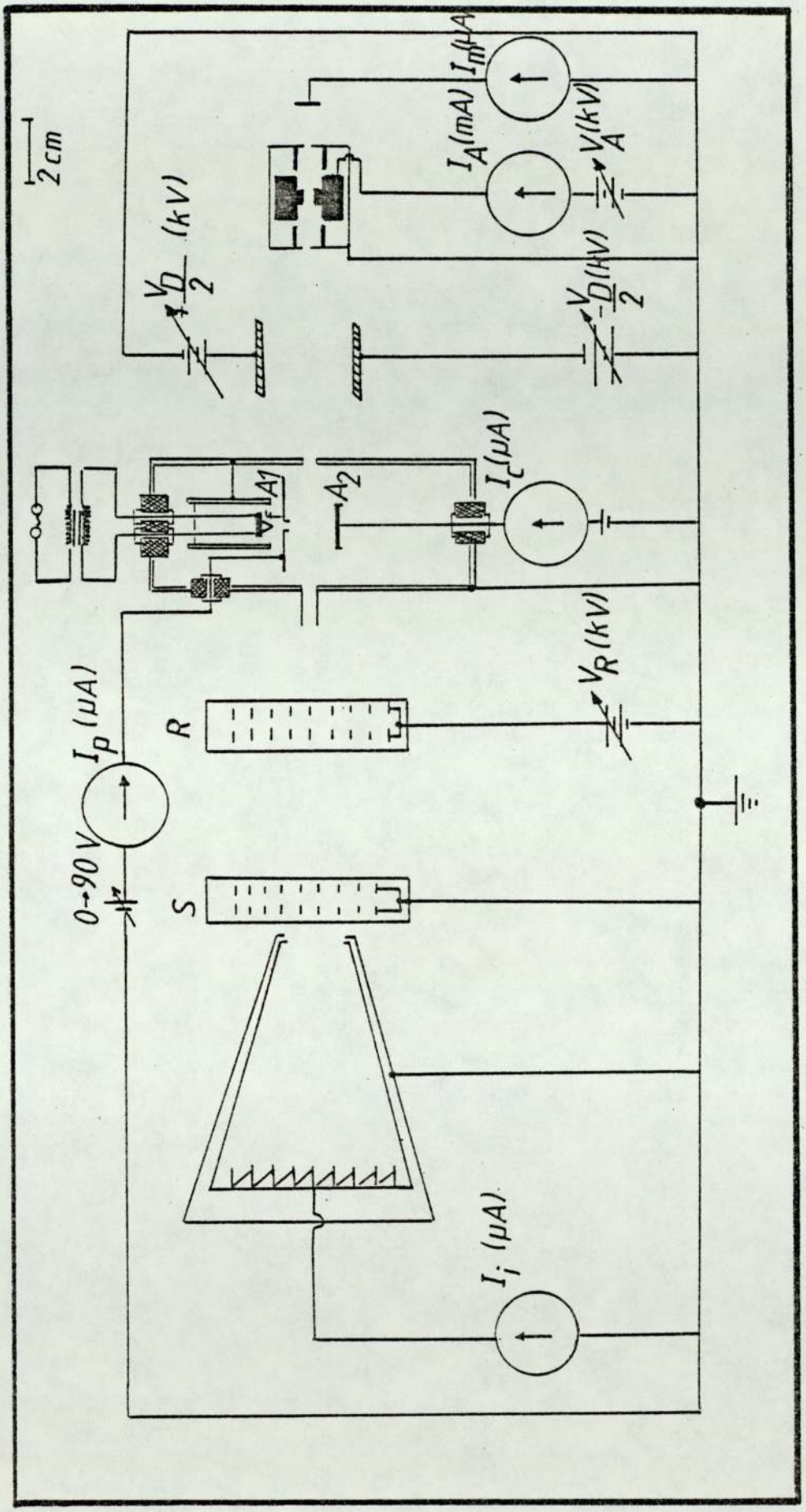

Figure 6.14 Schematic diagram of the ion source, deflectors, ionization chamber and retarding field analzer including Faraday cup.

anode, A_1 which was at +90 volts. In this situation the electrons transmitted through the ionization region are assumed to be reasonably well collimated and normal to the direction of the fast neutrals. The electrons were collected by a positive collector, A_2. The ionization chamber was made of aluminium 11 cm long, 2.5 cm wide and 6 cm high with two holes in the front and back sides to allow the neutrals to pass through from the source to the analyser. The size of both holes is important in this measurement. When the front hole is too small, this reduces the number of neutrals entering the chamber but if it is too large, the field produced from the electrostatic deflector can penetrate the ionization chamber.

Experiments showed that a good compromise could be achieved using a 3 mm diameter entrance aperture. For the same reason it was necessary to minimize the size of the exit aperture to be 5 mm to protect the ionization chamber from the retarding field, and a small stainless steel tube, 1 cm in length and 4 mm in diameter was added to reduce the beam divergence. The energy analyser used in this measurement consisted of double grids R and S, to give a large transparency yet still produce a reasonably uniform field. They were made by winding 0.1 mm diameter tungsten wire around an aluminium frame, 40 x 40 mm, such that the grid wires were spaced at a distance 5 mm. This gave a transparency of more than 90%. Grid R is the retarding grid and grid S, is the screen grid to shield the collector from the positive retarding field at R. The ion current, I_i was detected by a Faraday cup and was recorded with D.C. amplifier as a function of the regarding voltage V_R and the corresponding energy spectrum was obtained by differentiating I_i with respect to V_R.

Before any measurement was undertaken concerning the ionization of the neutrals the energy analyser was tested with the total beam of ions and neutrals with the filament switched off and A_1 and A_2 at earth potential. Figure 6.15a shows the variation of I_i with V_R for argon at V_A = 5 kV and I_A = 2 mA, and the corresponding energy distribution is shown in figure 6.15b. These curves are similar to that found by Khorassany (41) and show a small low ion energy background dominated by a high energy peak at about 0.75 V_A. This value is again in good agreement with Khorassany and thus the analyser was assumed to be satisfactory.

In order to measure the energy of the neutrals it was essential to maximize the efficiency of the ionization by using the maximum number of neutrals and an intense electron beam of the correct energy. The maximum ionization cross-section for electrons with gas molecules is in the region of 100-150 eV and thus if we assume the neutrals are of energy ofafew keV, then we can neglect any deflection because the electron collision will not produce any significant change in trajectory of the neutrals. The alignment of the apertures was also important to ensure the neutrals passed through the centre of the entrance aperture and this was achieved by etching thin copper film placed at the exit aperture. The source was operated at V_A = 3.6 kV and I_A = 2 mA and the neutrals entered the chamber after the ions had been deflected and the background current to the Faraday cup was recorded before the filament was switched on. This background current was assumed to be due to the escape of secondary electrons produced by neutral particles and possible collection of stray ions and was typically about 5×10^{-9}A. The background was always subtracted from the measured current to get a true signal due to the ionization of neutrals when the filament was switched on. The maximum ionization current obtained

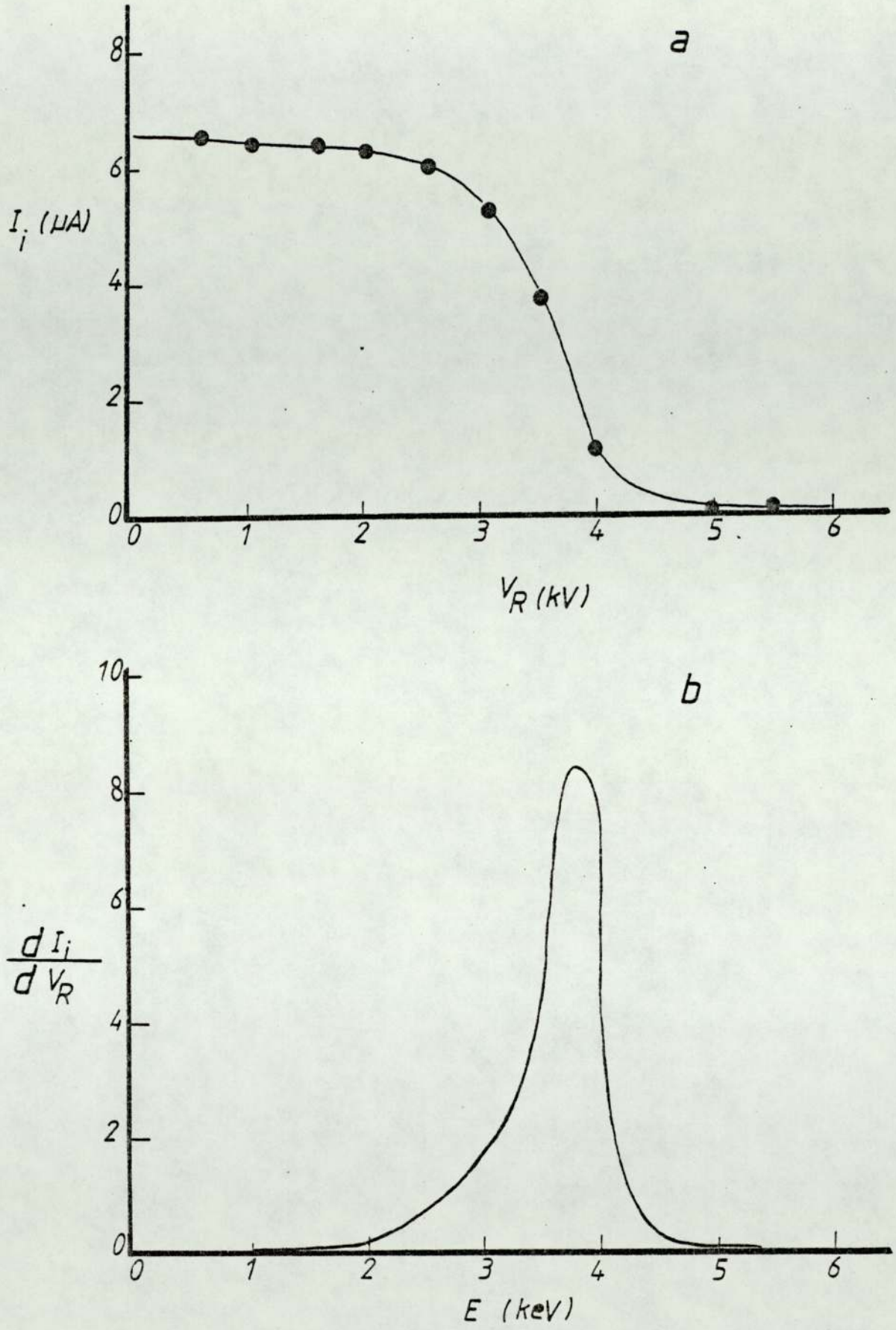

Figure 6.15 (a) Variation of ion current against retarding voltage, V_R, for argon ions

(b) The energy spectrum.

was no more than about three times the background current and was of the order of 1 to 2 x 10^{-8} A. A higher figure could not be expected if one takes into account the equivalent "neutral" current and the efficiency of ionization by the electron beam which would be less than 1%.

The variation of the true signal due to the ion current arriving at the Faraday cup as a result of the ionization of neutrals as a function of variation of V_R is shown in figure 6.16a and the corresponding energy distribution is shown in figure 6.16b. The energy distribution has two major features, firstly, a strong peak at very low energy which could be due to low energy ions arriving at the Faraday up by example reflection in the chamber. The second peak occurs at about 0.7 V_A which is the same energy as that of the ions and thus one can conclude that the neutrals have the same energy as the original ions. It was, however, not possible from these measurements to make any deductions about the energy spread of the fast neutrals. Further evidence in support of the conclusion that the neutrals have the same energy as the ions will be given in the following section.

6.3.2 Indirect method from sputtering yield

An indirect method of assessing the energy of the fast neutrals was devised by comparing the time for the total beam and for the neutrals to etch through a conducting copper film at different conditions for V_A and p_c at constant I_A. The film was prepared by evaporating a copper wire onto a clean glass slide 6 x 8 cm at about 1 x 10^{-5} Torr. This film as then placed in a solid frame containing a slot 1 x 3 cm to limit the etching area and also to protect the rest of the film from the deflected ions when only the neutrals were in use. In addition this made it possible to use

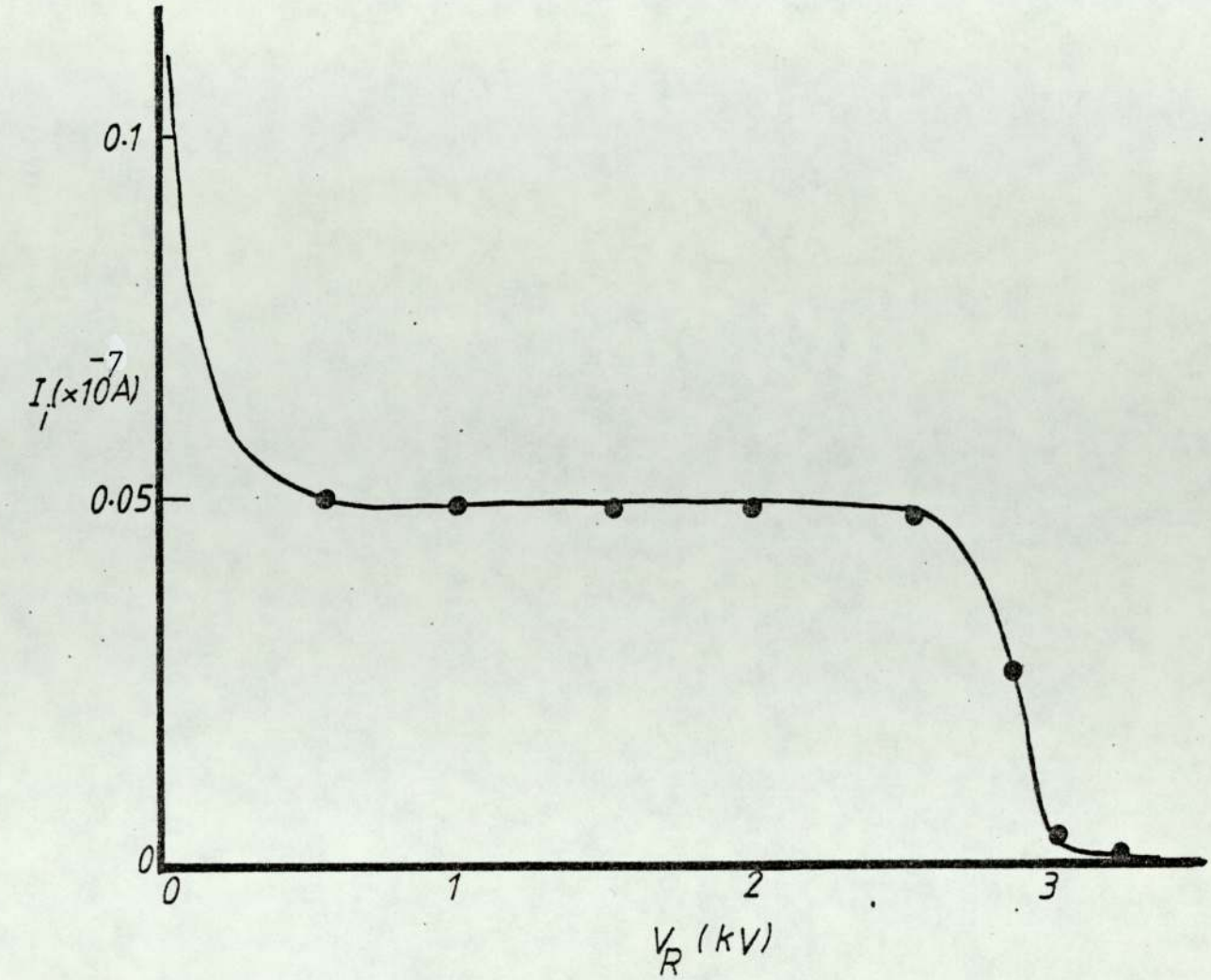

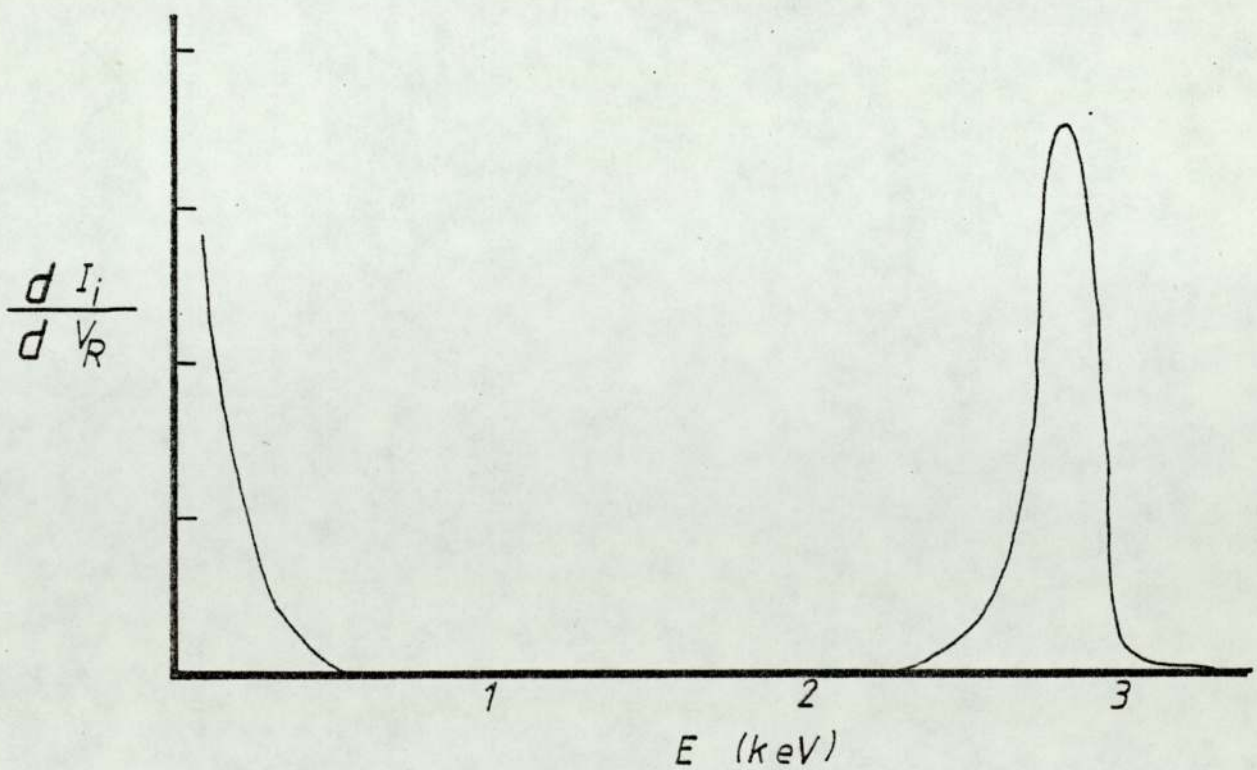

Figure 6.16 (a) Variation of ion current, I_i with retarding voltage, V_R for ionized fast argon neutrals

(b) The energy spectrum.

the slide for several etchings to ensure that the film was the same thickness. The etched area was observed through a window in the wall of the chamber so that the same etched area occurred for the total beam and also for the neutrals. The etching time for the neutrals $t(n_o)$ and the total beam $t(n_o+n_+)$ was recorded for each value of V_A. It can be seen that $t(n_o)$ and $t(n_o+n_+)$ are inversely proportional to (n_o) and (n_o+n_+) respectively and as $t(n_o)$ is always greater than $t(n_o+n_+)$, then we have a ratio of the time, r', given by:

$$r' = \frac{t(n_o+n_+)}{t(n_o)}$$

In addition

$$N_o = \frac{n_o}{n_o+n_+}$$

Figure 6.17 shows the values of r' plotted against the experimental values of N_o and also shows that the uncertainty in r' decreases as the uncertainty in N_o increases. The figure thus shows a linear relationship between r' and N_o and thus again gives evidence that the ions and neutrals have the same energy. Theoretically, one would expect this straight line to have a slope of unity. The fact that it is not unity suggests that there is a systematic error in the measurement of N_o or r', with the latter being the most likely case as it was difficult to judge when the correct area had been etched.

6.4 Discussion

The experimental work described in this Chapter has shown that the source produces fast neutrals and ions and the percentage of the neutrals varies with chamber pressure from about 20% at a

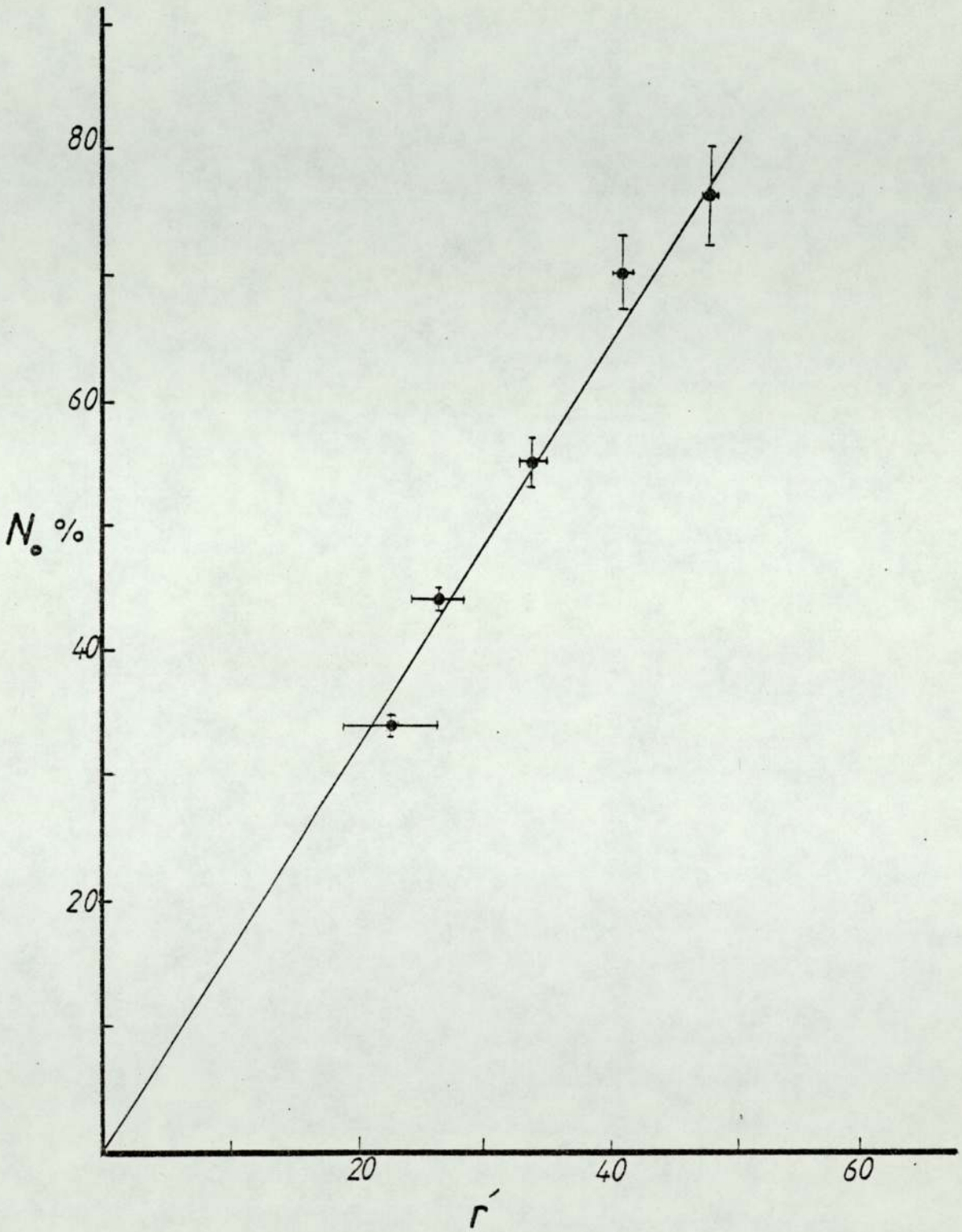

Figure 6.17 The variation of percentage of fast neutrals, N_o with the ratio of etching times for total beam and neutrals r´ using argon.

pressure of 10^{-5} Torr to 90% at 10^{-4} Torr. The energy of these neutrals has been shown to be equal to the corresponding ion energies and that the neutrals originate from a charge exchange process inside the source. This is contrary to the view of Franks[54] who claimed that the neutrals originate from the recombination of fast ions with slow secondary electrons produced at the edge of the ion exit aperture. This latter view has not been supported by the present work because the model described by Franks does not explain the variation of the neutral content with pressure. In addition, the model involving a charge exchange process seems also to adequately explain the small reduction in ion current as the detector is moved away from the source aperture. Franks claimed that when a positive electrode at about 300 volt positioned at 2 cm from the cathode was used, the the percentage of neutrals reduced to less than 5%.

This seems unlikely from the work discussed in section 5.22 as it was found that the Faraday current remained constant at this deflecting voltage. However in Franks' publication there are no details of the actual measurement and experimental techniques. Franks also claimed that neutrals have not been detected when the source cathode was held at a negative voltage (-4kV) and the anode at 0 to +4kV with a retarding cylinder outside the cathode aperture at earth potential. He claims that this is due to the earthed cathode producing a strong electron accelerating field and thus reducing the percentage of fast neutrals. An equally acceptable argument to this idea would be that the accelerated electrons re-ionize the neutrals of course one cannot discount the possibility that more than one mechanism is taking place under these conditions, although the present work strongly supports the model involving a charge exchange process.

CHAPTER 7

CONCLUSIONS AND SUGGESTIONS FOR FURTHER WORK

A study of the spherical version of the saddle field ion source has been made and a review of other types of ion sources is given in order to compare them in terms of their properties and suitabilities for various applications. It has been confirmed that the spherical source is relatively easy to construct and to operate and is particularly suitable for applications in situations where it is necessary to include such factors as the low operating pressure and freedom from magnetic fields yet still maintaining high current densities.

A careful study has been made of the modes of operation of the source. It has been found if the effective pump speed, source conductance, nature of the gas and interpretation of pressure measurements are taken into account the source is most efficient when the mean free path for ionization inside the source is greater than the radius of the source. However, measurements have shown that the current and power efficiency reach a maximum value at a particular pressure and the gas efficiency is greater for argon than for helium.

It has been established that the source produces not only energetic ions but also electrons and fast neutrals. The electrons are of low energy and originate from the edge of the cathode aperture due to secondary electron emission by ion bombardment. This has been confirmed by showing that the electron current is less when a high work function material such as stainless steel is used for the

cathode material. These electrons surround the ion beam but do not contribute to the use of this source for ion etching insulating materials as was reported previously.

The fast neutrals are contained in the ion beam and the neutral content varies with gas pressure such that it increases from about 20% in the efficient oscillating mode at chamber pressures of about 10^{-5} torr to 90% in the glow mode at 10^{-4} torr. Theoretical considerations have shown that these fast neutrals are produced by a resonance charge exchange process inside the source. This model is not in agreement with Franks[54] who proposed that the fast neutrals are produced by a recombination process between the ions and the low energy electrons but this seems unlikely as the cross-section for this process is very small. Furthermore, when these electrons are extracted from the beam the neutral to ion ratio remains the same which would not be the case if a recombination process has taken place. An analysis indicates that the energy of the fast neutrals is the same as that of the ions which is in agreement with a resonance charge exchange process. Advantage can be taken of these fast neutrals as they can be used to etch non-conducting materials, whereas a pure ion beam suffers from the disadvantage that a charge build occurs on any insulating surface.

It is appreciated that there are other aspects of the source which are not fully understood and other diagnostic techniques are necessary to confirm some of the above measurements. At present no attempt has been made to study the plasma characteristics and potential distribution in the source. It is possible that this could be achieved by the use of a very small Langmuir probe. The main problem is that the probe is likely to disturb the plasma which could make the measurement very difficult to interpret and in any case it would be preferable to establish the technique with

a large version of the cylindrical source in which it would be easier to manipulate the probe.

All measurements of the ions have been made with a Faraday collector designed in this laboratory and it has been assumed that it is quite efficient at retaining secondary electrons. Thus it would be very desirable to be able to confirm many of the measurements using an alternative technique such as an ion beam calorimeter in which the secondary electron emission can be neglected and is also suitable for fast ions and neutrals. However, precise measurements with either a Faraday cup or a beam calorimeter will not be possible until further information is known about the charge state of the ions.

In the present work, considerable difficulty was experienced in the energy measurements of the fast neutrals due to the low ionization efficiency in the crossed-beam experiments. It is proposed that a time of flight technique might be more suitable when the resolution will depend essentially on the length of the flight tube rather than the particle detector. In a very recent investigation by Dowset in collaboration with Franks[60] an alternative method has been used to determine the axial and radial variation of the ion/neutral content in the beam. They referred to this as a "punch-through" technique and it is essentially a combination of the method described in section 6.3.2 for etching thin films by ions and neutrals and that described by Fitch et al[43] for the determination of sputtering yields. The important difference is that Dowset and Franks used a series of apertures to determine the sputtered area whereas Fitch et al measured the area in a scanning electron microscope. The technique described by Dowset and Franks is a very interesting development but unlike the method used by Fitch et al, it is necessary to take considerable care to centralise the beam in the aperture.

Considerable developments have now taken place on the various geometries of the saddle field ion sources and this has been demonstrated by the range of applications already in use. These include such diverse techniques as shadowing of specimens for study in electron microscopy, ion etching of dental materials and cleaning of surfaces in ultra high vacuum. It is anticipated that as further developments take place these sources will continue to find new applications.

LIST OF SYMBOLS

A	Area of the two exit apertures
A_1, A_2	Anodes of the cylindrical source
A^{o}_{F}	Fast neutral
A^{+}_{F}	Fast ion
A^{o}_{s}	Slow neutral
A^{+}_{s}	Slow ion
B	Magnetic field
(Bx, By, Bz)	Magnetic field components along x, y and z directions
C	Conductance of the exit aperture
d	The distance between two parallel plates
e	Electron charge
E	Kinetic energy of the charged particle
E_i	Ionization energy
E_e	Electron energy
E.S.C.A.	Electron spectroscopy for chemical analysis
F	Force on the electron due to a magnetic field
(Fx, Fy, Fz)	Components of the force along x, y and z directions
g_1, g_2	Parallel grids
I_A	Anode current
I_B	Ion beam current
I_c	Ion current recorded by plate collector
$I_{(F, f)}$	Faraday current
I_e	Electron current
I_i	Ion current
I_2	Ion current plus secondary electron current produced by energetic neutrals and ions

I_3	Secondary electron current produced by the fast neutrals
I'	Probe current for the total beam
I''	Probe current for the neutral beam
I_i	Ion current after ionization of the fast neutrals
Im	Monitor current
l'	Average path length of ions
M	Molecular weight
m	Mass of the electron
N	Probability of charge exchange process
N_o	Percentage of the fast neutrals
N_+	Percentage of ions in the total beam
N_o (th)	Theoretical value of percentage of fast neutrals
N_o (exp)	Experimental value of percentage of fast neutrals
N (E)	Number of ions with certain energy
N_i	Pair of ions produced by electrons inside the ion source
n	Number of molecules per unit volume
n_o	Number of fast neutrals arriving per second
n_+	Number of ions arriving per second
n^+	Ionized atom
P_1	Deflector plate with positive voltage
p_2	Deflector plate with negative voltage
p_a	Atmospheric pressure
p_c	Chamber pressure
p_e	Equilibrium pressure
p_s	Source pressure
p_{ST}	Transition source pressure
Q	Gas flow
Q'	Work function

R	Retarding grid
R'	Ratio of molecular weight of gases
r	Radius of the electron deflection
r'	Ratio of the etching time for beam and fast neutrals
S	Screen grid
S_E	Effective speed of the diffusion pump
S.E.M.	Scanning electron microscope
T	Absolute temperature
T.E.M.	Transmission electron microscope
t	Time
$t(n_o)$	Etching time for neutrals
$t(n_o+n_+)$	Etching time for total beam
V'	Volume of the experimental chamber
V_A	Anode volume
V_1, V_R	Retarding voltage
V_2	Accelerating voltage
V_D	Total deflecting voltage
(V_x, V_y, V_z)	Velocity of the electron along x, y and z direction
X_D	Length of the electrostatic deflector
y_D	Deflection of ions by the analyzer
λ_e	Mean free path for electron molecular collision
α	Maximum total collision cross section
η_i	Current efficiency
η_p	Power efficiency
η_g	Gas efficiency
γ	Secondary electron coefficient
σ	Charge exchange cross section

REFERENCES

(1) NIER, O.A.
"A mass spectrometer for routine isotope abundance measurements"
The Review of Scientific Instruments, Volume 11, Page 212-216, (1940).

(2) BLEAKNEY, W
"The ionization potential of molecular hydrogen"
Physics Review, Volume 40, Page 496-501, (1932).

(3) PIERCE, J.R.
"Theory and design of electron beams"
New York, London, Van Nostrand 1954.

(4) SLABOSPITSKII, R.P. KARNAUKHOV, I.M. AND KISEL, I.E.
"A three-electrode electron gun ionizer with an ionization efficiency of 2 x 10^{-3}"
English Translation in Soviet Phys.Tech.Phys. (USA), Vol.11, No. 12 (1967).

(5) ARDENNE, M. VON, SCHILLER, S. AND WESEMEYER, H.
"On plasma researches with an electron beam probe of small diameter"
Exper. Tech. der Physics, Volume 6, No. 2, 49-62 (1958) in German.

(6) BAILY, C., DRUKY, D.L., AND OPPENHEIMER, F.
"A magnetic ion source"
The review of Scientific Instruments, Volume 20, Number 3, page 189-191, (1949).

(7) ATTERLING, H.

"Experiments with an arc ion source for the cyclotron"

Ark. Mat. Ast, FYS, 35A, paper 32, 16, (1948).

(8) MOAK, C.D., BANTA, H.E., THURSTONE, J.N., JOHNSON, J.W. AND KING, R.F.

"Duoplasmatron ion source for us in accelerators"

The Review of Scientific Instruments, Volume 30 , Number 8, page 694-699, (1959).

(9) CIUTI, P.

"A study of ion beams produced by a duoplasmatron ion source"

Nuclear Instruments and Methods, Volume 79, page 55-60, (1970).

(10) PENNING, F.M.

"Time-lag in dark discharge in gas filled photocell"

Physica, 3, page 563-568, (1936) in German.

(11) KELLER, R.

"Penning ion source"

Inds. Atomiques 2, No. 9-10, page 81-84, (1959)

(12) PRELEC, K., AND ISAILA, M.

"A small source for multiply charged heavy ions"

Nuclear Instruments and Methods, Volume 92, page 1-6, (1971)

(13) NAGY, J.

"The energy spectrum of ion beams emitted by a Penning-type ion source"

Nuclear Instrum. Methods (Netherland), Volume 32, Number 2, page 229-234, (1966).

(14) ANDERSON, C.E., EHLERS, K.W.
"Ion source for the production of multiply charged heavy ions"
The Review of Scientific Instruments, Volume 27, Number 10, page 809-817, (1956).

(15) THONEMANN, P.C., MOFFAT, J., ROAF, D. AND SANDERS, J.H.
"The performance of a new radio frequency ion source"
Physical Society Proceeding, Volume 61, page 483-485, (1948).

(16) VALYI, L.
"Investigation of a source of He^{++} ions"
Nuclear Instruments and Methods, Volume 79, page 315-319 (1970).

(17) HARRISON, E.R.
"Investigation of the perveances and beam profiles of an aperture disc emission system"
Journal of Applied Physics, Volume 19, Number 6, page 909-913, (1958).

(18) DATZ, S., AND TAYLOR, H.E.
"Ionization platinum and tungsten surfaces 1. The Alkali Metals"
The Journal of Chemical Physics, Volume 25, Number 3, Page 389-394, (1956).

(19) INGHRAM, G.M. AND CHUPKA, A.W.
"Surface ionization source using multiple filaments"
The Review of Scientific Instruments, Volume 24, Number 7, page 518-520, (1952)

(20) GRAIG, R.D.
"Surface ionization source for mass spectrometry"
Journal of Scientific Instruments, Volume 36, page 38-39, (1959).

(21) LIEBL, H.J. AND HERZOG, F.K.
"Sputtering ion source for solids"
Journal of Applied Physics, Volume 34, Number 9, page 2893-2896, (1963).

(22) HURLEY, R.F.
"The production of focused ion beams for surface and gas-phase collision studies"
Vacuum, Volume 25, Number 4, page 143-149, (1975).

(23) WILSON, R.G., BREWER, G.R.
"Ion beams with applications to ion implantation"
The publisher, John Willey & Son Inc. (1973) U.S.A.

(24) BARFORD, N.C.
"Space charge neutralization by ions in linear flow electron beams"
Journal of Electronics and Control, Volume 3, Number 1, page 63-86, (1957).

(25) HINES, M.E., HOFFMAN, G.W. AND SALOOM, J.A.
"Positive ion drainage in magnetically focused electron beams"
Journal of Applied Physics, Volume 26, Number 9, page 1157-1163, (1955).

(26) KLEMPERER, O., BARNETT, M.E.
"Electron Optics"
Cambridge University Press, London, Third Edition, page 225, (1971).

(27) HALL, J.H.
"Some applications of triode sputtering to integrated circuits"
Vacuum, Volume 17, Number 5, page 261-264, (1966).

(28) McILRAITH, A.H.
"A charged particle oscillator"
Nature, Volume 212, Number 5069, page 1422-1424 (1966).

(29) FITCH, R.K., MULVEY, T., THATCHER, W.J. AND McILRAITH, A.H.
"The oscillator gauge: A new type of ionization gauge"
Journal of Physics E: Scientific Instruments, Volume 4,
page 1-4, (1971).

(30) PEGGS, G.N. AND McILRAITH
"A sensitive time-of-flight molecular beam
Journal of Physics E: Scientific Instruments, Volume 6,
page 1137-1139, (1973).

(31) RUSHTON, G.J.
Ph.D. Thesis, Physics Department, The University of Aston
in Birmingham, page 61, (1972).

(32) FITCH, R.K., MULVEY, T., THATCHER, W.J. AND McILRAITH, A.H.
"A new type of ion source"
Journal of Physics D: Applied Physics,
Volume 3, page 1339-1402, (1970).

(33) RUSHTON, G.J. AND FITCH, R.K.
"The performance of twin wire electrostatic charged particle
oscillator"
Vacuum, Volume 21, Number 10, page 449-452, (1971).

(34) RUSHTON, G.J., O'SHEA, K.R., AND FITCH, R.K.
"Modes of operation of an electrostatic ion gun"
Journal of Physics D: Applied Physics, Volume 6,
page 1167-1172, (1973).

(35) RUSHTON, G.J. AND FITCH, R.K.
"The twin anode electrostatic ion gun with thermionic electron injection"
Journal of Physics E: Scientific Instruments, Volume 7, page 313-315, (1973).

(36) CLARK, R.B., FITCH, R.K., GHANDER, A.M., AND SMITH, A.G.
"The ionic charge states produced by the oscillating electron electrostatic ion source"
Journal of Physics E: Scientific Instruments, Volume 7, page 566-568, (1974).

(37) FITCH, R.K., GHANDER, A.M., RUSHTON, G.J., AND SINGH, R.
"Design and operating characteristics of a low pressure ion source"
Proceedings, 6th International Vacuum Congress, Japan Journal Appl ed Physics, suppl. 2, pt.1, page 411-413, (1974).

(38) FRANKS, J.
"Ion Tech. Ltd"
British Patent Appl.No. 44718/78 (1973).

(39) FRANKS, J.
"Proceedings of Conference on Low Energy Ion Surface Interaction", Liverpool, England (1974).

(40) GHANDER, A.M.
Ph.D. Thesis, Physics Department, The University of Aston in Birmingham, page 67, (1974).

(41) KHORASSANY, M. AND FITCH, R.K.
"Energy distribution of the ions produced by saddle field ion sources"
Vacuum, Volume 27, Number 3, page 159-162, (1975).

(42) FITCH, R.K., KHORASSANY, M. AND MAWLOOD, T.
"The production of energetic neutrals by saddle field ion sources"
Proceedings 7th International Vacuum Congress and 3rd International Conference of solid surfaces, page 285-288, Vienna, (1977).

(43) FITCH, R.K., MAHMOUD, E.A. AND GHAFOURI, S.N.
"The charge state of the ions produced by a saddle field ion source and its applications to the measurement of sputtering"
Paper to be presented at the 8th International Vacuum Congress, Cannes, September 1980.

(44) FITCH, R.K. AND RUSHTON, G.J.
"Low pressure ion source"
The Journal of Vacuum Science and Technology, Volume 9, No.1, page 379-382, (1971).

(45) GHANDER, A.M. AND FITCH, R.K.
"An improved form of the oscillating electron electrostatic ion source for ion etching"
Vacuum 24, Number 101, page 483-4871 (1974).

(46) FRANKS, J. AND GHANDER, A.M.
"A saddle field ion source of spherical configuration for etching and thinning applications"
Vacuum, Volume 24, Number 10, page 489-491, (1974).

(47) FRANKS, J., CLAY, C.C., AND PEAC , G.W.
"Ion beam thin film deposition"
Scanning Electron Microscopy (1980)
S.E.M. Inc. AMF, O'Hare (Chicago) U.S.A.

(48) DHARIWAL, R.S., FITCH, R.K., LAVELLE, C.L.B. AND JOHNSON, G.
"Artefacts observed on dental tissues during ion etching in scanning electron microscope"
J.Anat. Volume 122, Number 1, page 133-140, (1976).

(49) DHARIWAL, R.S. AND FITCH, R.K.
"In situ ion etching in a scanning electron microscope"
Journal of Materials Science, 12, page (1225-1232), (1977).

(50) KHORASSANY, M.
Ph.D. Thesis, Physics Department, The University of Aston in Birmingham, page 56, (1977).

(51) KHORASSANY, M.
Ph.D. Thesis, Physics Department, The University of Aston in Birmingham, page 78, (1977).

(52) MASSEY, H.S., AND BURHOP, E.H.
"Electronic and Ionic impact phenomena"
Oxford University Press, page 30, (1952).

(53) NAVEZ, M., SELLA. C., AND CHAPEROT
"Electron microscope study of the effects of ionic bombardment on glass"
International Symposium of the National Scientific Research Centre - Ionic Bombardment Theory and Application
Gordon and Breach, New York, page 339-359, (1962).

(54) FRANKS, J.
"Properties and application of saddle field ion sources"
Journal of Vacuum Science Technology, Volume 16, Number 2, page 181-183, (1979).

(55) RUSHTON, G.J.
Ph.D. Thesis, Department of Physics, The University of Aston in Birmingham, page 63-68, (1972).

(56) KLEMPERER, O.
"Electron Physics"
The Physics of the Free Electron, Butterworths, London, page 11, (1961).

(57) CARTER, G., AND COLLIGON, J.S.
"Ion bombardment of solids"
Heinemann Educational Books Ltd., London, page 54, (1969).

(58) SALSBORN, E.
"Charge exchange cross sections"
IEEE Transactions on Nuclear Science, Volume NS-23, Number 2, page 947-958, (1976).

(59) RAPP, D., AND FRANCIS, W.E.
"Charge exchange between gaseous ions and atoms"
Journal of Chemistry Physics, Volume 37, Number 11, page 2631-2645, (1962).

(60) FRANKS, J. AND DOWSETT, M.G.
"Characterisation of the B11 saddle field ion source"
Private communication, Ion Tech. Ltd., Teddington, August, 1980.

Proc. 7th Intern. Vac. Congr. & 3rd Intern. Conf. Solid Surfaces (Vienna 1977)

THE PRODUCTION OF ENERGETIC NEUTRALS BY SADDLE FIELD ION SOURCES

R.K.Fitch, M.Khorassany* and T.N. Mawlood

Department of Physics, University of Aston in Birmingham,B4 7ET,U.K

Abstract: An electrostatic analyser has been developed to investigate the production of energetic neutrals by saddle field ion sources using helium, argon and nitrogen. It has been found that with both the cylindrical and the spherical source operating at constant source current, the,percentage of energetic neutrals in the emerging beam increases from about 20% to 70% as the chamber pressure increases from 10^{-5} to 10^{-3} torr. This corresponds to a decrease in anode voltage from about 7 kV to 2 kV. Calculations have shown that these results can be explained in terms of a charge exchange process occurring inside the source. Advantage can be taken of this high neutral content when the source is used for ion etching insulating materials.

INTRODUCTION

The saddle field ion sources discussed in this paper are electrostatic devices which operate at low pressures without a magnetic field or thermionic filament. They originally arose from the idea of McIlraith /1/ for a charged particle oscillator which was similar to the energy analyser described by Mollenstedt /2/. Two forms of the ion source are now available, one employing cylindrical and the other spherical geometry. The former produces a wide ion beam with a fairly broad energy spread whereas the latter produces an intense fine beam of ions with a narrower energy spread /3/. The cylindrical source was first described by Fitch et al. /4/ and later in improved forms by Fitch and Rushton /5/ and Ghander and Fitch /6/. The spherical source was devised by Franks /7/ and the properties of this source are given by Franks and Ghander /8/.

These sources are particularly useful in high and ultra-high vacuum technology such as for ion cleaning of surfaces for surface analytical techniques. One particular application which has been in use for some time is for ion etching and thinning of materials for examination by transmission and scanning electron microscopy. In a recent paper Dhariwal and Fitch /9/ incorporated one of these sources into the specimen stage of a scanning electron microscope for in-situ ion etching and applied it to a variety of materials. They observed that the source could be used with electrically insulating materials as well as with conductors and suggested that this was due to the presence of energetic neutrals in the emerging ion beam. The purpose of this paper is to report the results of an investigation undertaken to determine the neutral content as a function of pressure and anode voltage for helium, argon and nitrogen.

* On leave from National University of Iran, Tehran.

DESCRIPTION OF THE ANALYSER AND EXPERIMENTAL PROCEDURE

The cylindrical source used in this work consisted of a stainless steel cathode, diameter 25mm and length 75mm, enclosing two tungsten rod anodes, diameter 1.5mm, disposed symmetrically about the cylinder axis at a separation of 4mm. The ions emerged through a circular aperture, diameter 5mm, positioned midway along the cathode and normal to the plane of the anodes. The spherical source was purchased from Ion Tech Ltd. The effective diameter is about 25mm, the anode aperture is 5mm and the two ion exit apertures, diameter 1.5mm, are positioned at diametrically opposite points in the cathode. Schematic diagrams of the source and analyser are shown in figure (1). The Faraday collector, C entrance aperture 27mm, was first used in this laboratory for ion energy analysis /3/. The two flat plates V_1 and V_2, were used when it was required to deflect the ions by applying potentials of $\pm \frac{1}{4}V_a$, where V_a is the source anode voltage. Three arrangements of the analyser are shown in the figure. In figure 1a, $V_1 = V_2 = 0$ and it is assumed that the current i_1 is

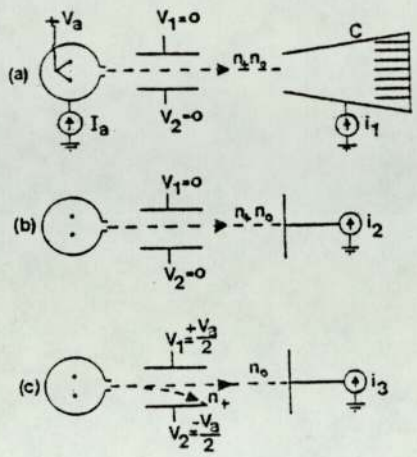

Fig. 1. Schematic diagram of the ion source and analyser.

proportional to the number of ions n_+. In figure 1b, $V_1 = V_2 = 0$, but the Faraday collector has been replaced by a flat nickel collector and it is assumed that the current i_2 is proportional to n_+ and the secondary electrons produced by n_+ and the energetic neutrals n_o. In figure 1c, $V_1 = +\frac{1}{2} V_a$ and $V_2 = -\frac{1}{2} V_a$ and the current i_3 is then only due to the secondary electrons produced by the energetic neutrals. These three situations can be represented by the following equations:

$$i_1 = n_+ e$$

$$i_2 = (n_+ + k n_+ + k n_o) e$$

$$i_3 = k\, n_o e$$

where e is the electron charge and k is the secondary electron coefficient assumed to be equal for ions and neutrals of the same energy. Thus any determination of i_1, i_2 and i_3 makes it possible to measure k given by:

$$k = \frac{i_2 - i_1 - i_3}{i_1} \quad \ldots\ldots\ldots (1)$$

and hence n_+ and n_o and thus the percentage of neutrals, N, in the beam where,

$$N = \frac{n_o}{n_o + n_+} \times 100\%$$

The source and analyser were operated in a stainless steel chamber pumped by a conventional rotary pump/diffusion pump system, using an alumina trap in the fore line and "Santovac 5" fluid in the diffusion pump. The pressure in the chamber, p_c, was measured with a Penning gauge calibrated for dry nitrogen.

EXPERIMENTAL RESULTS

Figure 2a shows the variation of k for helium as a function of V_a for anode currents I_a, of 1mA and 3mA using the spherical source. The values of k vary from about 0.3 to 0.8 as V_a increases and hence as the average ion energy also increases. The uncertainty in k, indicated by the error bars have been estimated from equation (1) and show that the uncertainty in k increases with decreasing V_a. These large uncertainties were expected on account of the limitation of the method and likely variation of the condition of the collector surface during the measurements. The figure does however show that k is independent of I_a. Figure 2b gives the corresponding variation of N and shows that N increases with decreasing V_a, which corresponds to an increase in the chamber pressure. However for all values of V_a, N is greater for I_a = 3mA. It should also be noted that the uncertainties in N are less than the corresponding uncertainties for k. This arises from the fact that N is relatively insensitive to the uncertainty in k.

Figure 3 gives two curves of the variation of N with V_a for argon - one for the spherical source and the other for the cylindrical source for I_a = 1mA. Both curves again show that N increases with decreasing V_a but at all values of V_a, N is greater for the spherical source.

In order to verify these measurements of the percentage of neutrals at different values of V_a, the spherical source was set up as in figure 1c with V_1 and V_2 just sufficient to separate the ion and neutral beams. The times required to etch a copper film evaporated onto a glass plate were then recorded for the ions (t_+) and the neutrals (t_o) using argon. The variation of the ratio $R = t_+/t_o$ with V_a is given in figure 4 and clearly follows the same variation as N does with V_a as given in figures 2b and 3. For example, for V_a = 4 kV, R is about unity and the corresponding value of N is about 40%. This agreement is as well as can be expected taking into consideration the various uncertainties in both experiments.

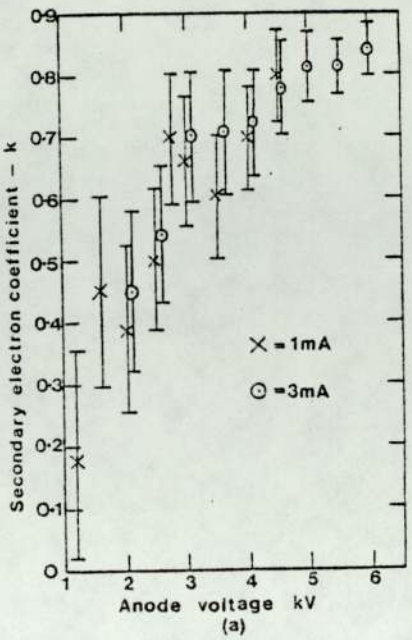

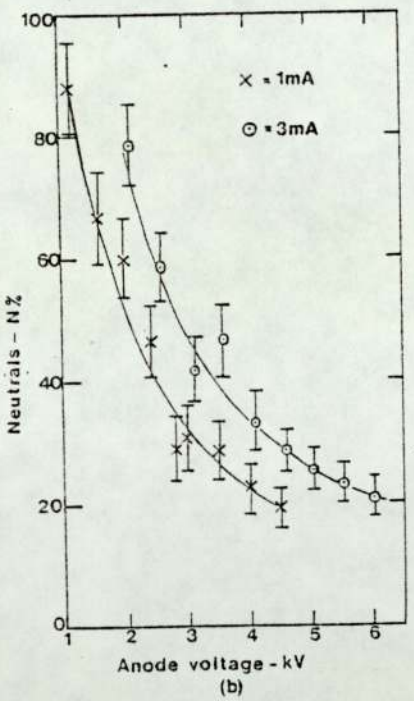

Fig. 2. The variation with anode voltage of (a) the secondary electron coefficient and (b) the percentage of energetic neutrals, using the spherical source with helium for I_a equal to 1mA and 3mA.

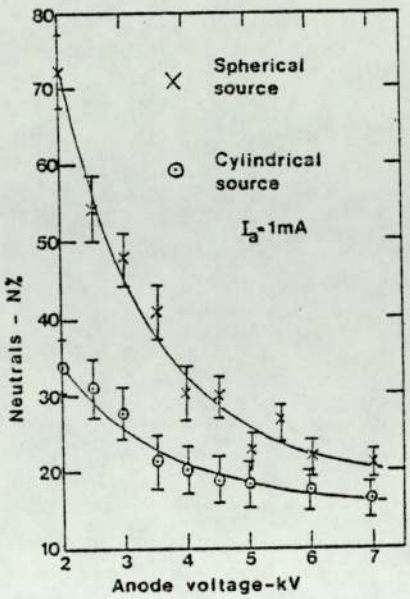

Fig. 3. The variation of the percentage of energetic neutrals for both sources using argon for I_a = 1mA.

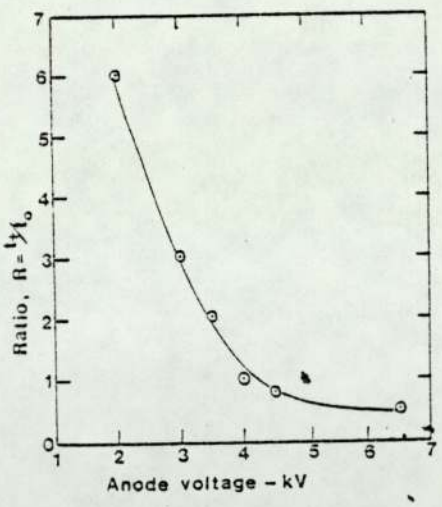

Fig. 4. The ratio of the etching times for ions and neutrals as a function of anode voltage using the spherical source with argon.

DISCUSSION AND CONCLUSIONS

It is clear from the results for helium and argon shown in figures 2 and 3 that both sources produce a significant proportion of energetic neutrals. Similar results have also been obtained for nitrogen. In all cases the percentage of neutrals increases with decreasing anode voltage which corresponds to an increase in chamber pressure, p_c. Furthermore figure 2b shows that at constant V_a the neutral content increases as I_a changes from 1mA to 3mA, because p_c is greater when I_a = 3mA. These results can be explained assuming a symmetric resonance charge exchange process occurring inside the source, in which a fast ion and a slow neutral produce a slow ion and a fast neutral. The probability of the charge exchange process, P, is given by:

$$P = \sigma \ell n$$

where σ = charge exchange cross section, ℓ average path length of the ions and n is the gas density.

This can be illustrated using the results for the spherical source with argon when V_a = 4kV, I_a = 2mA and p_c = 7×10^{-5} torr. The effective speed of the diffusion pump was measured and found to be about 100 ls^{-1}. Thus assuming molecular flow the total conductance of both apertures is 0.35 ls^{-1} which gives a pressure inside the source of 2×10^{-2} torr when p_c = 7×10^{-5} torr, and the corresponding value of $n = 2 \times 10^{14}$ $mol.cm^{-3}$. At 4kV the average ion energy is about 3keV/3/ giving a value of σ for argon as 14.5×10^{-16} cm^2 /10/. The radius of the spherical source is 1.3 cm so that it can be assumed that ℓ is about 1 cm. These figures give a value of P = 0.3 which is in reasonable agreement with the experimental value of N which is equivalent to about 0.4. Figures 3a and 3b show that at the same anode voltage N is larger for the spherical source. This arises from the fact that although ℓ is greater in the larger diameter cylindrical source, the source pressure is much higher in the spherical source due to the larger conductance of the aperture in the cylindrical source. This investigation has shown that with these sources it is possible to set the operating conditions to select the desired neutral content in the beam. This is particularly important when the source is being used for etching insulating materials. In one particular experiment the spherical source was used to etch a sample of P.T.F.E. using argon with the anode voltage selected to provide 50% neutrals and 50% ions at an anode current of 2mA. The etched specimen was examined in a scanning electron microscope and it was found that the etching rate of the neutrals was about 7μm hr^{-1} whereas the etching rate of the ions was only about 1.5μm hr^{-1}.

ACKNOWLEDGEMENTS

One of us (M.K.) would like to thank the National University of Iran for granting him study leave. Two of us would like to acknowledge support from the Iran Ministry of Science (M.K.) and the Royal Society and the University of Aston in Birmingham (R.K.F.) to attend the Congress.

REFERENCES

/1/ A.H.McIlraith: Nature, Lond., 212 (1966) 1422.
/2/ G.Mollenstedt: Optik.5 (1949) 499.
/3/ R.K.Fitch and M.Khorassany: Vacuum 27 (1977).
/4/ R.K.Fitch, T.Mulvey,A.H.McIlraith, and W.J.Thatcher: J.Phys.D, 3 (1970) 1399.
/5/ R.K.Fitch and G.J.Rushton: J.Vac. Sci. and Tech. 9 (1972) 379.
/6/ A.M. Ghander and R.K.Fitch: Vacuum 24 (1974) 483.
/7/ J.Franks: British Patent No.44718/ 73 (1973).
/8/ J.Franks and A.M.Ghander: Vacuum 24 (1974) 489.
/9/ R.S.Dhariwal and R.K.Fitch: J.Mat. Sci. 12 (1977) 1225.
/10/ E.Salzborn: IEEE Trans. on Nuclear Science 23 (1976) 947.